2014

EVALUATION OF THEORETICAL CAPACITY MODELS FOR PLATE ANCHORS IN SAND IN RELATION TO FLOATING OFFSHORE WIND TURBINES

Fabian C. Dietrich
University of Rhode Island, Fabian_Dietrich@my.uri.edu

EVALUATION OF THEORETICAL CAPACITY MODELS FOR PLATE ANCHORS IN SAND IN RELATION TO FLOATING OFFSHORE WIND TURBINES

BY

FABIAN C. DIETRICH

A MASTER'S THESIS SUBMITTED IN PARTIAL FULFILLMENT OF THE

REQUIREMENTS FOR THE DEGREE OF

MASTER OF SCIENCE

IN

CIVIL AND ENVIRONMENTAL ENGINEERING

UNIVERSITY OF RHODE ISLAND

2014

MASTER OF SCIENCE THESIS

OF

Fabian Dietrich

APPROVED:

Thesis Committee:

Major Professor Aaron S. Bradshaw

Christopher D.P. Baxter

Harold B. Vincent

Nasser H. Zawia

DEAN OF THE GRADUATE SCHOOL

UNIVERSITY OF RHODE ISLAND

2014

ABSTRACT

Increasing emission of carbon dioxide from combustion of fossil fuels its effect on the earth's climate has led to increased research into renewable, clean energy solutions. Wind energy has been used as an alternative energy source for hundreds of years, however current research proposes the deployment of offshore wind farms in the deep waters of the oceans. A major challenge of deploying offshore wind farms is to safely and economically fix the wind turbines by means of anchors in the seabed.

The objective of this study is to evaluate whether different anchoring concepts are suitable for securing floating offshore wind turbines in sandy soil conditions. For this purpose, an extensive literature review has been carried out to identify existing anchor capacity prediction models for three different anchor types. A 1-g model laboratory program was then developed and pullout tests using different anchor shapes in sand were performed.

The laboratory testing program included pullout tests on shallow, vertically loaded square plate anchors, inclined square plate anchors, and drag embedment anchors in sands. For this purpose a testing facility (1.2 m width, 2.4m length and 0.9m height) was developed and a total of 11 pullout tests were carried out. The sand samples were prepared at a relative density of 22% and the tested depths varied from 0.15 m to 0.45 m. Tests results show an increase in capacity with increasing inclination angles.

A comparison of the obtained test results and predicted capacities were used to evaluate the existing models. Best fit models were identified and loads derived from a state-of-the-art wind turbine were used to assess the feasibility of the proposed anchors to secure the 5-MW turbine. The results suggest that the examined anchor types are theoretically capable of mobilizing allowable capacities larger than the acting forces. The feasibility of anchor installation at the required embedment depths has to be proven in future research.

ACKNOWLEDGMENTS

This past year has been one of the most interesting years, both personally and professional and would not have been possible without the help of so many people on so many levels.

First of all I would like to thank my Major Advisor, Prof. Aaron Bradshaw, for his patience, encouragement, continual help and advice throughout my thesis. Without him this research would not have been possible.

I would like to address my thanks to Prof. Christopher Baxter for his time, insight, comments and ideas throughout my studies and to Joseph Giampa for his help and input towards this research.

I feel grateful for everyone who has been a part of my studies and contributed to it in any possible way.

To my parents, Susanne Rolf-Dietrich and Christoph Dietrich, for doing what great parents do. To my brother, Jan Andre, without you three I would not be the same person I am today. You influenced me in so many ways, guided me throughout my life and provided me with unconditional support. Thank you.

TABLE OF CONTENTS

LIST OF TABLES

LIST OF FIGURES

1 INTRODUCTION

1.1 Overview of Mooring Systems for Offshore Floating Structures

Offshore wind energy is a major focus of wind energy research and deployment both in Europe and in the United States. As the need for energy exponentially increases a steady desire for new energy resources exists (Musial and Butterfield, 2004). Although the concept of wind energy as a source of green energy was introduced in the 1970's (Heronemus, 1972), it was not until the 1990's that extensive research studies were carried out. While offshore wind turbines in shallow water depth are already widely distributed, there still is a lack in deepwater solutions due to technical and economical issues. Nevertheless wind power has established itself as a major source of non-polluting renewable energy and onshore wind farms have helped meet the large demand for electricity in the United States and Europe (Matha et al., 2009).

Currently the majority of wind farms are located either in shallow water or onshore. Shallow water depths allow the manufacturers to use conventional land-based turbines with upgraded electrical and corrosion control systems. These fixed-bottom structures are placed on a foundation in the seabed and are therefore limited to water depths of about 30 m. Unlike the waters surrounding most northern European countries, waters along the U.S. east coast are often deeper and there is pressure to move proposed wind farms out of the viewshed of the public. The result is that many offshore wind farms on the U.S. east coast are likely to be in

water depths greater than 30 m. Greater water depths lead to more severe loading conditions that make conventional anchoring systems extremely difficult and expensive (Butterfield and Musial, 2004). Fixed-bottom systems, such as monopoles, lattice-jacket, and tripods, are not practical in greater water depths and therefore new anchoring systems have to be developed that can withstand the wind, wave, and tidal forces (Butterfield et al., 2007).

A major concern with offshore wind energy is whether it is practical to provide renewable energy at low and competitive costs compared to traditional energy resources (Snyder and Kaiser, 2009). Several studies analyzing costs of offshore wind turbines (OWT) have been carried out (e.g. Hensel et al., 2012) and a comprehensive analysis of offshore floating wind turbines can be found in Green and Vasilakos (2011), Jonkman and Buhl (2007) and Breton and Moe (2009).

Only about 10% of the potential offshore wind resources available in the United States are in shallow water while the remaining ones are located in deeper water depths. Recent studies have indicated that for the New England States within a range of 40-90 kilometers off the coast, energy resources up to 166,300 MW are available in deep water. The potential of deepwater solutions can be emphasized when taking into account that only about 2,700 MW are available in shallow water. It is estimated that, in total, about 900 GW of wind potential is accessible in areas between 10 km and 100 km off the coast of the United States. In total, the offshore

wind resource potential is higher than the current U.S. electrical capacity (Musial and Butterfield, 2004).

It is not unreasonable to assume that the U.S. offshore wind industry will inevitably move towards deepwater floating platforms. Moving further offshore means not only an increase in water depth but also an increase in the uncertainties of the ocean conditions especially in the Atlantic Ocean. In contrast to the well defined wind, wave, tide, and current conditions in the North and Baltic Sea these conditions are less known in the Atlantic, particularly in the case of extreme events such as hurricanes and nor'easters (Musial and Butterfield, 2004; Aubeny et al., 2001).

The feasibility of floating structures has already been proven by the offshore oil and gas (O&G) industry for decades. Floating structures have been constructed in water depths up to 2,400 m. It is anticipated that the offshore wind industry will go through a similar development. In both industries the first developments were located relatively close to the shore in shallow water (Schneider and Senders, 2010). However it remains to be proven that the technology for floating wind platforms can be transferred to the offshore wind industry. The experience gained in the O&G industry can be used as a guideline but significant differences in loading conditions, soil properties, and foundation types must be considered.

In order to support a floating offshore platform, there are primarily three different designs being used in the O&G industry right now (Matha et al., 2009):

1. A ballasted deep-drafted spar buoy;
2. An unballasted tension leg platform;
3. A drafted barge.

For this thesis, floating production storage and offloading structures have been excluded because of their lack of application for offshore wind energy facilities.

The three concepts are displayed in Figure 1. The difference between these concepts lies in the way they try to achieve stability and resistance against the applied forces. The drafted barge generates stability by using the distributed buoyancy of the platform. The idea of the ballasted deep-drafted spar buoy is to create stability by hanging weights below a centrally installed buoyancy tank. This tank creates a righting moment and high inertial resistance. The tension leg platform (TLP) solely relies on the stability created by the line tension (Butterfield et al., 2005). A TLP provides the most stable form of floating platforms and with increasing numbers of tendons the stability can increase even more. Large parts of platforms anchored with vertical moorings usually are submerged and thus not exposed to wave loadings. In general, TLP anchors need to withstand larger moorings forces than an anchor in a catenary mooring system (Musial et al., 2004).

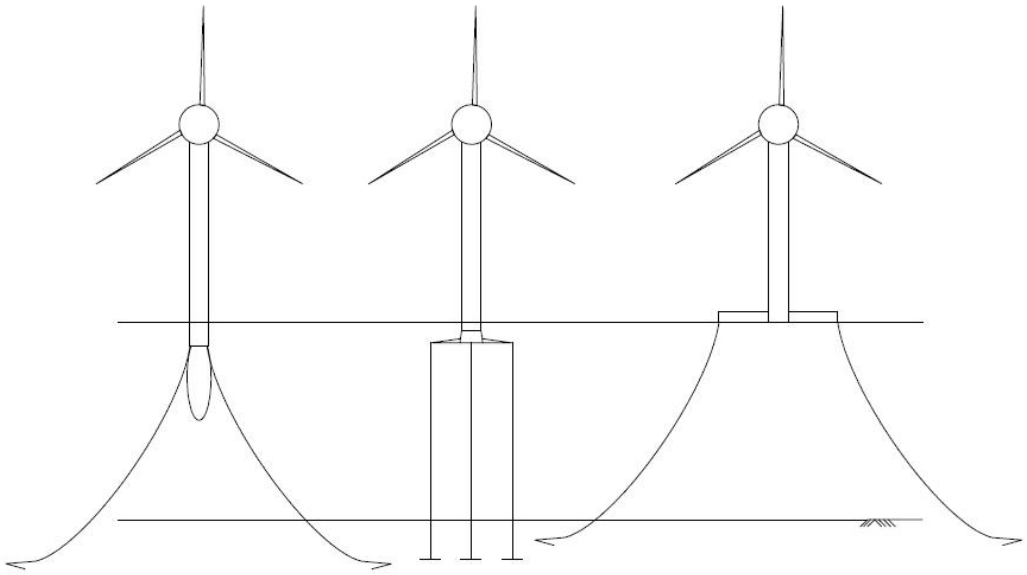

(a.) (b.) (c.)

Figure 1- Floating structures for OWT a.) ballasted buoy, b.) tension leg platform, c.) drafted barge (adapted from: Musial et al. 2005)

There are different alternatives on how to anchor floating structures to the seabed depending on the type of floating platform. The most common mooring systems in the O&G industry are catenary moorings, taut-leg moorings, and vertical tension legs (Musial et al., 2004). Catenary mooring systems are usually used with ballast stabilized buoys or buoyancy stabilized barges. The tension leg platforms meanwhile use taut, semi-taut leg or vertical mooring systems (Jonkman, 2007). There are multiple possibilities of the types of mooring cables used, such as chains, steel, or synthetic fibers.

Catenary systems have been used for a long time to secure floating structures. They were named after the curve the mooring line forms between the floating platform and the seabed because of its flexible structure. Due to this bending, the mooring touches the seabed before it reaches the anchor and the angle of the anchor chain and mudline is close to zero. This results in almost entirely horizontal forces on the anchor. It is not uncommon for catenary mooring systems to have large footprints and to be anchored in the seabed at a radial distance close to the water depth (Randolph and Gourvenec, 2011). The scope of a mooring system, defined as the ratio of the total length of the mooring components to the water depth, can be as high as 5 for catenary mooring systems.

As the water depths increase, the heavy weight of anchor chains can become a limiting parameter in deep water applications. Thus taut or semi-taut moorings with smaller scopes become a more desirable solution in deeper water. Another advantage of the taut or semi-taut moorings is the smaller footprint that they require (Butterfield et al., 2005).

The main difference between taut moorings and catenary mooring for the geotechnical anchor system is the angle at which the mooring enters the seafloor. In taut moorings the line usually arrives at an angle between 30 and 45 degrees relative to the horizontal at the seabed, and the anchor has to withstand horizontal and vertical forces (Randolph and Gourvenec, 2011).

Tension-leg platforms are usually anchored with vertical moorings that arrive at an angle close to 90 degrees and will result in mainly vertical forces. The steeper the angle between mudline and floating platform is, the shorter and lighter the anchor line will be (Randolph and Gourvenec, 2011).

The different moorings systems are displayed in Figure 1 with a vertical mooring line system in Figure 1b and a caternary mooring system on the right and left hand side (Figures 1a and 1c).

There are numerous variations of anchors available today to use with both canetary and taut mooring systems. The load capacity of an anchor-system always depends on the seabed soil conditions. These conditions vary for each site so usually the anchor will specifically be designed for the conditions found (Musial et al., 2004a). The typical anchor of a catenary mooring system is the drag embedment anchor (DEA). Inclined plate anchors can be used for taut-leg and semi taut-leg systems and vertically loaded plate anchors are usually used with vertical moorings. Plate anchors, in contrast to pile anchors for example, achieve their capacities from a combination of bearing and friction and not solely from friction on the sides. This results in significant higher anchor efficiencies and plate anchors are less susceptible to friction fatigue failure that might occur when using pile anchors. Therefore this study subsequently focuses on plate anchors.

The design of DEAs is dominated by empirical design charts and equations published by a variety of authors (NCEL, 1987; NAVFAC, 2012). The values used in these curves

were developed from actual test data and extrapolated to fit a wide range of soil conditions and anchor sizes. Most of the design charts and equations published by manufacturers for vertical and inclined anchors are for clay conditions and usually based on empirical results as well (Vryhof Anchors, 2010).

1.2 Statement of the Problem

The pullout capacity of each anchor depends on the individual soil conditions at the site. The standard design procedures using empirical models might be insufficient, as these models do not take any soil specific parameters into consideration. Theoretical models have also been developed to predict the pullout capacity of a vertical loaded anchor and a few models cover inclined anchors. Using soil specific models might be desirable as they include the effects of the actual soil profile of the site more accurately and therefore could be a better choice to precisely predict the anchor capacity.

1.3 Objective of the study

The objective of this study is to analyze and evaluate existing theoretical and empirical capacity prediction models for vertically loaded and inclined plate anchors in sand. A best fit model for each anchor type will be chosen. The feasibility of vertically loaded anchors and inclined anchors to be used to secure floating offshore wind turbines in deep water is assessed.

1.4 Scope of the Study

To meet the objective of this study, small-scale, 1g anchor pullout tests are performed on local beach sand. The tests include the testing of a squared plate drag embedment anchor, vertically loaded plate anchor, and inclined plate anchor. An analytical study, using published models, is also performed in order to evaluate which model fits the experimental results best. The chosen model is then used to assess the feasibility of plate anchors to secure floating platforms, by designing the anchor accordingly to actual loads, derived from a standard 5-MW offshore wind turbine. This turbine and the resulting loads have been proposed and developed by the NREL and therefore represent a realistic approach (Jonkman et al., 2009; Musial et al., 2004; Sclavounos et al., 2010).

2 LITERATURE REVIEW

2.1 Introduction

The focus of this study is on the evaluation of proposed theoretical capacity models for inclined and vertically loaded plate anchors. To accomplish that, the study will be carried out in two sections. The first part will consist of a laboratory testing program and the second section will contain an analytical study of different theoretical anchor capacity models.

The experimental program consists of a series of different pullout tests. These tests will include strict vertically loaded anchors, inclined anchors, and drag embedment anchors. The anchors will be placed at different embedment depths and the mobilized resistance will be measured.

The analytical study will include a comparison of the predicted and measured capacities of a drag embedded anchor, a vertical loaded anchor, and an inclined anchor. Different theories will be used to predict the capacities and a parametric study will be carried out to analyze different parameters and settings. In order to compare the near-normally loaded anchor with the conventional drag embedment anchor the anchors will be simulated having the same fluke area and anchor weight for each setting. As a simplification, the drag embedment anchor is assumed to have a squared fluke area. Real loads for a typical floating wind turbine will be used to design the anchors according to a realistic loading condition.

The following chapter will provide a theoretical review of important considerations, such as sample preparation and scaling issues for 1g tests, and anchor capacity prediction models. This literature review does not claim to be complete but is used to understand the state of knowledge on relevant work.

2.2 Physical Modeling

2.2.1 Sample preparation at large scale

The preparation of sand specimens for laboratory testing can be generally achieved with several methods. Butterfield and Andrawes (1970) distinguish between two groups:

(1) Methods where the density is adjusted after the deposition (e.g. shoveling, tamping and vibrating)

(2) Methods where the density is adjusted during deposition (e.g. wet and dry pluviation).

The pluviation method, or raining of sand through the air, is today widely used in different forms and by various researchers. Some of the advantages of this method are the ability to achieve higher dry densities, minimal particle crushing, reduced segregation, and better repeatability (Okamoto and Fityus, 2006). Compared with other sample preparation methods, pluviation through air can be performed with greater flexibility in less time than other methods. It not only results in homogeneous samples with a desired relative density but also enables to simulate a soil fabric that is similar to the soil fabric found in natural deposits formed by sedimentation (Okamoto and Fityus, 2006).

This technique also allows samples to be prepared in different layers and to place instruments, testing equipment, or density caps at desired depths in the process of

pluviation (Gade et al., 2013). This is a big advantage compared to the other methods given the importance of preparing undisturbed sand specimens.

Several studies have shown that the deposition rate (i.e. in kg/m^2/min) has the greatest effect on relative density. Greater deposition rates yield samples with lower densities. Other parameters such as diffuser sieve size, fall distance between diffuser sieves, and number of sieves used in a diffuser, have shown to have only minor contributions to the relative density (Rad and Tumay, 1987). The effect of the fall height on the relative density has been discussed controversially in the literature. Vaid and Negussy (1984) found out that the influence of the fall height on the relative density seems to be most important for fall heights smaller than 50 cm.

Gade et al. (2013) proposed the usage of a portable pluviator developed by Dave and Dasaka (2012). Figure 2 shows the suggested setup with the proposed dimensions. The pluviator is based on concurrently controlling the number of sieves installed, drop height (referring to the distance between the last sieve and the top of the soil layer), and deposition rate depending on the desired relative density. One of the main advantages of this setup is the good accessibility and mobility when preparing large scale laboratory tests. The authors concluded that the relative density of the samples increases with an increase in drop height. Relative densities also decrease with increasing deposit rates and numbers of sieves for any particular drop height used. The maximum and minimum relative densities obtained in that study are respectively 41% and 100%.

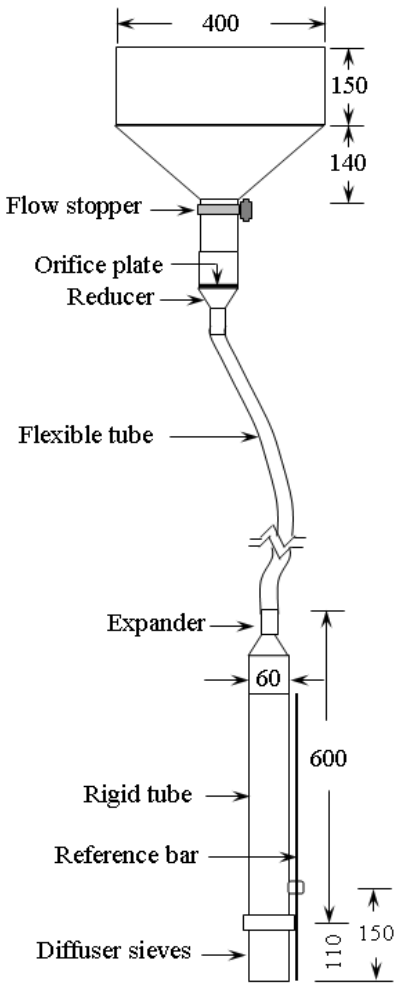

Figure 2- Portable pluviator (adapted from Gade et al., 2013)

A pluviator developed by Purdue University consists of a system of shutter plates and diffuser sieves with a diameter of 2 m. The pluviator is hung on a steel gantry above a soil tank with the same inside diameter. A mechanical hoist is used to adjust the height and keep a consistent drop height. Holes to control the deposition rate are drilled in the top of the pluviator and two sieves beneath the top part are used to evenly distribute and rain the sand. This pluviator has been used to prepare

samples with relative densities ranging from 38% to 91% depending on the setup (Prezzi, 2009).

Tufenkjian et al. (2010) and Giampa (2014) used a pluviator developed by NAVFAC to create a uniform sand bed. The pluviator consisted of a frame, hopper, internal distribution drum, dispensing tray, drive wheels, and an electric motor. It was mounted on top of a trench and four guide wheels allowed it to traverse the length of the trench while depositing sand. With this setup three configurations control the relative density of the trench: (1) drop height, (2) opening size, and (3) the angle of deposition. It has been shown that with the right combination of those three variables relative densities between 10% and 88% can be achieved.

2.2.2 Scaling effects in 1g experiments

Physical modeling of various problems has been performed for many years in geotechnical research. Physical modeling has been used to test theories that need to be proven by field tests or to validate numerical models. However, field testing at full scale is often impossible due to high costs, time consumption, and the lack of full scale facilities. Large scale test results are also often difficult to interpret and compare due to the variability of soil conditions, layering, and inhomogeneity in in-situ soils (Kirsch, 2009). For these reasons, testing is often performed on small scale models that represent the actual structure or prototype at some scale. They can be used to identify the behavior of the soil, its interaction with existing structures, or modeling the construction process.

Soil response is controlled by the effective stress within the soil mass. This applies especially for granular soils that at a given relative density and stress level behave in either a contractive or dilative manner. Thus when using small scale models, the results have to be evaluated carefully and scaling laws and scaling effects have to be taken into consideration (Yan and Byrne, 1989).

A distinction is usually made between model tests conducted at 1g-conditions and centrifuge tests conducted at *n*g-conditions. According to scaling laws, the centrifuge model will represent the prototype at a scale:

$$n = \frac{B_p}{B_m} \qquad (1)$$

where n= geometric scaling factor and B_p and B_m are the prototype and model dimensions, respectively.

The stresses acting in a model scaled in this way will be identical with the stresses of the prototype, but the displacements anticipated in the prototype will be larger than those of the model by the scaling factor n = N (Yan and Byrne, 1989).

A centrifuge test uses the rotation of a centrifuge to increase gravitational forces on the model, so that stresses in the model are the same as stresses occurring in the prototype. A model is build with a scale 1/n from the assumed prototype and is tested under an "n" times bigger gravity field. The typical radius of a centrifuge is between 0.2 and 10 meters. Due to the radial acceleration and increase in gravity on the model, the self-weight of the soil is scaled up. This results in a stress distribution with depth comparable or equal to the stress distribution in the prototype. Therefore the stress dependent soil characteristics can be reproduced correctly (Kirsch, 2009).

Although centrifuge testing is seen as the most favorable method for small scale testing, limitations exist. Since the acceleration depends on the distance of the soil to the centre of the centrifuge, the mass forces are not equal over the height of the model. However, the main drawbacks are the high costs of centrifuge testing, the long preparation time, and the need for specially trained personnel to run these tests (Laudahn, 2005).

An alternate to centrifuge testing is 1g scale model tests. If a soil is being tested under conditions of normal gravity, simply scaling to the ratio of geometric size is not sufficient. Yan and Byrne (1989) presented a method to overcome this insufficiency by employing a high hydraulic gradient within the soil. This has the effect of creating a high body force and therefore stress levels are created that are close to field conditions. By applying seepage through the sample basically the same principle is applied as in the centrifuge test, namely an increase in the vertical effective stress. When using this principle certain scaling rules have to be applied. If a downward hydraulic gradient (*i)* is used in a model, the effective unit weight of the soil will be increased by a seepage force of magnitude $i\gamma_w$

$$\gamma_m = i\gamma_w + \gamma' \qquad (2)$$

where

γ_m = effective unit weight of the soil in the model

i = applied hydraulic gradient

γ_w = unit weight of water

γ' = buoyant unit weight of the soil.

The ratio of the unit weight of the model and the prototype is denoted with the unit weight factor N and is defined as

$$N = \frac{\gamma_m}{\gamma_p} \qquad (3)$$

where

γ_p = effective unit weight of the soil of the prototype.

Depending on the groundwater conditions in the prototype this could be total or buoyant unit weight.

Alternatively, tests at 1g conditions can be scaled by linking stress and strain to changes in void ratio or density of the soil following the change of stress.

The effect of a change in soil volume caused by a change in shear stress was linked by Casagrande (1936). Casagrande introduced the expression “critical void ratio” which is defined as the void ratio at which deformations continuously occur without changing the principal stress difference (Holtz et al., 2011). Typically loose sands (high void ratio) contract and dense sands (low void ratio) dilate when sheared. Contractive behavior describes a reduction in volume and an increase in density when being sheared under drained conditions. Dilative behavior describes an increase in volume and decrease in density during drained shear. This means that the volume change behavior of a soil subjected to shear is controlled not by the void ratio alone, but rather the void ratio in relation to the critical void ratio (Fellenius and Altaee, 1994).

Roscoe et al. (1958) defined a state at which the soil deforms at constant stresses and constant void ratio. This state is called the critical state and was based on the results on a series of extensive laboratory tests on remolded clays. During similar studies later, this concept was found valid for cohesionless soils as well.

Poulos (1981) defines steady state as a state in which the mass continuously deforms while volume, normal effective stress, shear stress, and velocity stay constant. The steady state line is therefore defined as the curve constructed by all steady state points in the void ratio – mean stress plane. Every point on that line can be determined by means of triaxial testing on a soil sample with differentiating mean stresses. The relationship is typically linear on a plot of void ratio vs. log effective stress.

Fellenius and Altaee (1994) introduced a concept that uses the steady state as a reference state for physical modeling. The concept takes advantage of the uniqueness of the state for each soil and the relative ease of experimentally reaching the state.

Figure 3 shows the steady state line for three drained compressions tests, tested at different initial void ratios and different initial mean stresses. P represents the prototype situation and samples M1 and M2 represent smalls scale model situations. The vertical distance from the samples to the steady state line is named “upsilon parameter” by Fellenius and Altaee (1994), “*e*-prime” by Roscoe and Poorooshasb (1963) and “the sate parameter” by Been & Jefferies (2002). Sample

M1 was prepared to have the same vertical distance or upsilon parameter to the steady state line as sample P, while sample M2 had the same void ratio as sample P. The consolidation stress for samples M1 and M2 were the same and the stress for sample P was much higher.

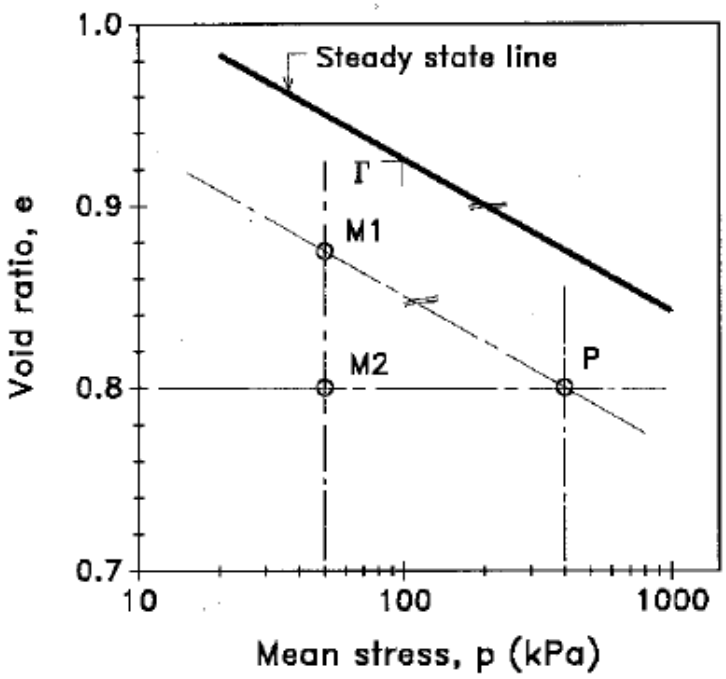

Figure 3- Steady state line (Fellenius and Altaee, 1994)

When analyzing the Mohr circles shown in Figure 4 for these tests one can see that sample M2 would exhibit a higher friction angle than sample M1 and P; the two samples with the same upsilon parameter. Fellenius and Altaee (1994) also proved that testing at the same upsilon parameter not only results in the same friction angle but also reflects the entire behavior of the soil. Hence the volumetric strain vs. axial strain behavior of sample M1 and P are identical.

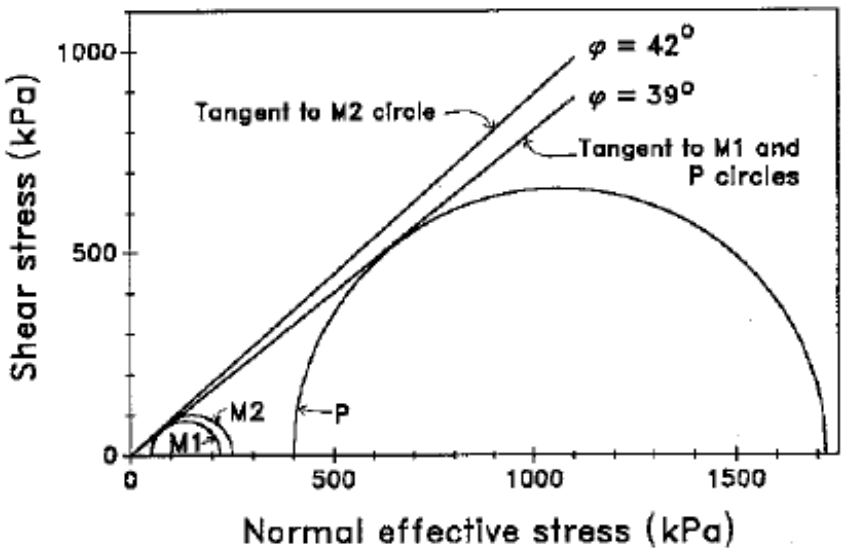

Figure 4- Mohr circles (Fellenius and Altaee, 1994)

Figure 5 shows the volumetric strain vs. axial strain of the samples. At low stresses a contractive behavior can be observed and with increasing stress the behavior changes to dilative while sample M2 behaves only dilative.

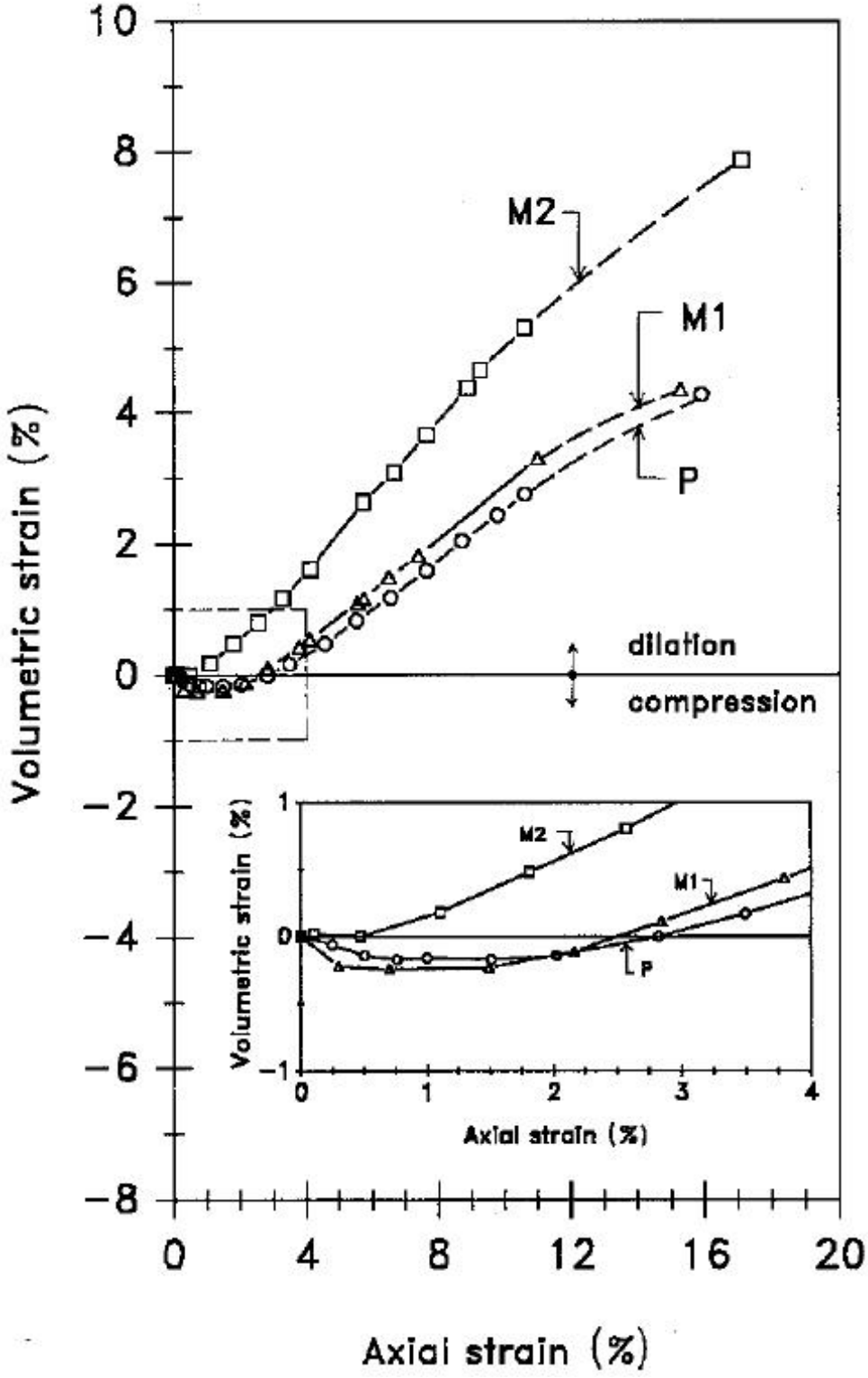

Figure 5- Volumetric strain vs. axial strain (Fellenius and Altaee, 1994)

Therefore only a small scale model with the same upsilon parameter, in this case sample M1, truly represents the prototype conditions. Thus the behavior of the sample M2 cannot correctly been used to analyze the prototype behavior.

Still there are some drawbacks to the theory proposed by Fellenius and Altaee (1994). One of the key points is the knowledge of the initial void ratio and mean stress for the prototype. These values can easily be determined for laboratory tests but are hard to determine for in-situ tests (Fellenius and Altaee, 1994).

Houlsby (1991) found out that the dilatancy angle effects volume changes of soil as well as the apparent strengths. This means a model needs to be prepared in such a way that the soil peak friction angle and dilatancy angle are the same for the model and the prototype and therefore the soil behaves the same way. This can be achieved by preparing the test sample in a looser state. Figure 6 shows curves of different relative density as a function of friction angle (ϕ) and effective stress (p'). This shows that for the particular soil and geometric scaling factor a friction angle of 43 degrees at a prototype relative density of 75% correspond to a relative density of 38% for the model (Leblanc et al., 2010).

However this concept also has certain limitations. First, the sample cannot be prepared looser than the maximum void ratio and thus certain prototype conditions cannot be modeled. Secondly, the sample must not be prepared in a denser conditions that the minimum void ratio of the prototype soil.

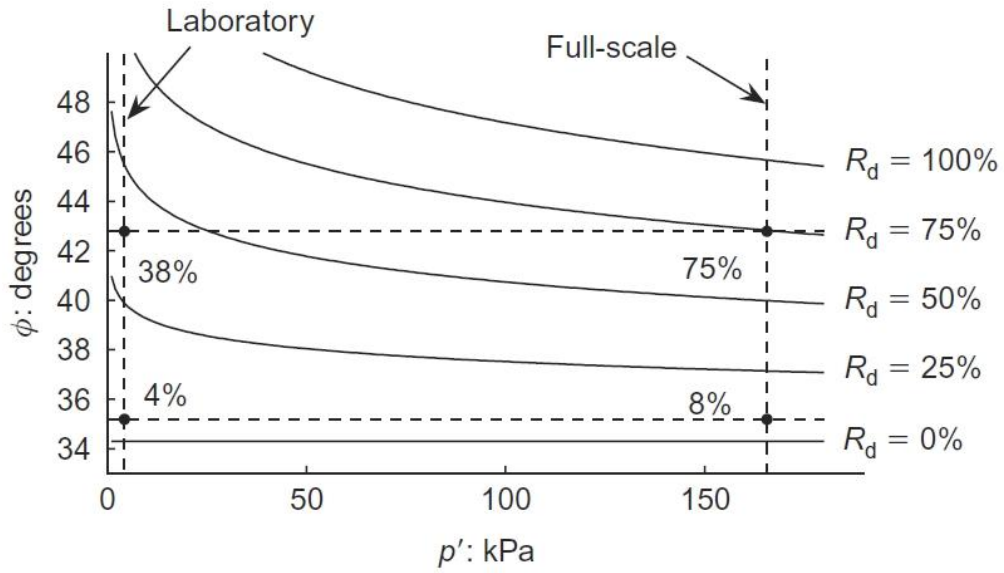

Figure 6- Friction angle as function of effective stress and relative density (Leblanc et al, 2010)

Considering these limitations, it is clear that proper scaling is an important part of 1g testing. When using the results of a small scale test model to predict the prototype behavior, it is important to apply the according scaling relations to calculate stresses, strains and displacements. If the scaling issue is not addressed, the results of 1g tests cannot be used to predict prototype behavior.

2.3 Anchor Capacity Models

At the present day there are a variety of anchors commercially available. They can generally be divided into gravity anchors and embedded anchors. Gravity, or surface, anchors generate their capacity by their self-weight and the friction between its base and the seabed. Because of limitation in size and therefore capacity, gravity anchors are restricted to shallow water depths. Embedded anchors can be used in deeper water and are able to generate larger holding capacities. In practice, three different types of embedment anchors have generally been accepted: driven or drilled and grouted piles, suction caissons, and plate anchors (Randolph and Gourvenec, 2011).

The major difference of the three anchor types is the way these anchors achieve pullout capacities. Anchor piles are installed and used in the same way as piles used for foundations. Pullout capacity is achieved by friction on the side of the pile and lateral soil resistance. Anchor piles are able to withstand both horizontal and vertical forces and are known to give the highest absolute capacity of all embedded anchors. With increasing water depth the installation of pile anchors becomes more complicated and special equipment is needed. This makes pile anchors unattractive in very deep water.

Suction caissons are made of large cylinders that are open at the bottom and closed at the top. The initial penetration is achieved by self-weight while the top cap is left open to de-air. The remaining penetration is accomplished with suction forces as

the top cap is closed and a vacuum is applied to the top with a pump. The pullout capacity is created by bearing resistance between soil and projected area of the caisson and frictional resistance on the outsides of the shaft. Suction caissons have mainly been used in clay up to this date.

The pullout capacity of different plate anchors will be discussed in detail in the following chapter and various prediction models will be analyzed. This study focuses on shallow plate anchors, including drag embedment, vertically, and inclined loaded anchors.

2.3.1 Drag Embedment Anchors

One of the most used forms of anchors for floating structures is the drag embedment anchor (DEA). Its use with floating platforms has been well documented for some time (Schneider and Senders, 2010). Some of the advantages of a drag embedment anchors are the high ratio of anchor capacity to anchor weight of the anchor (usually in the range of 20-50), the minimum of specialized support needed, and that the anchor potentially can be reused. One major disadvantage is the poor performance in very hard soils, which refers to the stability of the anchor in the soil after penetration. Another disadvantage is the high uncertainty in the exact positioning on the seafloor (Liu et al., 2010; Liu et al., 2012a). DEAs are usually referred to by their manufacturer's name. Typical types of DEA anchors are: Stockless, Danforth, BRUCE, STEVFIX, and STEVMUD. Typical manufacturer are: Sotra anchor & chain, Bruce anchor group, and Vryhof anchors (NAVFAC, 2012).

Most of the common anchors share similar features that are illustrated in Figure 7. The anchor usually consists of a shank, which is used to direct the line load to the anchor and one or more flukes to dig the anchor into the seabed and create bearing capacity through the mobilized soil wedge. One vital part of the anchor system is the attachment of the chain or wire to the anchor at the tip of the fluke. Usually a relatively small part of the chain is below the soil surface while the larger part is in the water. Since the self weight of the chain is dragging the chain towards the seabed, the chain arrives at an angle close to zero at the anchor-chain connection.

This is a desirable feature of the anchor system as the anchor is used to mainly withstand horizontal forces in catenary mooring systems (NAVFAC, 2012).

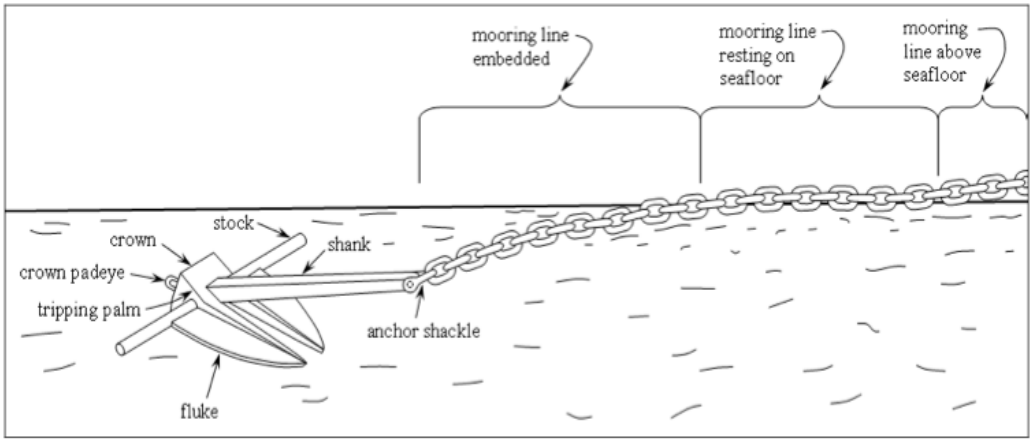

Figure 7- Typical drag embedment anchor (NAVFAC, 2012)

The angle between fluke and shank, β, plays an important role in the design considerations to achieve maximum penetration depth. Depending on the soil condition at each site the angle is adjusted. Different studies showed that an angle around 50° for clay-like soil conditions and 30° for sands seems to be optimal. The penetration depths vary on the material. To achieve penetration, the anchor is placed on the seabed and embedded by applying horizontal tension forces to the attached chain. The anchor penetrates the soil until it reaches equilibrium and therefore its final position (Miedema et al., 2005). This ultimate penetration depth depends on the type of mooring line, anchor size, and soil conditions at the installation site. Typical penetration depths are between one and five fluke lengths. Figure 8 illustrates the penetration motion of a drag embedment anchor.

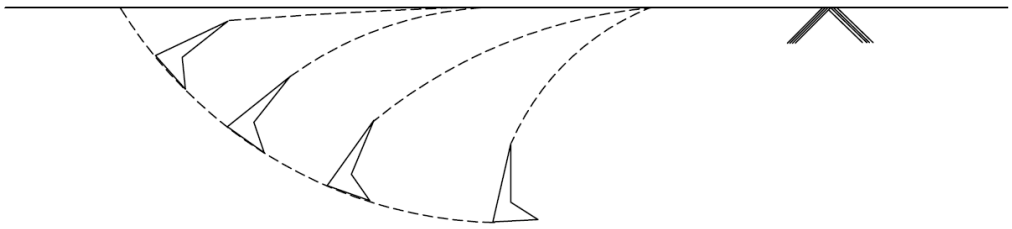

Figure 8- Penetration of a drag anchor (adapted from Thorne, 1998)

Due to complexities in shape and uncertainty concerning the variables affecting the performance, the capacity of DEAs is often extrapolated from empirical databases.

In efforts to aid in the design steps, the Naval Civil Engineering Laboratory (NCEL) developed a first series of figures and tables in 1987. These curves provide a holding capacity for DEA depending on the anchor weight and specific anchor type chosen. Figure 9 shows an example of anchor capacity curves for sand. The manual proposes a specific procedure in order to use these standard values properly. As a first step the ultimate horizontal holding capacity of the desired anchor has to be determined. This is done by calculating the maximum design horizontal load and multiplying this by a factor of safety proposed by NCEL. Next, an anchor that satisfies the needs has to be chosen. A convenient way to determine the ultimate holding capacity is to make use of the relationship between anchor efficiency and anchor weight, the simple efficiency ratio method.

$$T_M = e * W_a \qquad (4)$$

where

T_M is the ultimate holding capacity, e is the anchor efficiency and W_A is the weight of the anchor. The anchor efficiency is defined as the ratio between the ultimate holding capacity divided by the weight of the anchor (NAVFAC, 2012).

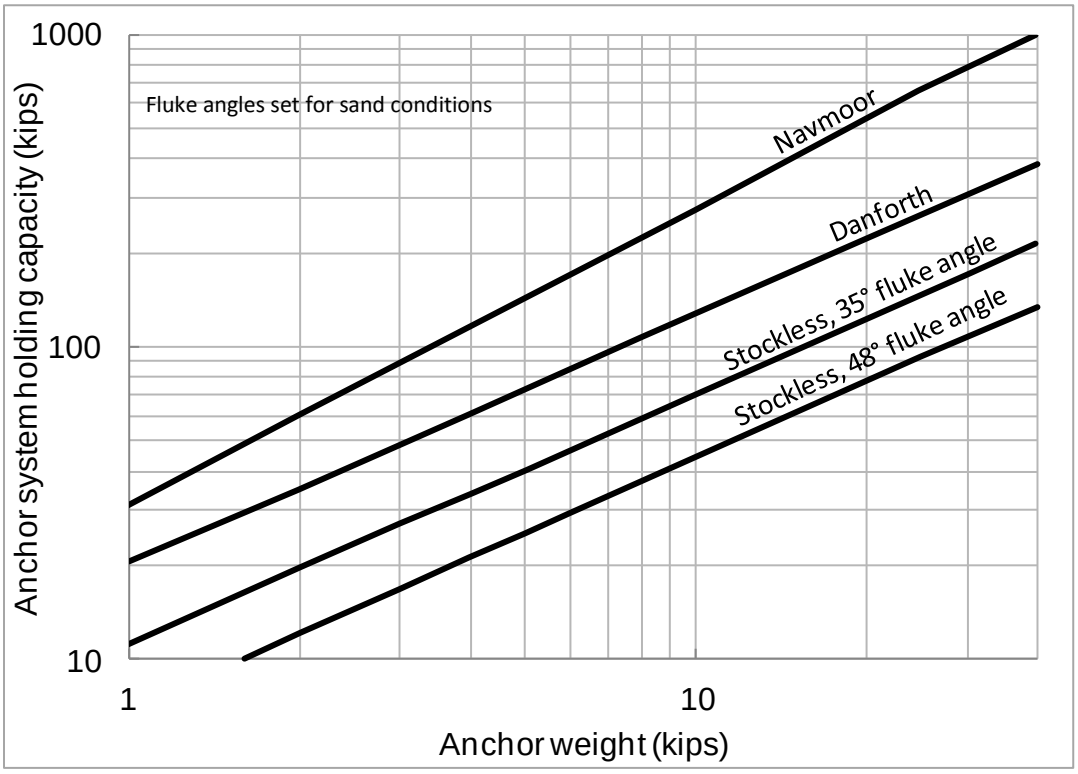

Figure 9- Anchor capacity curves (adapted from: NCEL, 1987)

To use this method several assumptions have to be made. As a first assumption, the anchor efficiency is assumed to be constant for a specific soil type over a range of anchor sizes and weights. Secondly, the anchor is installed properly and safely, and thirdly, the necessary embedment depth and embedment distance in order to develop the maximum capacity is reached. As these assumptions sometimes prove

not to be true, this method may over-predict holding capacities, especially as tests have showed that a constant relationship between anchor efficiencies and anchor weight is untrue. The efficiency tended to decrease with increasing anchor weights. Nevertheless this method is still widely used because of its simplicity and its history of usage (NAVFAC, 2012).

To account for the nonlinear relationship between anchor weight increase and capacity NAVFAC (2012) proposed the Power Law Method. This method is results in a straight line of anchor capacity and anchor weight on logarithmic axis. The general form of such a line is described by:

$$H_M = m*(W_a)^b \qquad (5)$$

where m, b are dimensionless soil and anchor dependent parameters and W_a is the weight of the anchor.

Values for parameters *m* and *b* are found using field test data and are given in the manual. This relationship proved to be valid for anchor weighing 200 lb or more. Table 1 shows typical values describing the performance of a specific anchor in a given soil. The capacities shown in these figures and tables include chain and anchor holding capacities and do not differentiate between them. For anchors smaller than 200 lb a similar table exists.

Table 1- Proposed values power law

Anchor Type	Soft Clays and Mud		Stiff Clays and Sand	
	m	b	m	b
Stockless (fixed fluke)	5.5	0.92	11.1	0.8
Danforth	10.5	0.92	20	0.8
BRUCE Cast	3.9	0.92	39.6	0.8
STEVFIX	22.7	0.92	46	0.8
STEVMUD	30	0.92	-	-

Currently there is no complete method for the prediction of a DEA holding capacity based on geotechnical considerations alone. This is due to the vast of variables involved, the uncertainty of the anchor trajectory after penetration, and anchor movement during loading. The two most important papers published on the behavior of drag embedment anchors are published by Neubecker and Randolph in 1996 (Neubecker and Randolph, 1996a; Neubecker and Randolph, 1996b). They investigate the static and kinematic behavior of drag anchors in sand. In order to predict the static holding capacity, a limit equilibrium approach is used.

The method is a modification of a more simplistic approach proposed by Le Lievre and Tabatabaee (1981). The theories differ in the way the failure wedge is assumed. Contradictory to Le Lievre and Tabatabaee's suggestion, Neubecker and Randolph assume three dimensional failure wedge which resembles a more realistic failure mode. This is again an idealized failure mode.

Figure 10 shows the considered forces acting on the anchor under equilibrium at a certain depth. Depending on the embedment depth the forces will change in magnitude and in direction. The holding capacity of the anchor increases as the

anchor penetrates deeper until it reaches a maximum. When loaded beyond this threshold failure will occur. Neubecker and Randolph define failure as the point where the line tension applied at the shank exceeds the holding forces created by the anchor.

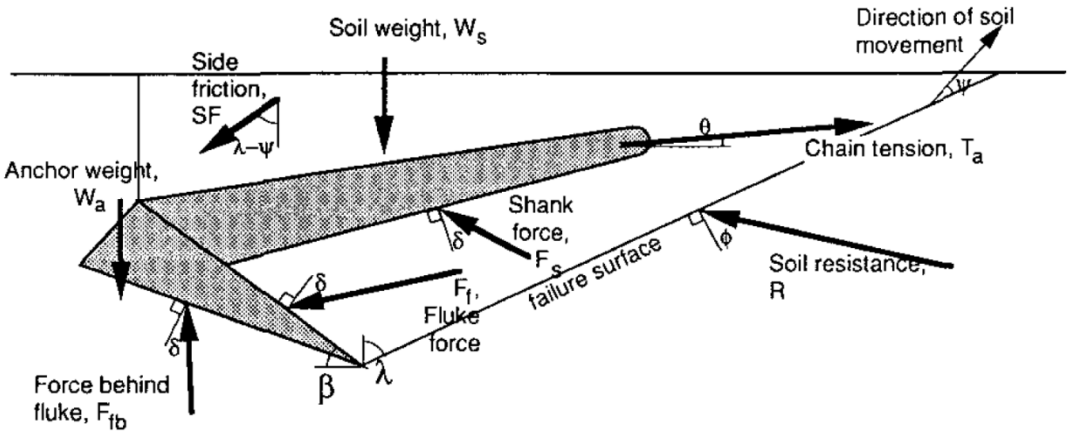

Figure 10- Forces acting on a drag embedment anchor (Neubecker and Randolph, 1996).

The calculation of the ultimate holding capacity consists of several steps described in the paper. First of all a failure wedge angle λ has to be assumed. Using this angle the mobilized soil mass, W_s, and the side friction (SF) can be calculated. Both calculations consider a three dimensional soil wedge where the fluke area is mapped onto the soil surface and results in a pyramidal shape. The standard bearing capacity equation is used to calculate the shank force (FS). In order to calculate the remaining forces, Neubecker and Randolph treated the force polygon of the soil wedge and the force polygon of the anchor individually. These polygons are shown in Figures 11 and 12.

There are only two unknown forces in the soil wedge force polygon. These are the fluke force, F_f, and the soil reaction, R. They can be calculated by applying vertical and horizontal force equilibrium.

When considering the anchor force polygon individually again only two forces are left unknown, which are the force on the back of the fluke, F_{fb}, and the chain tension, T_a. They also can be calculated using force equilibrium.

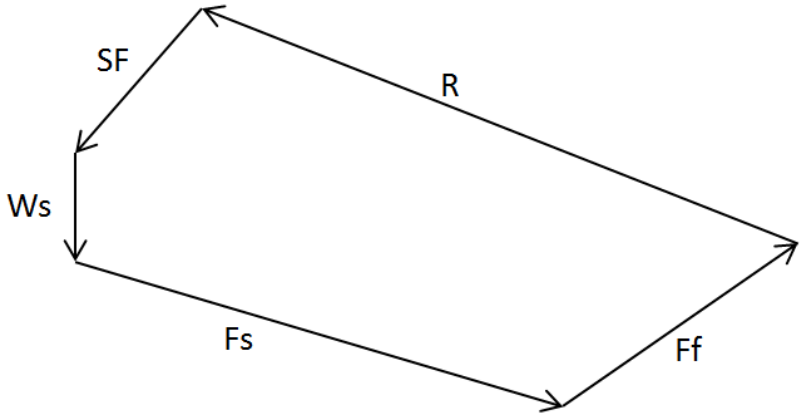

Figure 11- Soil wedge forces only (adapted from: Neubecker and Randolph, 1996)

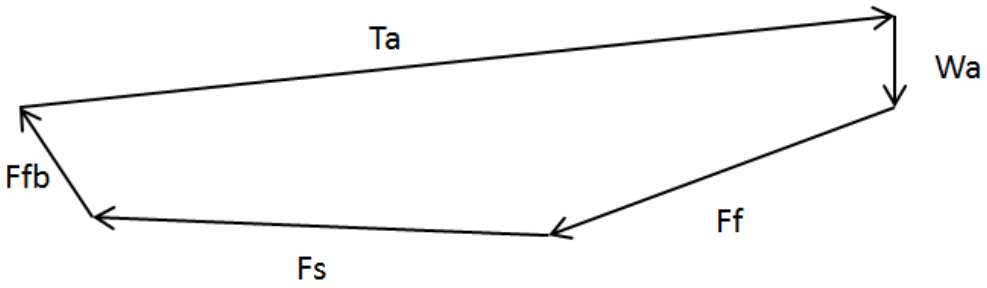

Figure 12- Anchor forces only (adapted from Neubecker and Randolph (1996))

The weight of the soil plays a main part in this analysis and it adds a major contribution in the development of pullout capacity. The correct prediction of the weight of the soil appears to be the most difficult part since the anchor could already mobilize the maximum holding capacity before it is fully embedded (Monaco, May 2013).

Due to the high uncertainty in the design of DEAs it is general practice to design the anchor as the “weaker link” of a mooring system. This means that the anchor is preferred to drag instead of breaking the mooring line. Further dragging of the anchor does not necessarily mean a catastrophic failure of the anchor and sometimes even results in an increase of the capacity as the anchor penetrates deeper. The drag of an anchor then results in the redistribution of the mooring line forces in a mooring system to the neighboring lines.

2.3.2 Vertically loaded plate anchors

The following section summarizes different installation methods of plate anchors and describes already proposed models to predict the vertical uplift capacity of square plate anchors in cohesionless, dry sands. Generally plate anchors are embedded using pile driving techniques or suction pile followers, while drag-in plate anchors are today only theoretically possible due to accuracy issues in positioning the anchor. When the driving method is used, the plate anchor is driven into the sand by a follower. These followers could be hydraulic hammers or, if the underwater situation does not allow a hammer to be used, suction followers (SEPLA). SEPLAs have been used in clays for the O&G industry but the use of such a suction follower in sand is still being researched. The follower ensures that the desired embedment depth and position of the plate anchor is reached but is removed before the mooring line is loaded and therefore can be reused. Another possible option to achieve anchor penetration is the use of the jetting technology. A pulsating supply of water at the anchor tip is used to loosen soil and allow the anchor to penetrate. This is specifically used in very dense sands to assist penetration. This technique can also be used to develop sufficient soil densities around the anchor after the placement (NAVFAC, 2012; Randolph and Gourvenec, 2011).

As most of the prediction models have been developed by different researchers in different years, various definitions have been used to characterize capacity. For

numerical convenience, ultimate anchor capacities will be presented in a standardized form of a dimensionless breakout factor N_γ, where N_γ is defined as:

$$N_\gamma = \frac{Q_u}{\gamma * A * H} \qquad (6)$$

where Q_u is the ultimate pullout capacity, γ is the unit weight of the soil, A is the area of the anchor and H is the embedment depth of the anchor.

A good overview of different capacity models for vertically loaded anchors is given by Merifield (2006) and is displayed in Table 2.

Table 2- Overview of vertical plate pullout prediction models (adapted from Merifield, 2006)

Author	Analysis Method	Anchor Shape	Friction Angle	H/B
Meyerhof & Adams (1968)	Limit equilibrium: semi-analytical	strip, sqr/circ	-	-
Vesic (1971)	Cavity expansion	strip/circ	0-50°	0-5
Rowe & Davis (1982)	Elastoplastic finite element	strip	0-45°	1-8
Vermeer & Sutjiadi (1985)	Elastoplastic finite element/ upper bound	strip	all	1-8
Tagaya et al. (1988)	Elastoplastic finite element	circ/rect	31.6°, 35.1°	0-30
Tagaya et al. (1983)	Elastoplastic finite element	L/B = 2	42°	
Saeedy (1987)	Limit equilibrium	circ	20-45°	1-10
Murray & Geddes (1987)	Limit analysis and limit equilibrium	strip, rect, circ	all	all
Koutsabelouis & Griffiths (1989)	Finite element: initial stress method	strip/circ	20°, 30°, 40°	1-8
Sarac (1989)	Limit equilibrium	circ/sqr	0-50°	1-4
Basduhar & Singh (1994)	Limit analysis: lower bound	strip	32°	1-8
Kanakapura et al. (1994)	Method of characteristics	stip	5-5-°	2-10
Ghaly & Hanna (1994)	Limit equilibrium	circ	30-46°	1-10
Smith (1998)	Limit analysis: lower bound	strip	25-50°	1-28
Sakai & Tanaka (1998)	Elastoplastic finite element	circ	Dense	1-3

The models of interest are those that present solutions for square and rectangular anchors. These are in particular Meyerhof and Adams (1968), Murray and Geddes (1987), Sarac (1989), and Merifield et al. (2006).

Meyerhof and Adams (1968) presented a limit equilibrium solution to predict the pullout capacity of strip, horizontal and rectangular plate anchors. Based on tests carried out by the authors simplifying assumptions were made. The failure surface was assumed to be inclined and shaped like a truncated cone and will reach the soil surface for shallow depths. The failure surface is illustrated in Figure 13.

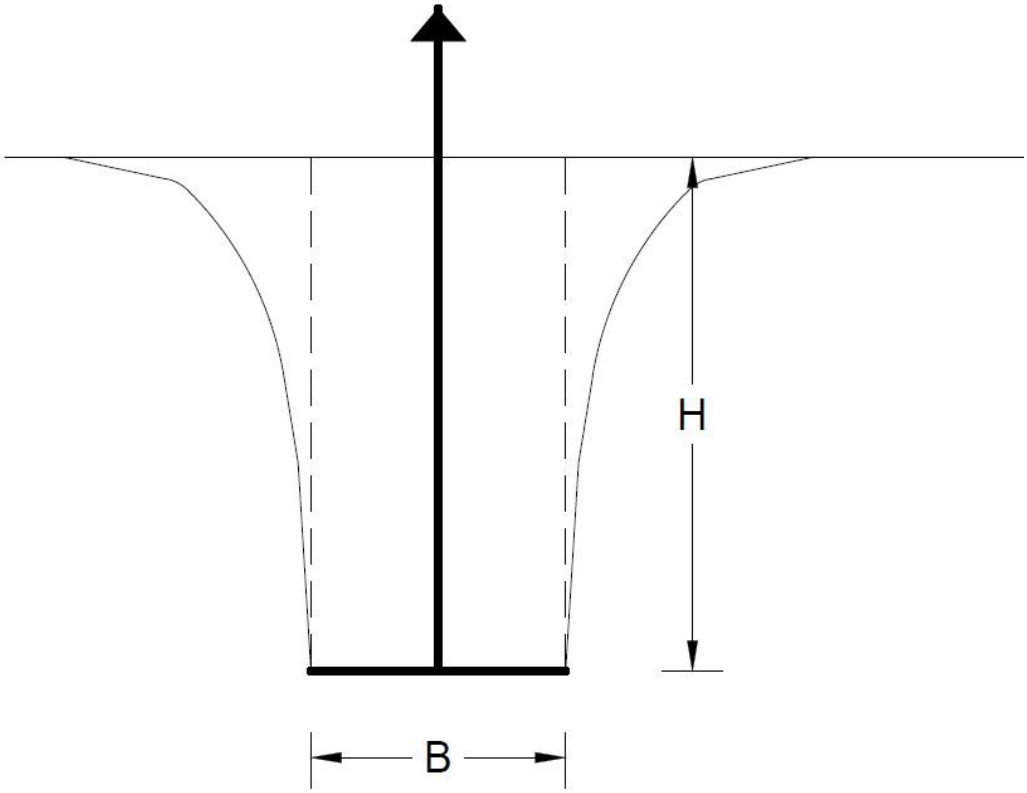

Figure 13- Failure surface assumed (adapted from: Meyerhof and Adams, 1996)

Meyerhof and Adams (1968) determined the average angle of the failure surface for sands to be $\frac{\phi'}{3}$ with respect to the vertical, where ϕ' is the effective friction angle of the sand. The first solution was found for strip and continuous footings and then modified for use in sands and clays for both circular and rectangular footings. It was found that the passive earth force was governing the pullout resistance. To find the corresponding passive earth pressure coefficients, the theory of Caquot and Kerisel (1949) was used. A theoretical shape factor (s) is introduced to extend the theory from strip footings to square and rectangular plates and to account for the differences in shapes. For shallow depths s can be calculated with:

$$s = 1 + m\frac{H}{B} \qquad (7)$$

where s is the shape factor, m is a coefficient depending on the friction angle, H is the embedment depth, and B is the plate width.

The pullout capacity for the model proposed by Meyerhof and Adams (1968) can be calculated with:

$$N_\gamma = \frac{2sK_u H \tan\phi'}{B} + 1 \qquad (8)$$

where N_γ is the breakout factor, s is the shape factor, K_u is a theoretical uplift coefficient, ϕ' is the effective friction angle, H is the embedment depth, and B is the plate width.

Murray and Geddes (1987) developed a limit analysis approach to create an envelope for the predicted capacities. Contrary to limit equilibrium approaches, a limit analysis method does not provide an exact prediction but deliver a bounded solution. Upper bound solutions usually over-predict capacity and by obeying the associated flow rule (θ= ϕ' =ψ) are searching for a failure mechanism that is as close as a bound as possible to the ultimate uplift resistance. The lower bound solution is merely defined as the soil block located vertically above the anchor base. Murray & Geddes (1987) conclude that the most appropriate failure boundary consists of a straight-line failure plane inclined at the friction angle ϕ to the vertical at the edges of the plates. The failure surface is illustrated in Figure 14.

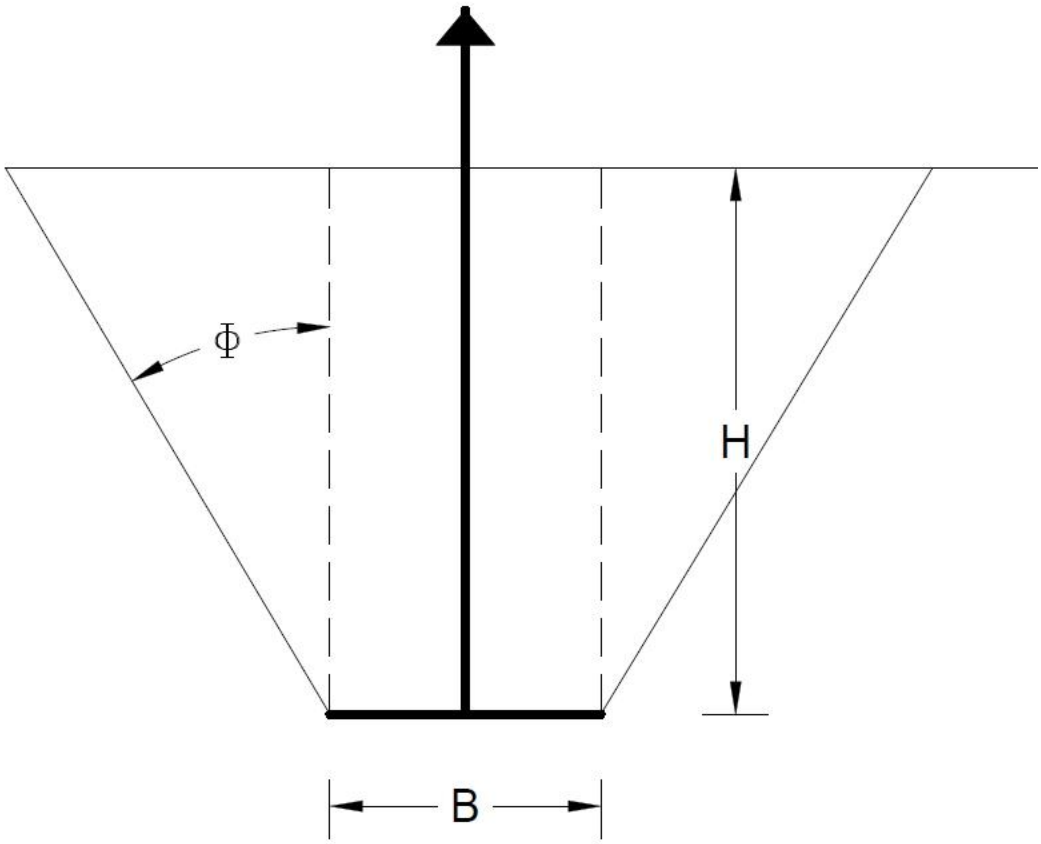

Figure 14- Failure surface assumed (adapted from Murray and Geddes, 1987).

The upper bound solution can be found using the following equation:

$$N_{\gamma} = 1 + \frac{H}{B}\tan\phi\left(1 + \frac{\pi H}{3B}\tan\phi\right) \qquad (9)$$

where N_{γ} is the breakout factor, H is the embedment depth, B is the plate width, and ϕ is the friction angle.

A limit equilibrium solution for circular and square anchor slabs is presented by Sarac (1989) in form of a design chart. The breakout factor can be determined depending on the ratio of embedment depth to plate width (H/B) and friction angle.

The author assumes, based on experimental tests, the failure surface to be shaped like a convex curve that met the soil surface at an angle of $45 - \frac{\phi'}{2}$. A logarithmic spiral failure plane is proposed by the author to approximately display the real rupture line. The solution to the limit equilibrium approach is found using a finite difference method and the stresses on the rupture line are calculated with Bereyancev's theory of complete limit equilibrium. Figure 15 shows the failure geometry.

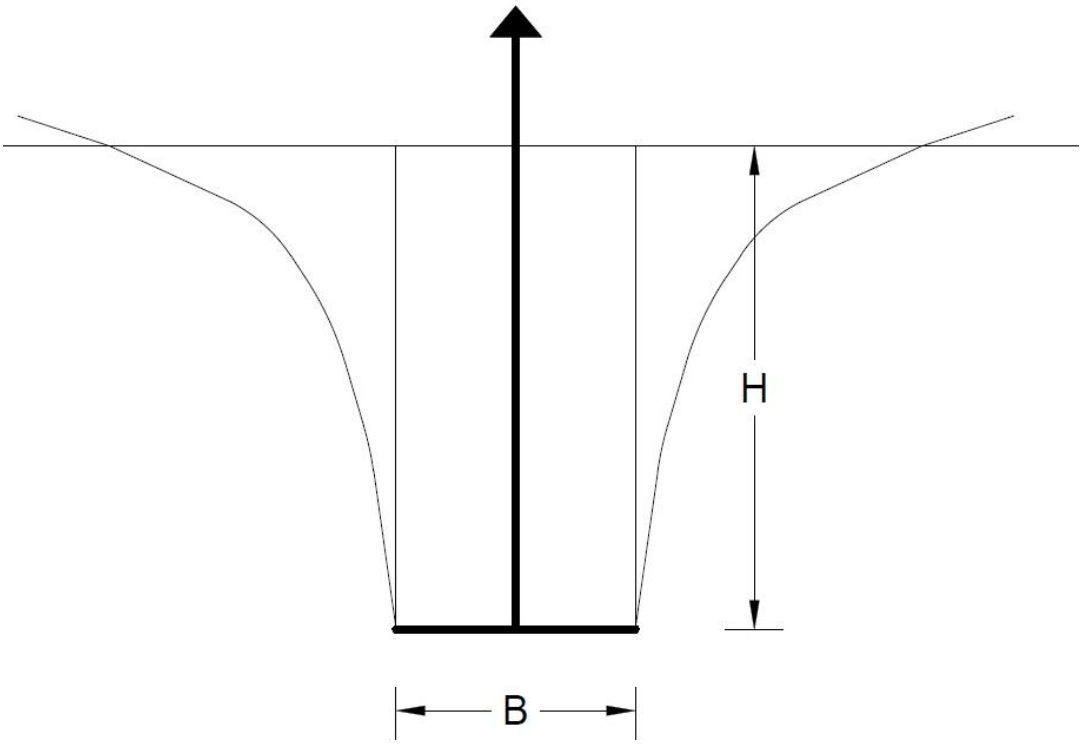

Figure 15- Failure surface assumed (adapted from: Sarac, 1989)

Merifield et al. (2006) points out that very few rigorous numerical analyses have been performed to determine the pullout capacity of anchors in sand. To close this

gap, the authors present a three-dimensional lower-bound limit analysis solution. Developing a lower-bound solution, the authors expect the soil to still be in equilibrium. The associated flow rule is used, assuming the friction and dilatancy angle to be equal. Using the research software SNAC a finite analysis is carried to estimate the capacity of circular anchors utilizing axisymmetrical elements. The results, dimensionless breakout factors, were presented as a function of friction angle and the ratio of embedment depth to plate width, in the form of charts.

2.3.3 Inclined plate anchors

In this section, the pullout capacity of inclined anchors in cohesionless soil will be examined. Various theories and models have been published that use empirical relationships to predict anchor capacities or consider circular and strip anchor geometries. Some of these include Murray and Geddes (1989), Ghaly (1997), Choudhury and Subba Rao (2005), Ghosh (2010). As this study focuses on theoretical models for square anchors, these models are not part of this study. For a more detailed literature review on vertical and horizontal plate anchors see Das (2013) and Hanna et al. (1988).

The considered problem geometry is shown in Figure 16. The shallow plate anchor is inclined at an angle α relative to the horizontal at an embedment depth H measured from the soil surface to the bottom of the plate and a width of the anchor plate B.

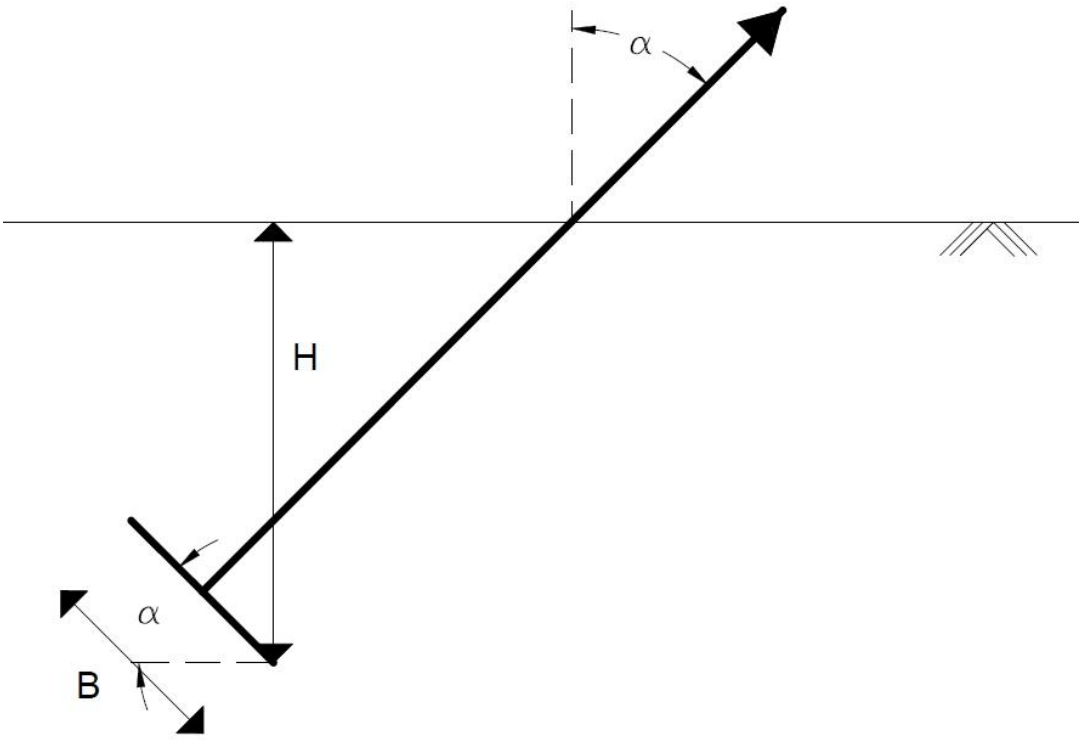

Figure 16- Anchor geometry used (adapted from: Meyerhof (1973)

In this study a number of existing numerical and laboratory studies that address the inclined capacity of anchors in cohesionless soils have been analyzed. In particular the research carried out by Meyerhof (1973), Hanna et al. (1988), and Goel et al. (2006) demonstrated to be of interest and the corresponding models have been used in a parametric study.

Meyerhof (1973) extended a previous theory of vertical uplift capacity of anchors published by Meyerhof and Adams (1968) to inclined anchors and piles under axial load. Depending on the depth of embedment two different failure mechanisms can be differentiated:

1: The failure surface of shallow anchors will reach the ground level and will be considered as a general shear failure;

2: For greater embedment depths a local shear failure will occur close to the anchor.

For loose sands, Meyerhof states that at a ratio of embedment depth to anchor width of 4 the failure mode changes from a general shear type of failure to a local shear type.

The theory is based on active and passive earth pressure theory and the ultimate pullout capacity can be interpreted as the difference in active and passive earth pressure above and below the anchor plate. When the anchor reaches failure, the mobilized soil wedge is assumed to be in the shape of a truncated pyramid.

In order to calculate the ultimate holding capacity in form of the dimensionless breakout factor N_γ for inclined plate anchors, the following equation is proposed:

$$N_\gamma = \frac{H * K_b * s}{2B} + \cos^2 \alpha \qquad (10)$$

where N_γ is the breakout factor, K_b is a net earth pressure coefficients, s is a shape factor, H is the embedment depth, B is the plate width, and α is the inclination angle with respect to the vertical.

The uplift coefficients used are obtained from the earth pressure coefficients for an inclined wall (Caquot and Kerisel, 1949). The value of K_b increases for a given friction angle ϕ with increasing load inclination α. A maximum value is reached at an

inclination of α equals 90 degrees with respect to the vertical which corresponds to horizontal pull. A minimum value of K_b represents vertical uplift (α equals zero degrees). Meyerhof presents a chart, which displays the variations of the uplift coefficients for shallow strip anchors, deep strip anchors, and deep square anchors. To account for shallow square anchors, the uplift coefficient, K_b, for shallow strip anchors is used and a shape factor (s) is introduced. The shape factor can be found in Meyerhof and Adams (1968) and in Equation 7. The coefficient K_c can be neglected in this work since the focus is on cohesionless, dry sands.

Hanna et al. (1988) developed a theoretical model to estimate ultimate holding capacities of an inclined shallow strip anchor using limit equilibrium analysis. Despite the fact that strip anchors are not part of this study, Hanna et al. (1988) is included as the authors compare their theory to square anchor laboratory test. The theory is proposed for inclination angles α ranging from zero to 60 degrees. It is assumed that at an inclination larger than 60 degrees the failure mechanism is closer to a failure mechanism proposed for vertical retaining walls. Figure 17 shows the failure planes assumed by Hanna et al. (1988).

In this method the failure planes are assumed to be parallel to the anchor chain and therefore in line with the pullout force. This assumption is used as a simplification of the problem but does not reflect the actual failure plane. Along the assumed failure planes, two passive forces will act inclined at an angle δ. To account for the simplification, δ is an angle smaller than the peak friction angle ϕ. The angle δ also

depends on the inclination angle of the anchor α and on the embedment depth as only the end points of the plate anchor are located on the actual failure surface.

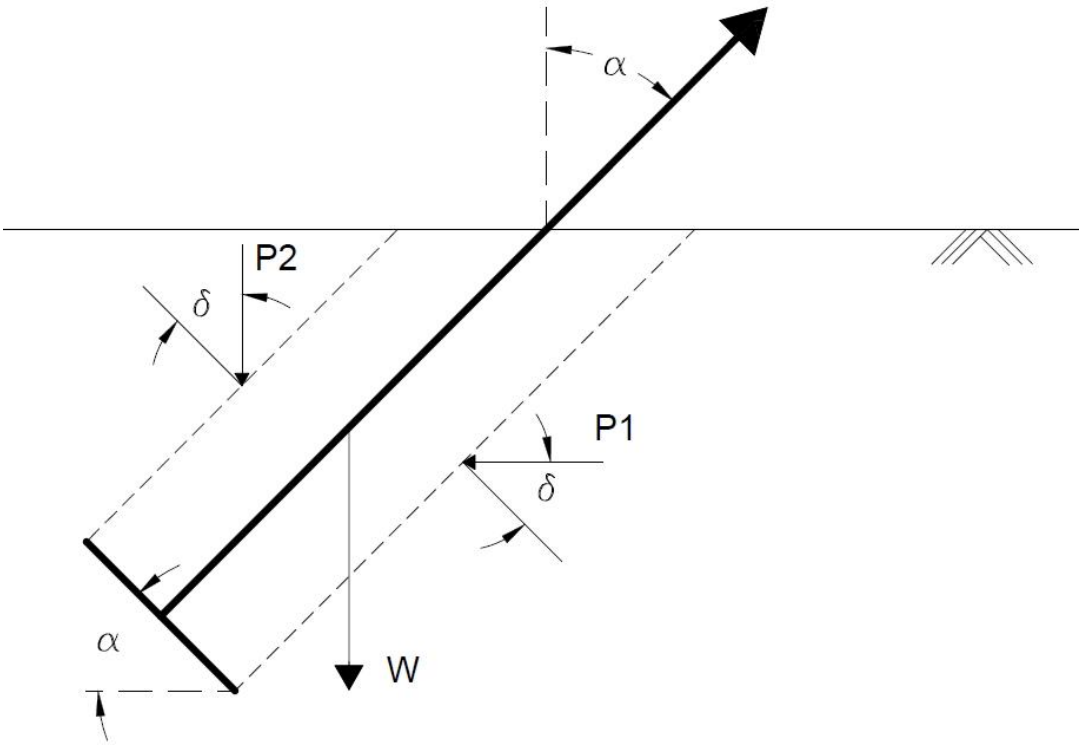

Figure 17- Failure planes (adapted from: Hanna et al., 1988)

The forces P_1 and P_2 can be determined using passive earth pressure theory and passive earth pressure coefficients (Caquot and Kerisel, 1949 and Sokolovskii, 1965). Depending on the ratio angle of mobilized shearing resistance and peak friction angle, δ/ϕ, a reduction factor is applied. This reduction factor accounts for the oversimplification of the assumed failure surface. A generalized solution for this problem is presented in the study and as a simplified result a punching uplift coefficient is introduced. The punching uplift coefficient K_s depends on friction angle of the soil ϕ, inclination of the anchor α, and embedment depth. The variation of

this coefficient is presented for ease in design charts. Introducing this coefficient to the previous equation Hanna et al. (1988) concluded:

$$N_{\gamma} = \frac{1}{2} * \frac{k_s \sin\phi\left(L_1^{\,2} + L_2^{\,2}\right)}{BH} + \frac{1}{2} * \frac{\left(L_1 + L_2\right)\cos\alpha}{H} \qquad (11)$$

where N_γ is the breakout factor, α is the inclination angle of the anchor, K_s is the punching uplift coefficient, L_1 and L_2 are the length of the assumed failure planes, B is the plate width, and H is the embedment depth.

The authors conclude that the anchor capacity increases with increasing inclination angle α and with increasing embedment depth H. Experimental tests carried out by the authors support this conclusion.

Goel et al. (2006) proposed a theory to predict breakout resistances for inclined circular anchors for deep and shallow conditions using a limit equilibrium solution. This theory is also included because the authors compare their theoretical approach to laboratory results for inclined square anchors. The geometry used is the same used by Meyerhof (1973) and shown in Figure 16. A solution is found analyzing an elemental length of anchor cable at a certain depth. The pressures on that cable are calculated using an elliptical horizontal section and earth pressure theory for lateral pressures and uplift respectively. This resistance is assumed to be symmetrical for the elliptical periphery. A coefficient I_i is introduced by the authors. This coefficient accounts for the unit resistance at any point in the ground and depends on the angle on inclination α, the coefficient of lateral earth pressure used in the analysis,

and the position of this one point with respect to its position on the cable. When integrated over the embedment length of the anchor cable the following equation is found (Goel et al., 2006):

$$N_\gamma = \frac{4H}{\pi D} * K * \tan\phi * I_i * \sec^2 \alpha \qquad (12)$$

where N_γ is the breakout factor, D is the diameter of the plate anchor, K is the coefficient of lateral earth pressure, α is the inclination angle of the anchor, I_i is a coefficient for unit resistance.

An overview over different failure patterns for shallow inclined anchors is presented by Ghaly (1997). A differentiation between four major failure surfaces is presented in the reference. Only two proposed failure surfaces correspond to failure surfaces for square or rectangular anchors. One surface is shaped like a truncated pyramid, identical to Meyerhof's (1973) proposal. The second surface is a pattern of a straight line – log spiral – straight line, proposed by Wang and Wu (1980). The other two surfaces are proposed for circular anchors.

3 LABORATORY TESTING PROGRAM

As described at the beginning of Chapter 2, a laboratory testing program was developed to perform model tests on drag embedment and inclined embedment anchors. This chapter presents a summary of results for the element testing (e.g. sieve analysis, maximum and minimum density, specific gravity and drained triaxial tests) carried out on the sand used for this investigation. A detailed description of the 1g model testing facilities built for the project at the University of Rhode Island is also presented. Results from the pullout tests performed on the anchors are discussed. The results of these tests will be used for the analytical study presented in Chapter 4.

3.1 Soil Properties

This section presents a brief discussion and results of the tests performed to characterize the beach sand from Rhode Island used in this investigation. These tests include classification tests, isotropically consolidated drained triaxial compression tests, determination of the critical state line

3.1.1 Soil properties

The sand used for this study was obtained from a local Rhode Island beach. Figure 18 shows the grain size distribution for the sand. The gradation curve presented in this figure shows the sample exhibits a fairly uniform gradation with grain sizes ranging from 0.2 to 1 mm and no fines. According to the Unified Soil Classification System (ASTM D 2488-00), the soil classifies as poorly graded sand.

Minimum and maximum dry unit weight of the sand was determined according to the procedure described in the ASTM D 4254 (Method C) and ASTM D 4253 (Method 1A). The soil properties are summarized in Table 3.

Table 3- Soil Properties Rhode Island beach sand used in this study

Parameter	Rhode Island beach sand	ASTM standard
D_{10} (mm)	0.19	ASTM D 422
D_{30} (mm)	0.27	
D_{50} (mm)	0.30	
D_{60} (mm)	0.31	
C_u	1.63	
C_c	1.24	
γ_{min} (kN/m^3)	14.1	ASTM D 4254
e_{max}	0.844	
γ_{max} (kN/m^3)	18.1	ASTM D 4253
e_{min}	0.436	

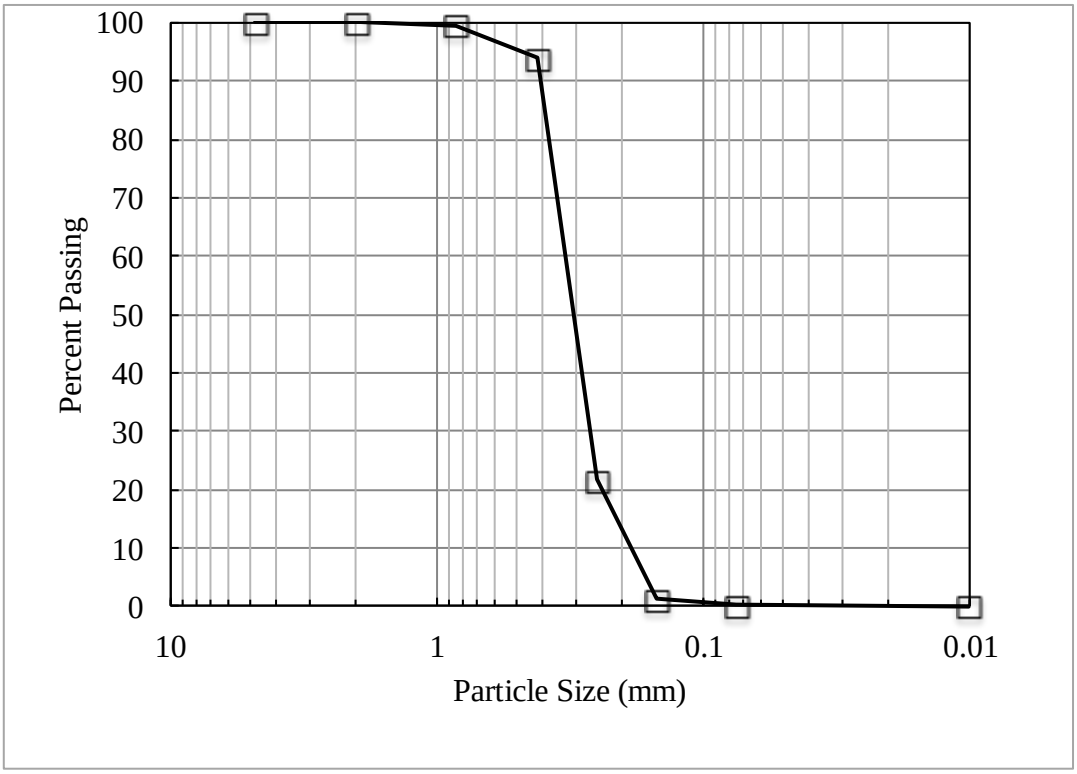

Figure 18- Particle size distribution (ASTM Standard D 422)

3.1.2 Shear Strength of the Rhode Island Beach Sand

In order to determine the shear strength properties of the sand (i.e. effective internal friction angle, ϕ'), a series of monotonic isotropically consolidated drained triaxial tests were carried out on reconstituted specimens. Samples were sheared at various confining stresses (30, 50, 100 kPa) and a Mohr Failure Envelope was developed for the soil in question.

The following subsections describe the methodology used for triaxial testing.

Sample Preparation:

In this study, samples were prepared in three different states: very loose (Dr≈ 15%), loose (Dr≈ 30%), and medium dense (Dr≈ 55%) using the dry pluviation method. The samples were placed in layers by pouring the sand into the mold using a funnel. Depending on the desired relative density, different opening sizes were used. A smaller opening size resulted in a higher relative density. Denser samples were additionally tapped with a small hammer after every other lift. The drop height was kept constant during sample preparation to ensure homogenous samples.

Once the sample was in the mold within the membrane, the porous stone and top cap were placed and the triaxial chamber was assembled. The chamber was filled with distilled water and a small vacuum was applied to the sample to ensure sample stability. Samples were flushed with CO_2 to substitute the air in the pores and then inundated with deaired water, through the bottom and top cap. This flushing of CO_2

and deaired water helped achieve saturation. Table 4 shows a summary of the dimensions of the samples, density and void ratio.

Table 4- Summary of results from sample preparation

σ3 [kPa]	Weight (g)	Height (mm)	Density (g/cc)	Dr (%)
30	935.20	144.37	1.64	56
50	910.90	140.25	1.64	56
100	926.75	142.51	1.64	58
30	869.41	142.92	1.54	31
50	891.40	143.86	1.56	36
100	866.18	141.60	1.55	26
30	835.58	143.33	1.47	13
50	844.77	143.99	1.48	16
100	850.61	144.75	1.48	10

Note – The diameter of the samples was 71 mm

Test procedure

Samples were sheared using the triaxial apparatus manufactured by Geocomp® which consists of a Load Track II load frame to apply the deviator stress and a set of Flow Track II flow pumps. The pumps apply, monitor and control cell and sample pressures. All samples were saturated until a B value of approximately 0.95 was reached.

Monotonic triaxial tests are carried out in two separate phases: (1) consolidation and (2) shear. During the consolidation phase, an isotropic pressure was applied to specimen until the desired vertical effective stress was reached. During the shear phase, in addition to the vertical effective stress, a deviator stress is applied to the specimen until failure. For these tests, samples were sheared at a strain rate of 0.5% / min up to a maximum axial strain of 20%. Failure was defined as maximum

deviator stress. Friction angles were calculated using Equation (13) where q_f is the shear stress at failure and p'_f is the mean effective confining pressure at failure. The results of the triaxial tests are presented in Table 5. Figures 19 shows volumetric strain vs. axial strain behavior and Figure 20 shows deviatoric stress vs. axial strain behavior for different relative densities respectively. Figure 21 shows a Mohr Coulomb circle with the corresponding failure envelope for the dense specimen. The calculations include corrections for the area and for piston friction.

$$\phi_{peak} = \sin^{-1}\left(\frac{q_f}{p'_f}\right) \qquad (13)$$

Table 5- Summary of results for the CD triaxial tests

Very Loose Samples				
σ'_3 (kPa)	$\sigma_{d\,Max}$ (kPa)	p' (kPa)	q (kPa)	ϕ' (°)
30	98.22	79.1	49.1	38
50	116.24	134.6	84.6	39
100	322.84	261.4	161.4	38
Loose Samples				
σ'_3 (kPa)	$\sigma_{d\,Max}$ (kPa)	p' (kPa)	q (kPa)	ϕ' (°)
30	116.26	88.1	58.1	41
50	190.77	145.4	95.4	41
100	369.89	284.9	184.9	40
Medium Dense Samples				
σ'_3 (kPa)	$\sigma_{d\,Max}$ (kPa)	p' (kPa)	q (kPa)	ϕ' (°)
30	161.94	110.0	81.0	47
50	244.43	172.2	122.2	45
100	480.14	340.1	240.1	45

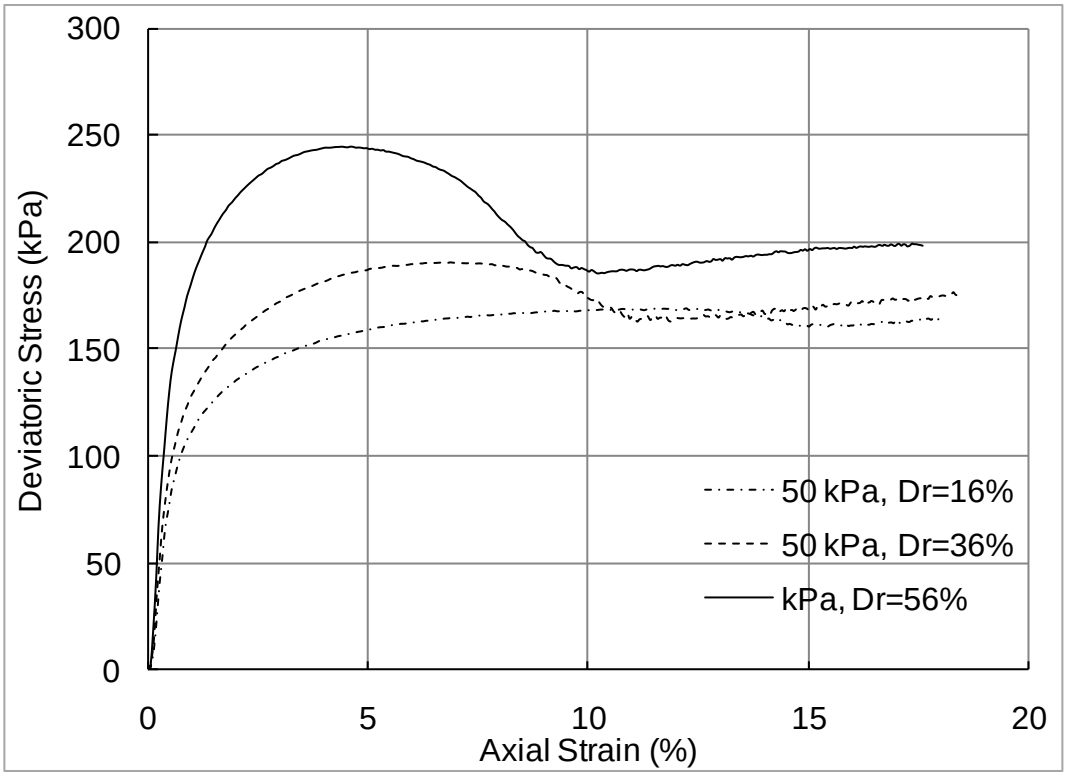

Figure 19- Deviatoric Stress vs. Axial Strain for different relative densities

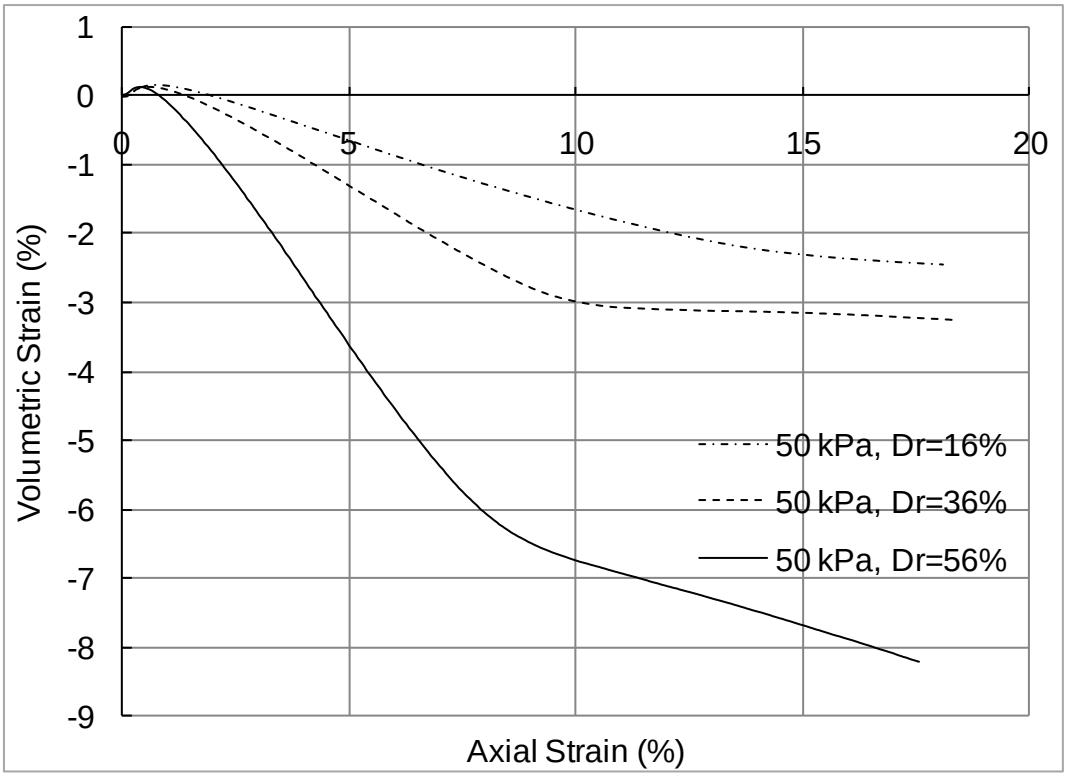

Figure 20- Volumetric Strain vs. Axial Strain for relative different densities

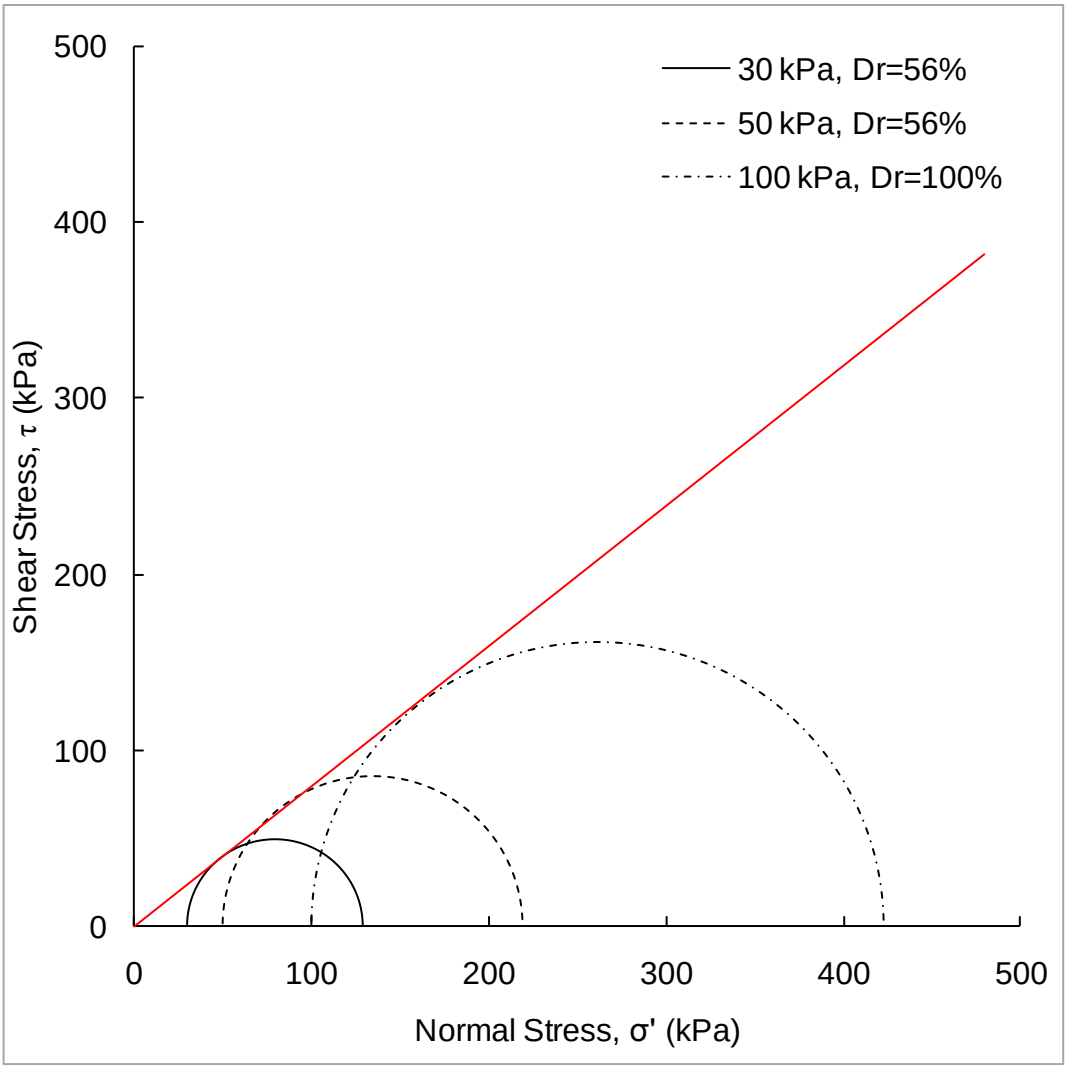

Figure 21- Mohr Coulomb Circles and Failure Envelope for dense specimens

3.1.3 Critical state friction angle

Critical state friction angles can be obtained by means of drained triaxial tests or a simplified procedure developed by Santamarina and Cho (2001). Both procedures were carried out in this study and will be discussed briefly.

Santamarina and Cho (2001) proposed that the critical state friction angle can be found using a graduated cylinder. Sand was poured in a cylinder filled with water. The cylinder was then tilted and slowly brought back to its initial position. The angle of repose in the middle region of the slope is the critical state friction angle. This procedure was repeated ten times and an average was taken. The results are summarized in Table 6.

Table 6- Critical state friction angle Santamarina and Cho

Test # [-]	ϕ_{CS} [°]
1	30.0
2	31.0
3	32.5
4	32.0
5	30.0
6	32.0
7	32.0
8	31.0
9	31.5
10	32.0
Average	31.4
COV	0.0265

The use of drained triaxial tests to determine critical state friction angle is described in Salgado et al. (2000). The authors found out that the critical state friction angle can be obtained at the point, where the volumetric strain vs. axial strain plot for a given test becomes horizontal. At this point the dilatancy angle becomes zero. The critical state friction angle can be determined using the deviatoric stress at that particular axial strain. Table 7 summarizes the results and Figures 22 and 23 illustrate this procedure. For further calculations the critical state friction angle calculated using Salgado et al. (2000) was used. This angle was calculated using Equation (13) with the values σ_1 σ_3 corresponding to the point where the change in axial strain is equal to zero.

Table 7- Critical state friction angle Salgado et al.

Test [-]	ϕ'_{cs} [°]
2	32.5
3	30.6
4	31.7
7	29.9
8	29.7
9	29.4
10	30.9
11	30.0
12	28.7
Average	30.4
COV (%)	0.0367

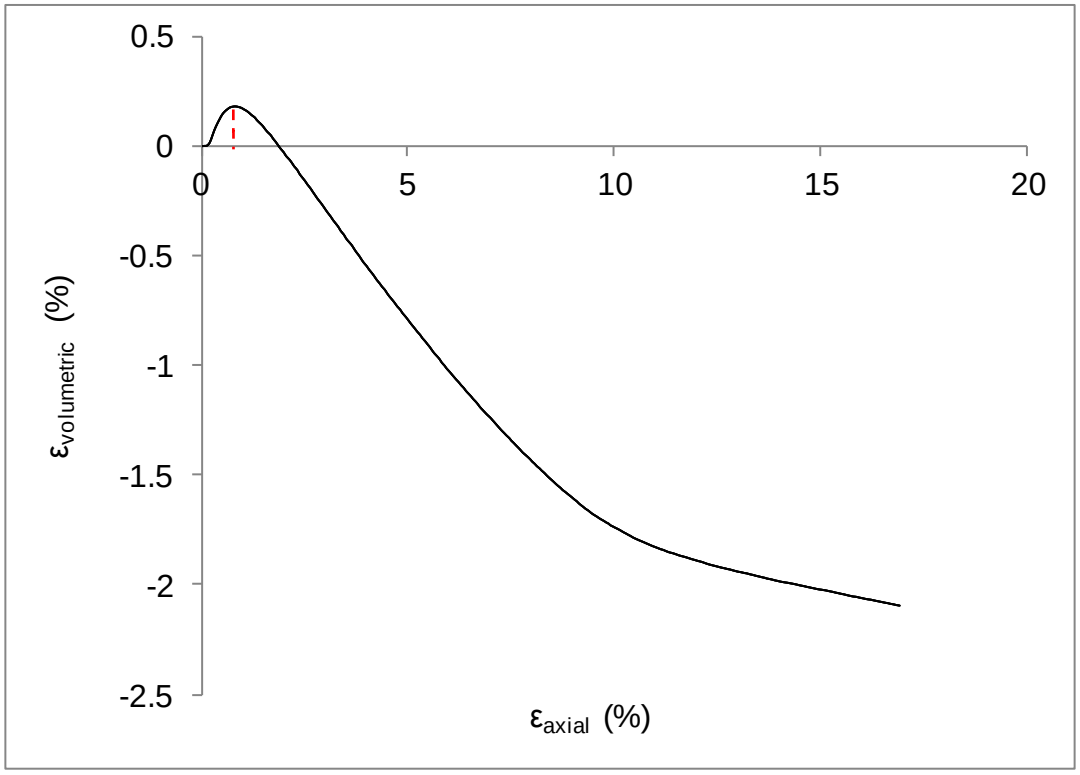

Figure 22- Volumetric strain vs. axial strain

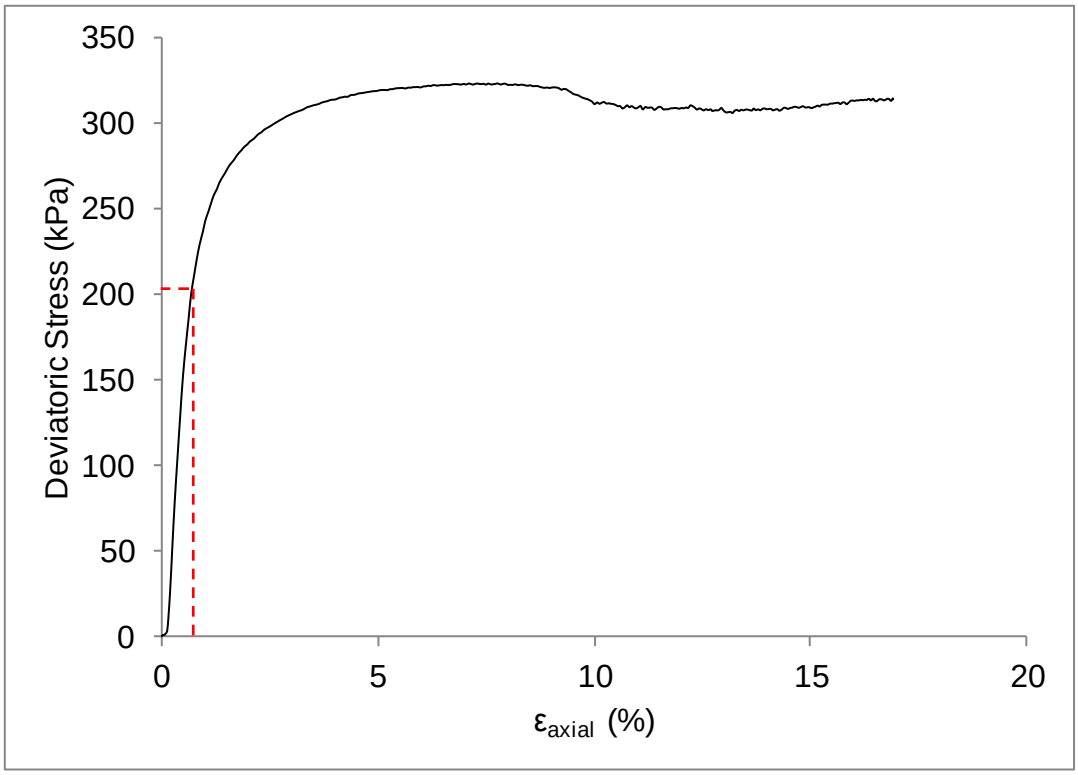

Figure 23- Deviatoric stress vs. axial strain

3.1.4 Bolton's stress dilatancy relationship

Bolton (1986) studied the relationship between strength and dilatancy of sands. He presents an empirical correlation to calculate dilatancy angles. The dilatancy angle is a function of peak friction angle, critical state friction angle, relative density, mean effective stress, and two fitting parameters. Peak friction angles for triaxial strain can be determined using:

$$\phi'_{peak} - \phi'_{cs} = 3 * I_D (Q - \ln p') - R \qquad (14)$$

where ϕ'_{peak} is the effective peak friction angle, ϕ'_{cs} is the effective critical state friction angle, p' is the mean effective stress, and Q and R are fitting parameters.

Q and R can be found by performing a linear regression using the data obtained in the triaxial tests and the average critical state friction angle calculated using the approach developed by Salgado et al. (2000). The confining pressures expected in the model tests are in the range of 1 to 4 kN / m^3 while the lowest confining pressures in the triaxial tests were 30 kN/ m^3. For this reason the relationship described above is assumed to be also true for smaller stresses and extrapolated to the smaller stress levels occurring in the model.

The best fit line is represented in Figure 24 with Q= 10.46 and R=-1.89 (r^2=0.988).

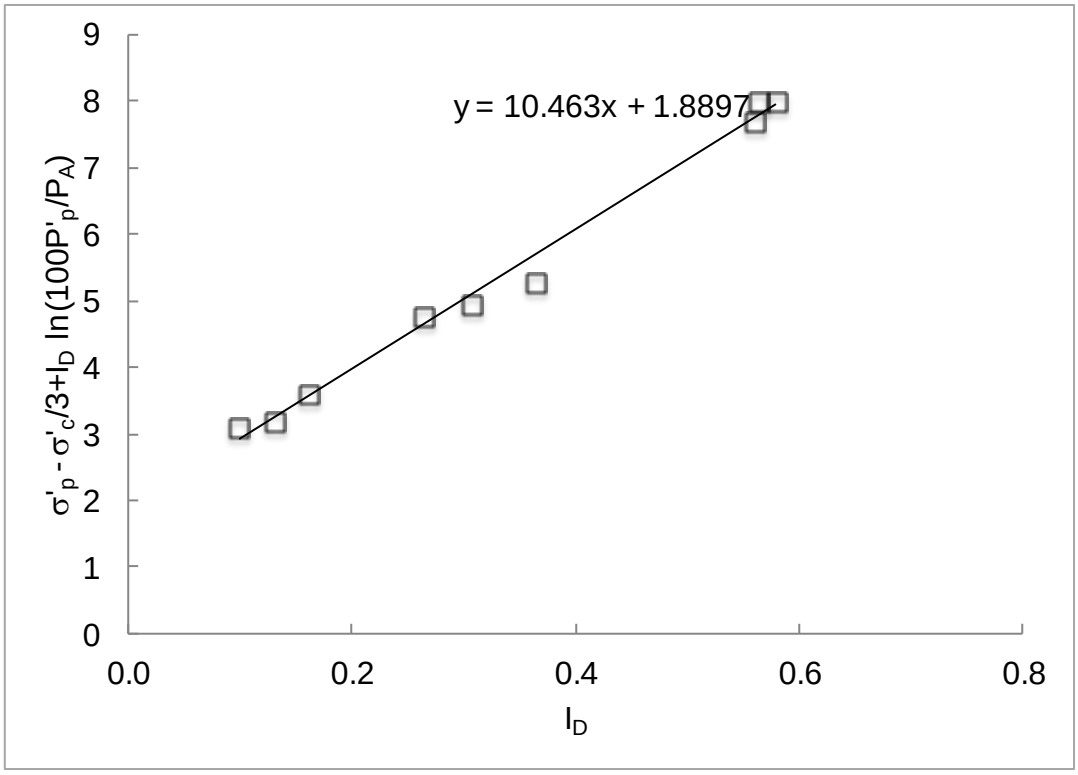

Figure 24- Determination of Bolton's parameters for the sand used in this study

The angle of dilation, ψ, can be calculated when rearranging Equation 14 to the following:

$$\psi = \frac{\phi'_{peak} - \phi'_{cs}}{0.8} \qquad (15)$$

where ψ is the dilatancy angle.

This stress – dilatancy relationship was used to address scaling issues in 1g model tests as it accurately characterizes the strength of a soil at low stress levels. This can be used to interpret the behavior of the soil at prototype scale. To model the constitutive response of a full scale soil, the model has to be prepared in a looser state with corresponding lower stress levels. To evaluate which relative density

corresponds to the in-situ relative density Equation (14) was used. A relationship between the prototype relative density and the model relative density can be established when equating the right hand side of Equation (14) for both cases. If the new equation is solved, the following ratio can be obtained:

$$\frac{I_{Dm}}{I_{Dp}} = \frac{Q - \ln p'_p}{Q - \ln p'_n} \qquad (16)$$

where I_{Dm} and I_{Dp} are the respective relative densities for the prototype and model, Q is a fitting parameter, p'_p and p'_m are the respective mean effective confining pressures at failure.

If a prototype anchor is considered with a width of 3048 mm in a 1:20 scale, the corresponding model has a plate width of 152.4 mm. Assuming both anchors are installed to an embedment ratio of 3 and the in-situ sand is at a relative density of 30%, Equation (16) indicates that the model sand needs to be prepared to a relative density of about 24%. This rather small difference in relative density is caused by the different soil conditions in the model and prototype. The model is prepared in dry sand while in the prototype saturated conditions are considered and buoyant unit weights are used. This results in only a small difference between the respective mean effective confining pressures when considering K_0 conditions in the calculation. At an embedment ratio of H/B = 1, the effective mean confining pressure of the model was determined to be 1.27 kN/m^3 and 5.76 kN/m^3 for the prototype respectively.

The just described relationship was used to prepare the soil samples for the study.

3.2 1g Model anchor tests

The following chapter describes the experimental testing program and the small-scale pullout tests carried out at the University of Rhode Island to model the breakout behavior of shallow square plate anchors in sand. The main focus was to represent the in-situ conditions in the best way possible and to perform repeatable and comparable anchor pullout tests. It was ensured that the prepared samples represented the desired in-situ conditions.

3.2.1 Model Test Experimental Setup

Two test tanks were set up to perform pullout tests on small scale anchors. The equipment consisted of a gantry crane, a winch and pulley system, load cells, string potentiometers, a data acquisition system, and the different miniature anchors. The completed tests included drag embedment, inclined and vertically loaded plate anchor tests.

The testing tanks used in this study were designed and built at the University of Rhode Island. The inside dimensions of the tank were 1219 mm wide, 2413 mm long, and 914 mm high. The bottom and sides were made out of plywood and reinforced by wooden beams. Two identical boxes were set up alongside one another but tests were only performed in one box. The second box was meanwhile used as a storage box for the used sand.

The overhead crane was set up in a way that the pluviator could be adjusted laterally and vertically while preparing the sample. The frame also allowed inclining the loading chain and anchors at any desired angle. The winch was placed and fixed on the floor and the steel cable was connected with a pulley system to the frame. A schematic diagram of the experimental setup is presented in Figure 25.

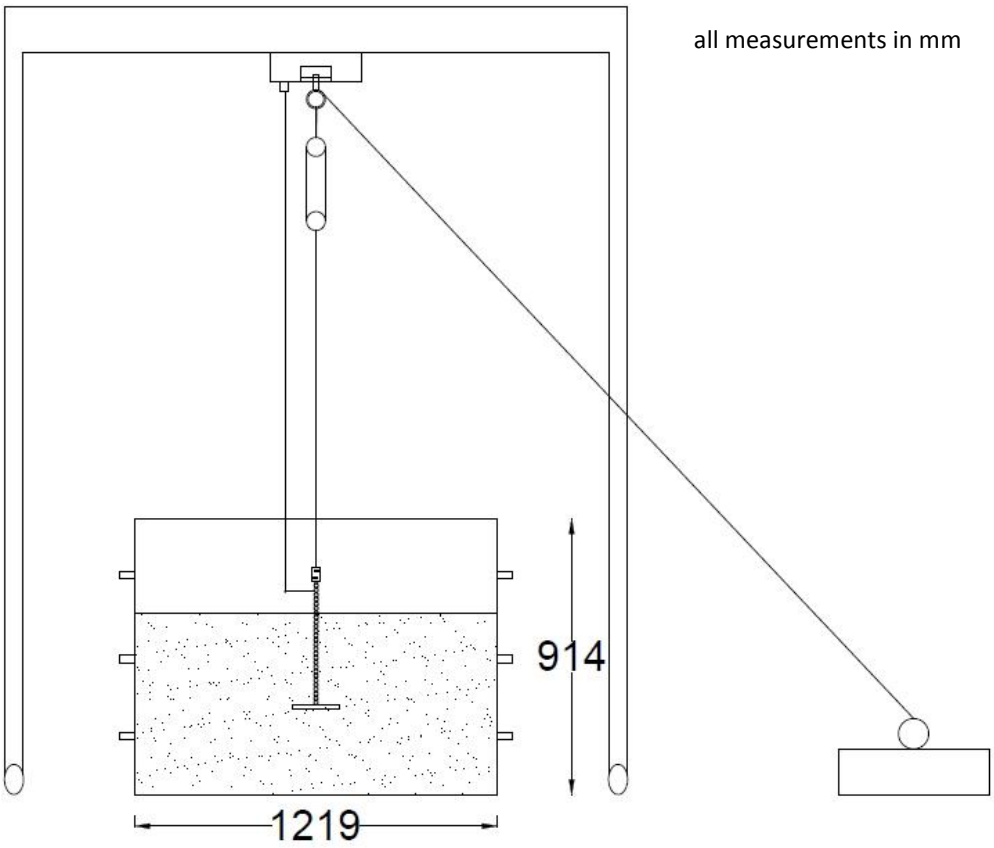

Figure 25- Schematic test setup

Model anchors were fabricated from steel. Tables 8 and 9 give an overview of the anchor properties. The plates were assumed to be rigid enough to not bend for the expected loading conditions. A steel chain was connected to the anchor and embedded in the sand to simulate the anchor chain. Figures 26 and 27 illustrate plate anchor and drag embedment anchor used in this study.

Table 8- Summary square plate anchor properties

Anchor #	*Height (mm)*	*Width (mm)*	*Length (mm)*	*Weight (N)*
1	12.7	152.4	152.4	27.02
2	12.7	152.4	152.4	27.73
3	12.7	304.8	304.8	96.42

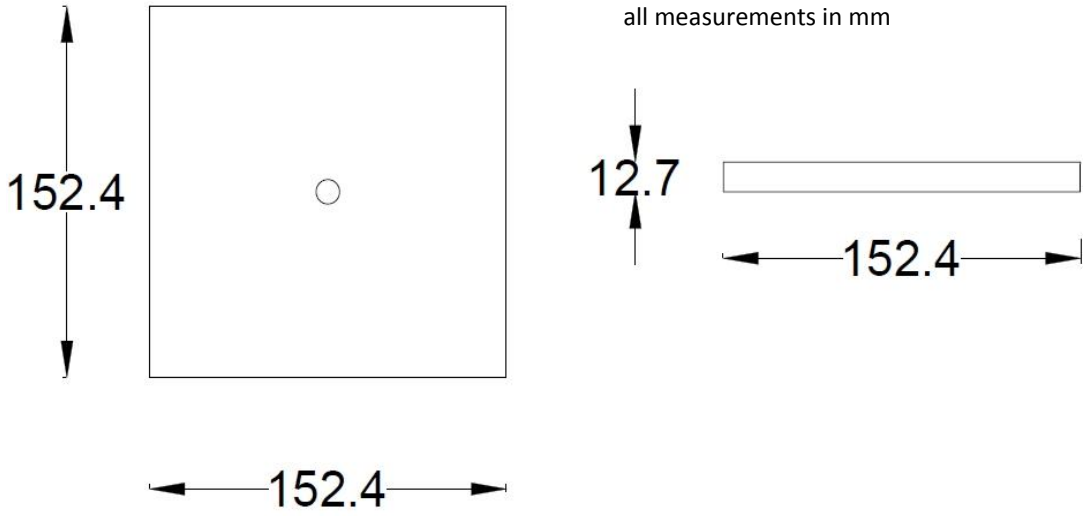

Figure 26- Dimensions square plate anchor

Table 9- Summary drag embedment anchor properties

Anchor #	*Height (mm)*	*Width (mm)*	*Length (mm)*	*Weight (N)*
4	12.7	152.4	152.4	26.56

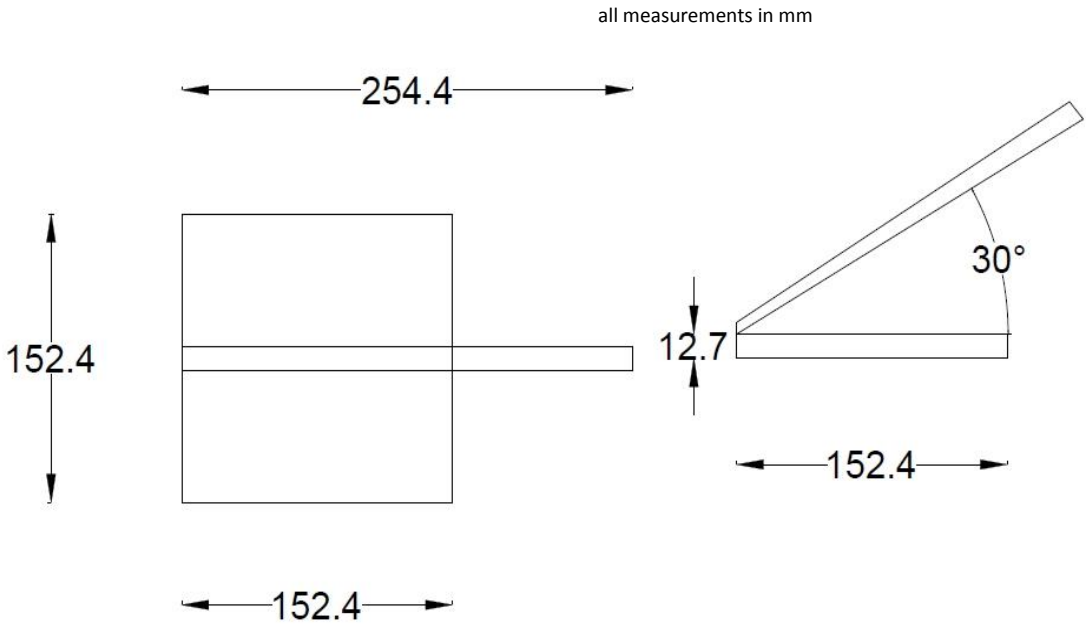

Figure 27- Dimensions drag embedment anchor

A load cell was connected in line between the cable and the anchor and a data acquisition system was installed to measure the loads in the pullout process. In the course of the pullout tests, two different load cells, with capacities of 200 and 500 lb were used depending on the expected loads. The smaller load cell was used for shallower anchors because of its higher precision with lower loads. A string potentiometer was attached to the steel frame and the anchor chain to measure the anchor displacement. The tests were recorded using the i100 instruNet data

acquisition system that was connected to a laptop and the load cells and string potentiometer. Pictures of the setup and the anchors can be found in Appendix B.

3.2.2 Sample preparation

The preparation of a uniform and repeatable sand bed with a desired relative density was required in this study. In order to achieve this, three different pluviation methods were tried in this study. The portable pluviator proposed by Gade et al. (2013) proved to meet the requirements best and was therefore used in this study. The pluviator is described in detail in Chapter 2.

One of the main selection criteria was the desired relative density. For this purpose the pluviator was calibrated by varying the drop height (50.8 mm to 190.5 mm) and alternating the number of installed sieves. A drop height of 152.4 mm and two 6.35 mm sieves resulted in a desired relative density of about 23%.

Six tests samples were prepared with relative densities ranging from 18-24%. The average unit weight for the six tests was 14.84 kN / m^3. The height of soil placed in the box was 609.6 mm for each box and a total of 11 anchor tests were performed. To ensure a homogenous sample, the drop height was adjusted every 50.8 mm and the pluviator was moved laterally throughout the box using the steel frame. The test anchors were placed at different embedment depths during the pluviation. For the placing of the anchors, possible boundary issues were considered and it was ensured that boundary effects were minimized. An advantage of the portable pluviator was the anchors could be put into place without disturbing the soil around and above it.

Minicone penetrometer tests (mCPT) were performed for each box at six different locations. The locations were carefully chosen to minimize possible boundary effects from box edges and to eliminate soil disturbance for the anchors. The miniature cone had a tip area of 1 cm^2 and was pushed in the sand using the pulley system and weights stacked on the cone to simulate a downward force. The cone was calibrated beforehand using the Geocomp® system. A known load was applied to the cone and the corresponding reading was recorded. A relationship between the applied weight and recorded values was then established and used throughout the tests for the cone.

A correlation between tip resistance and relative density was used to determine the density at each location and an average was taken for the whole box. The equation was proposed by Kulhawy and Mayne (1990) and is as follows:

$$D_R{}^2 = \frac{1}{305 * Q_c * OCR^{0.18}} * \frac{\left(\frac{q_c}{pa}\right)}{\left(\frac{\sigma_v}{pa}\right)^{0.5}} \qquad (15)$$

where D_R is the relative density, Q_c is a compressibility factor, OCR is the overconsolidation ratio, q_c is the measured tip resistance, σ_v is the overburden stress, and pa is the atmosphere pressure (100 kPa).

Typical tip resistance and sleeve friction profiles with depth are presented in Figure 28 and 29, respectively. Figure 30 shows a typical result of the relative density with depths and Table 10 summarizes all collected data.

Additionally, density was measured directly during the pluviation using caps of a known volume. While pluviating a layer of soil the caps were filled and weighed. Densities were then calculated using the known volume of the caps and the measured weight of the soil. Figure 31 shows a typical result of the relative density with depths and Table 11 summarizes all data. Both density readings showed comparable results. For the following calculations the density readings obtained from the density caps were used.

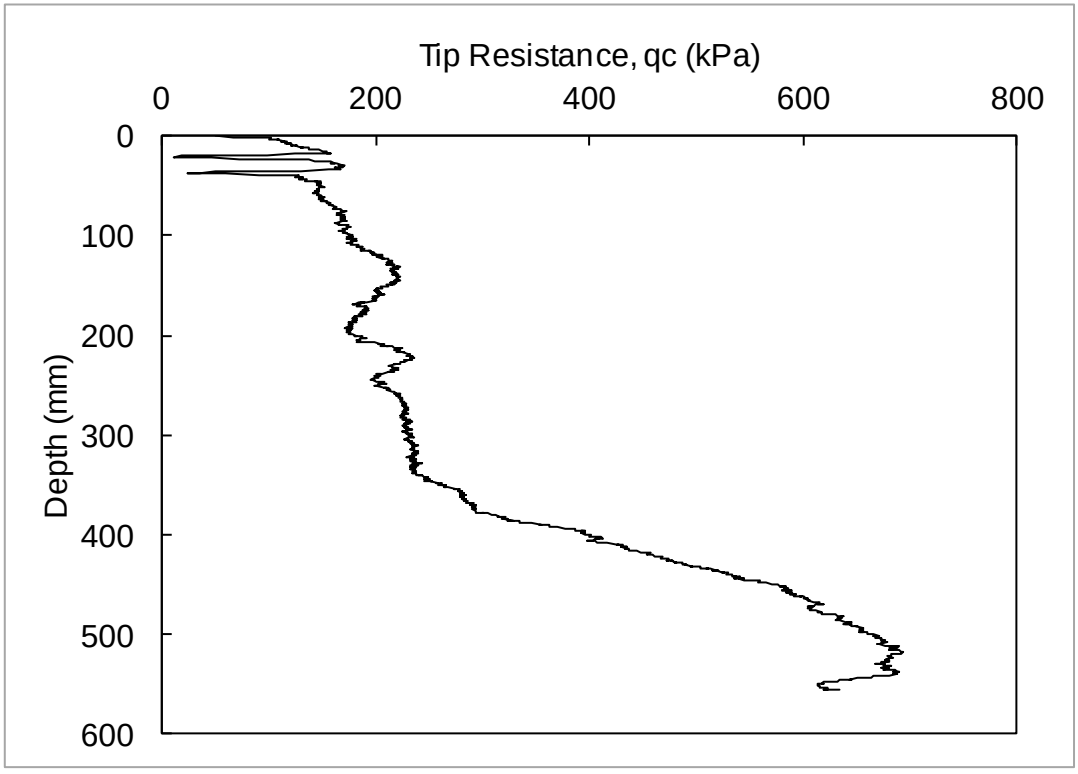

Figure 28- Typical tip resistance profile

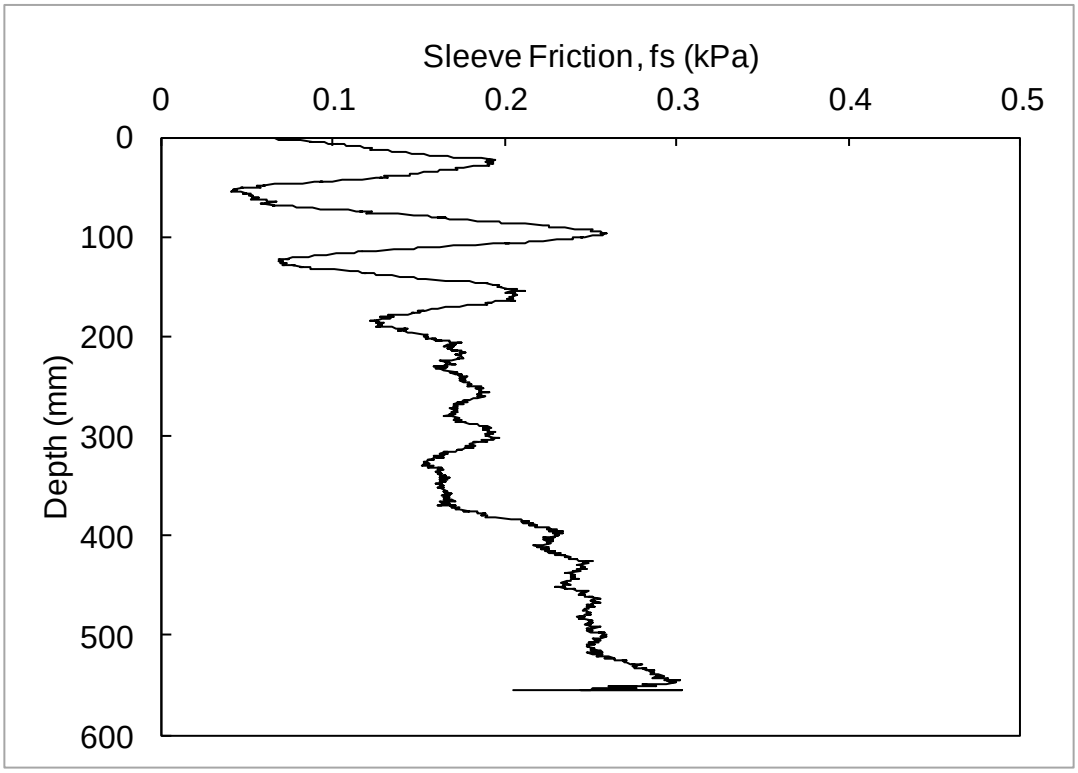

Figure 29- Typical friction sleeve profile

Table 10- Summary mCPT density readings

Box #	*Average Density Readings*
1	19.64
2	19.66
3	19.80
4	17.09
5	21.18
6	19.09
Average	19.41
COV	0.0687

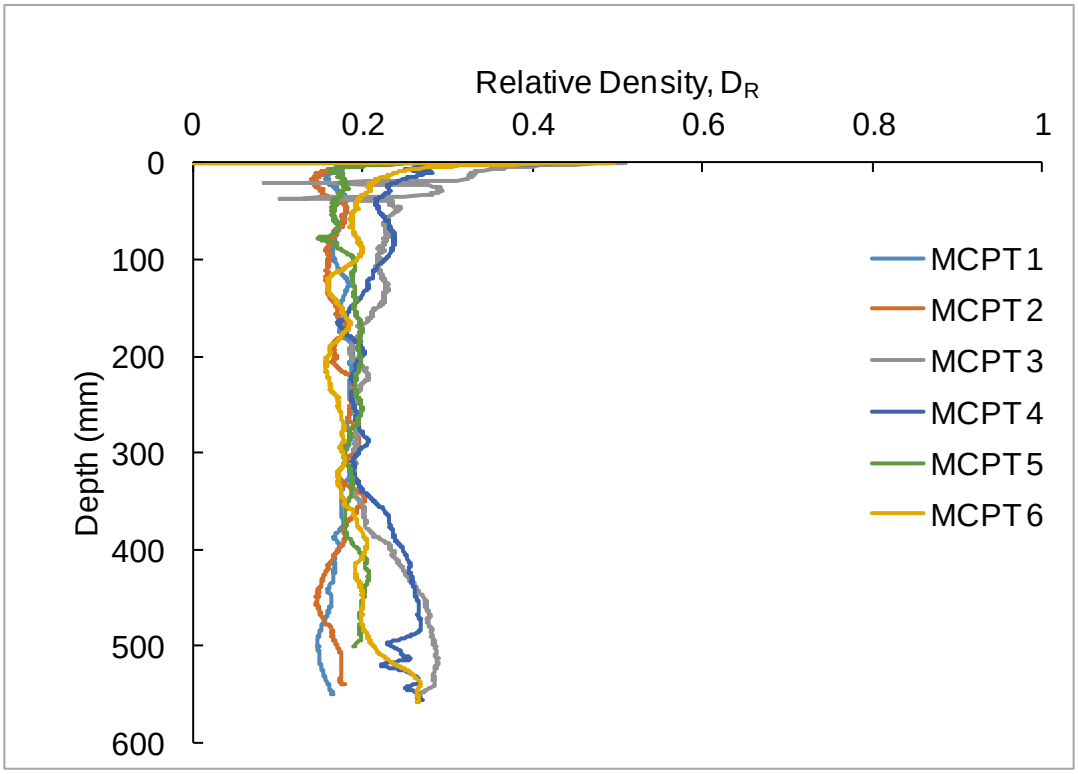

Figure 30-Minicone penetrometer tests density readings

Table 11- Summary density caps density readings

Box #	*Average Density Readings*
1	24.4
2	22.7
3	22.5
4	22.1
5	21.9
6	18.6
Average	22.0
COV	0.086

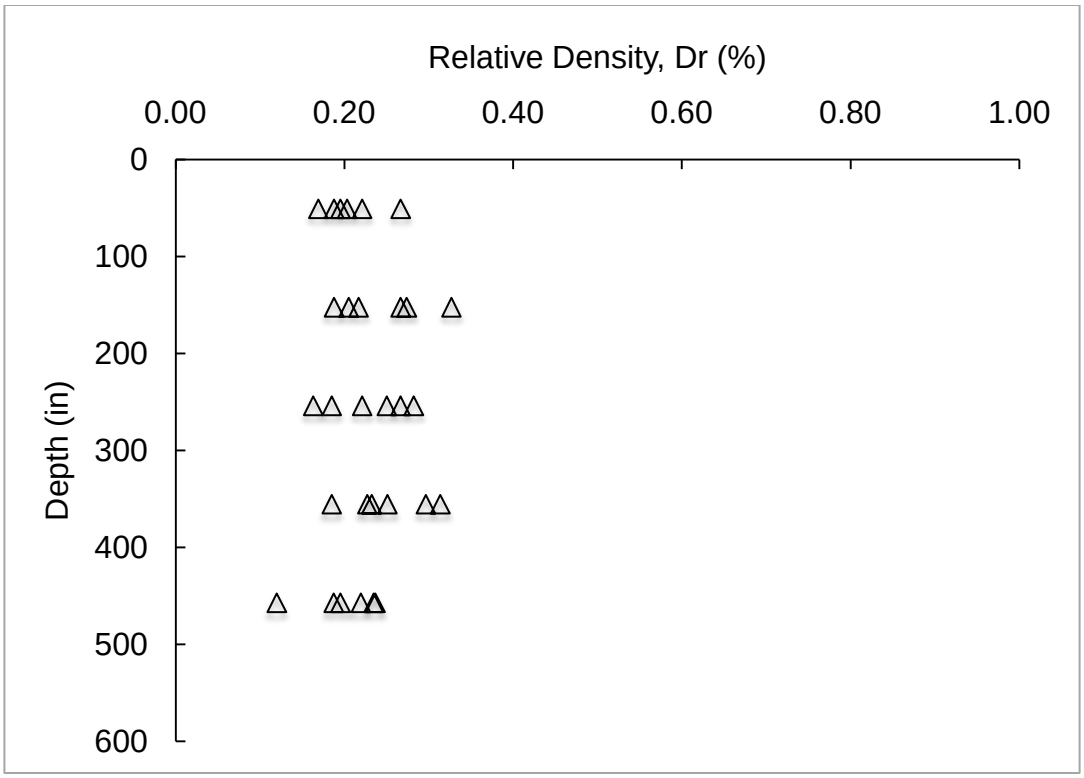

Figure 31- Density caps density readings

3.2.3 Anchor Pullout tests

The anchor pullout tests were performed using an electrical winch connected to a pulley system on the steel frame. The anchors were pulled at a constant rate of 5 cm / s, which was controlled by the pulley system and the winch speed. The acting forces and resulting displacements were measured as described before. Figures 32, 33 and 34 show typical load–displacement curves for vertically pulled anchors, inclined anchors and drag embedment anchors, respectively. Tables 12, 13, 14 summarize the obtained results for the corresponding tests. The ratio H/B, used in the table, is the embedment depth over the plate width. The soil parameters were calculated for each anchor position individually based on the density cap readings. Friction and dilatancy angles were calculated using Bolton's approach at the depth of the anchor. The unit weight is an average value of the soil between the anchor location and soil surface.

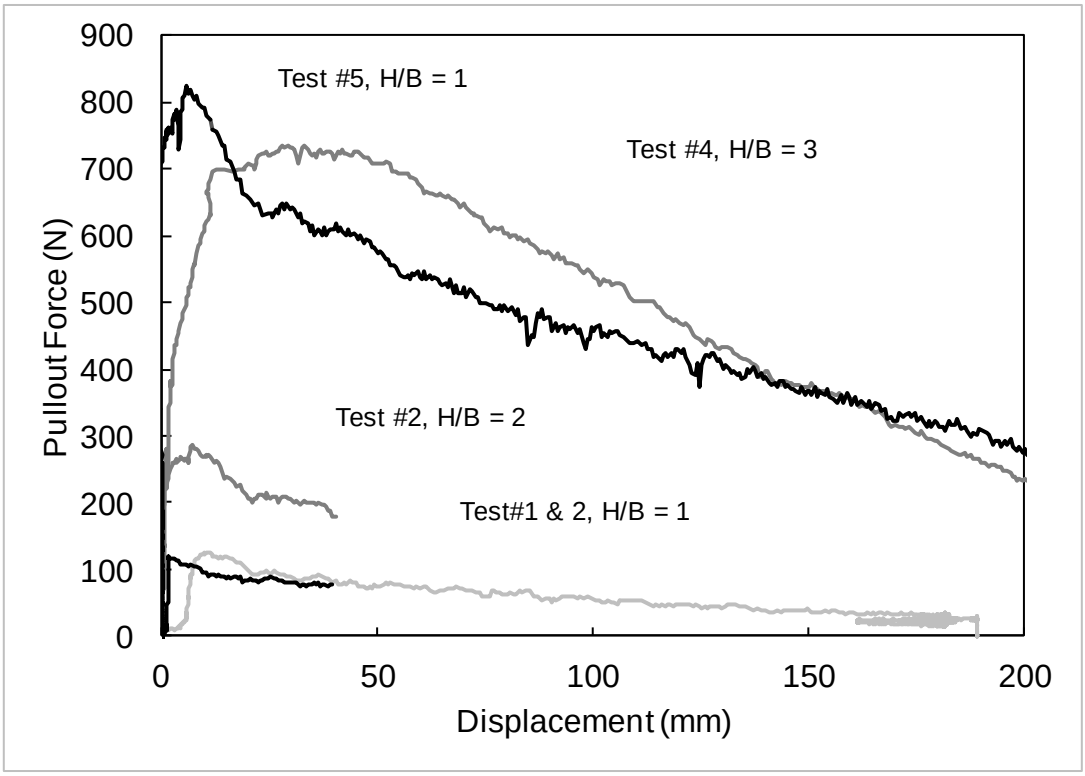

Figure 32- Load vs. displacement curve vertically loaded anchors

Table 12 Summary of vertically loaded anchor test results

Test No.	H/B	B (mm)	γ (kN/m^3)	σ_v (kN/m^2)	Dr (%)	ϕ (deg)	Ψ (deg)	Qu (N)	N_γ
1	1	152.4	14.96	2.27	25	44.0	15.1	91	1.72
3	1	152.4	14.76	2.25	21	42.2	13.1	98	1.88
5	1	304.8	14.84	4.52	22	42.5	13.4	727	1.73
2	2	152.4	14.89	4.54	27	44.4	15.6	258	2.45
4	3	152.4	14.76	6.81	21	41.8	12.7	708	4.52

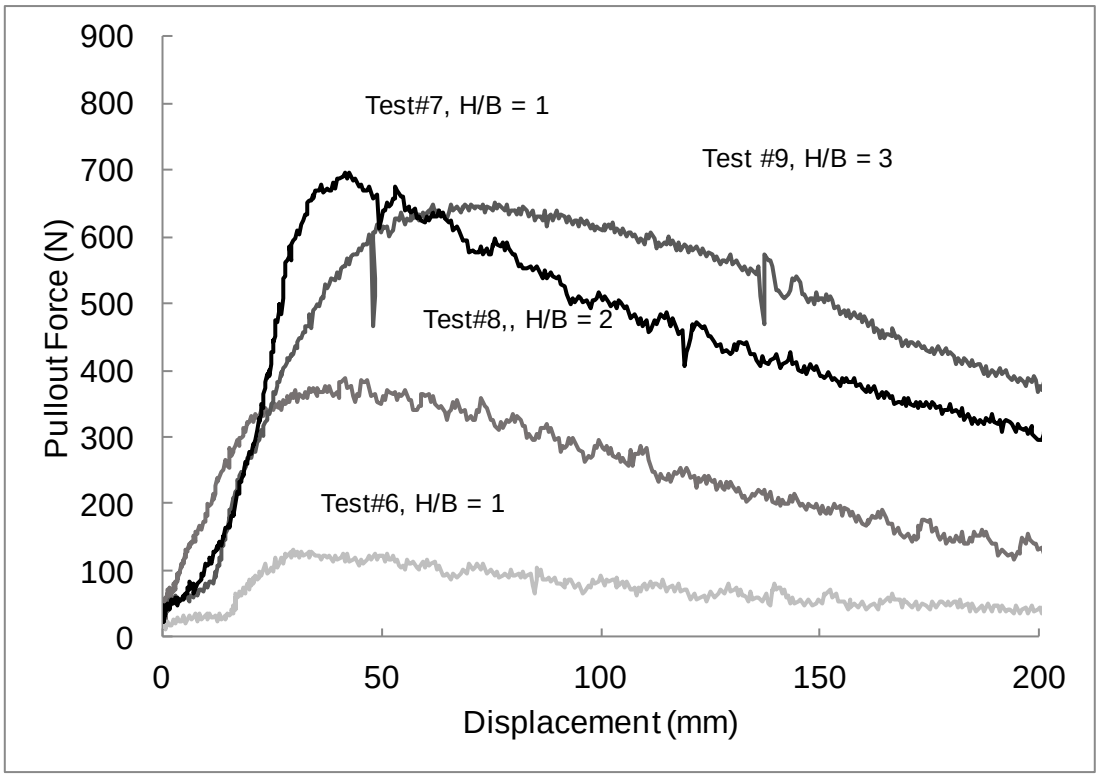

Figure 33- Load vs. displacement curve inclined anchors

Table 13- Summary of inclined anchor test results

Test No.	H/B	B (mm)	γ (kN/m^3)	σ_v (kN/m^2)	Dr (%)	ϕ (deg)	Ψ (deg)	Qu (N)	N_γ
6	1	152.4	14.85	2.26	23	43.0	14.0	102	1.94
7	1	304.8	14.91	4.53	23	42.7	13.8	601	1.42
8	2	152.4	14.81	4.51	21	42.2	13.1	363	3.46
9	3	152.4	14.80	6.77	21	41.9	12.8	621	3.99

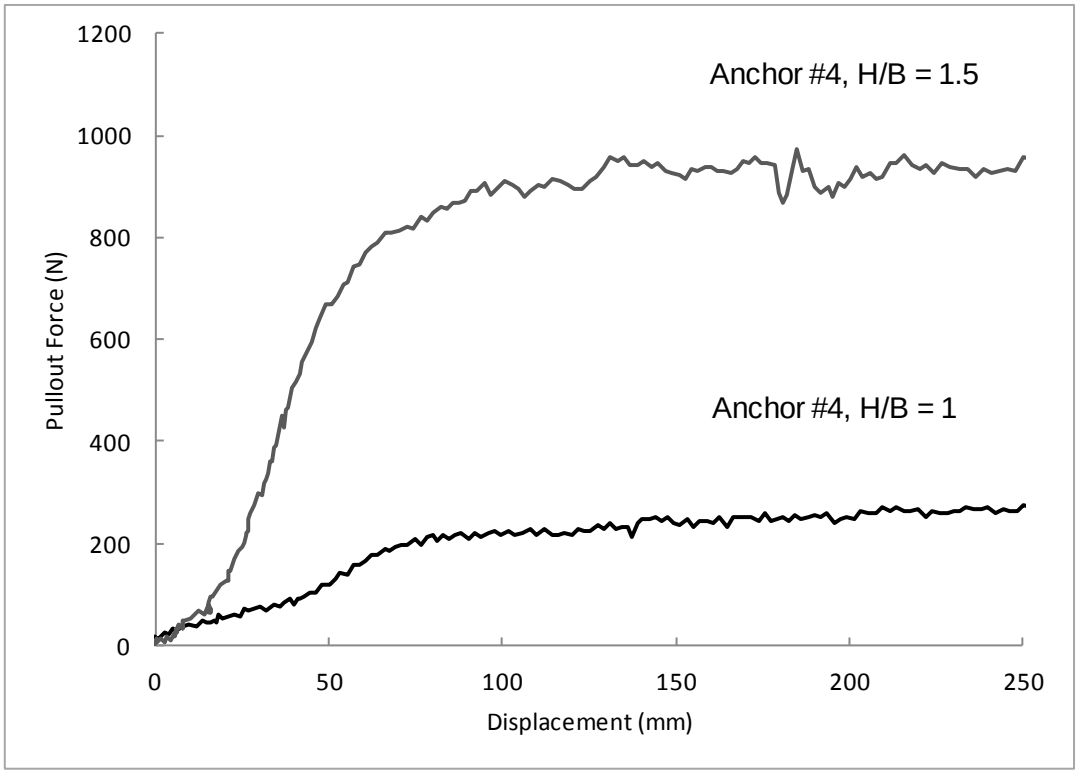

Figure 34- Load vs. displacement curve drag embedment anchors

Table 14- Summary of drag embedment anchor test results

Test No.	H/B	B (mm)	γ (kN/m^3)	σ_v (kN/m^2)	Dr (%)	ϕ (deg)	Ψ (deg)	Qu (N)	N_γ
10	1	152.4	14.85	2.26	23	42.99	14.0	272	5.19
11	1.5	152.4	14.66	3.35	19	41.13	12.0	945	12.15

The results show that the pullout capacity increases with an increase in the embedment ratio. This is consistent with the existing theories as the pullout capacity is a combination of the mobilized soil wedge and the friction on the sides of the wedge. Also, the capacity increases with an increase in inclination angle. This is due to the larger soil wedge mobilized in inclined tests. The load- displacement curves for both tests show a clear peak in capacity with relatively small

displacements. The vertically loaded anchors reached their peak capacity with displacement in the range of 1- 11 mm and the post peak load rapidly decreased. The needed displacements corresponding to the peak capacity for inclined anchors are larger and in the range of 30- 70 mm. Furthermore, the post peak softening behavior of the inclined anchors were not as distinctive but for both anchor types the mechanism was catastrophic.

Two different sized plate anchors (152mm and 304mm) were tested at the same H/B ratio to study scaling effects in the test tank. For the vertical pullout tests basically no difference in breakout factors between the anchors can be observed as the larger plate's breakout factor was 9% higher than the breakout factor of the small plate. Different sized anchors were also used in the inclined pullout tests. For these tests, the smaller plate recorded a 36% higher breakout factor. In total the results suggest that the size of the anchor does not affect the results.

The drag embedment anchor tests exhibited larger pullout capacities than plate anchors. On the contrary no distinctive peak was observed with drag anchors. This is due to the fact that the failure for drag embedment anchor is not a catastrophic failure. Even after the initial movement the anchor is still dragged horizontally through the soil and resistance is mobilized. The load- displacement curves also show this behavior. After a peak is reached almost no strain softening behavior can be observed. The recorded displacements for drag embedment anchors were larger than the displacements for plate anchors.

The recorded pullout test results are used in the following analytical program to evaluate existing prediction models and to assess their accuracy with regard to the specific soil conditions used in this study. In order to fully describe the behavior of the different anchor types, tests in denser conditions should be performed; however this is beyond the scope of this study.

4 ANALYTICAL PROGRAM

The following chapter presents a summary of the analytical study carried out for this investigation. First, a parametric study was performed to study the effects of inclination angle, H/B ratios, and friction angles on the predicted capacity of inclined square plate anchors. Second, a variety of anchor capacity prediction models, described in Chapter 2, were used to estimate breakout resistance factors for the anchor tests presented in Chapter 3. A comparison between the experimental results and the model predictions led to a choice of a single model that is used in a later part of this chapter to model the anchoring of a floating platform using real loads derived from a 5-MW offshore wind turbine.

4.1 Parametric Study of Analytical Models for Inclined Anchors

The use of taut, semi-taut mooring or vertical mooring system instead of catenary mooring system can be favorable in deep and ultra-deepwater. This is mainly due to the high weight of the anchor chain in the catenary system at large depths and uncertainty in the positioning of drag embedment anchors in the soil. Because of this, the use of plate anchors in semi-taut mooring systems seems promising. In semi-taut mooring systems the anchor has to withstand both vertical and horizontal mooring forces. To achieve this, the anchor is penetrated in the soil and then pulled until its final position is achieved as described in Chapter 2.3.3 (Randolph et al., 2011).

Three analytical models, described in Chapter 2, are used to investigate the influence of load inclination and embedment depth on the breakout capacity for inclined square plate anchors. These models include Meyerhof (1973), Hanna et al. (1988), and Goel et al. (2006). Three different sand conditions, with friction angles ranging from ϕ= 30, 40, 50 degrees, are used to investigate a broad range of sands. The inclination angle, α, of the anchor is taken with respect to the vertical, and H/B is the ratio of embedment depth to fluke width. The results are presented in terms of the dimensionless breakout factor, N_γ,

4.1.1 Effect of inclination angle

Generally, the breakout capacity increases with increasing inclination angle. An inclination of zero degrees corresponds with vertical uplift and 90 degrees means horizontal pull. Hanna et al. (1988) limit their theory to an angle of 60 degrees because in their observations greater inclination angles change the failure mechanism. Meyerhof (1973) and Goel et al. (2006) are modeled to inclination angles of 75 degrees. This range captures the typical mooring angles being used in practice up to this date. For this investigation the H/B ratio is fixed to 2.

Meyerhof (1973)

As described in Chapter 2, Meyerhof proposed the following breakout factor:

$$N_\gamma = \frac{H * K_b * s}{2B} + \cos^2 \alpha \qquad (10)$$

In this form the breakout factor is not very sensitive to the inclination angle. This might be due to the small changes in the uplift coefficient K_b, utilized in the model to account for changes in inclination angle. Dense sands show an increase in capacity of 20% when comparing vertical uplift and an inclination of 60 degrees, while in case of very low friction angles the breakout capacity even decreases with increasing inclination angles. This behavior is illustrated in Figure 35.

Hanna et al. (1988)

The breakout factor was described by Hanna et al. (1988) as:

$$N_\gamma = \frac{1}{2} * \frac{k_s \sin\phi\left(L_1{}^2 + L_2{}^2\right)}{BH} + \frac{1}{2} * \frac{\left(L_1 + L_2\right)\cos\alpha}{H} \qquad (11)$$

Figure 36 shows the breakout factor as a function of inclination angle for friction angles of 30, 40, and 50 degrees. Similar to the Meyerhof (1973) approach, the Hanna et al. (1988) breakout factor is insensitive to inclination angle and friction angle for inclination angles less than 40 degrees. The breakout factor ranges from approximately 2 for inclination factors less than 40 degrees to 5-9 for an inclination factor of 60 degrees.

Goel et al. (2006)

The breakout factor was described by Goel et al. (2006) as:

$$N_\gamma = \frac{4H}{\pi D} * K * \tan\phi * I_i * \sec^2\alpha \qquad (12)$$

The variation of this breakout factor as a function of inclination angle for friction angles of 30, 40, and 50 degrees is shown in Figure 37. These breakout factors increase both with increasing inclination angle and friction angle. The dense sand showed an increase of capacity of almost 450% over the course of the variation of α. Contrary to the other two methods notable increases in capacity for small inclination angles (α ≤ 40°) can be seen. It is observed that for any friction angle, the breakout factor shows a continuous increase with an increasing inclination angle.

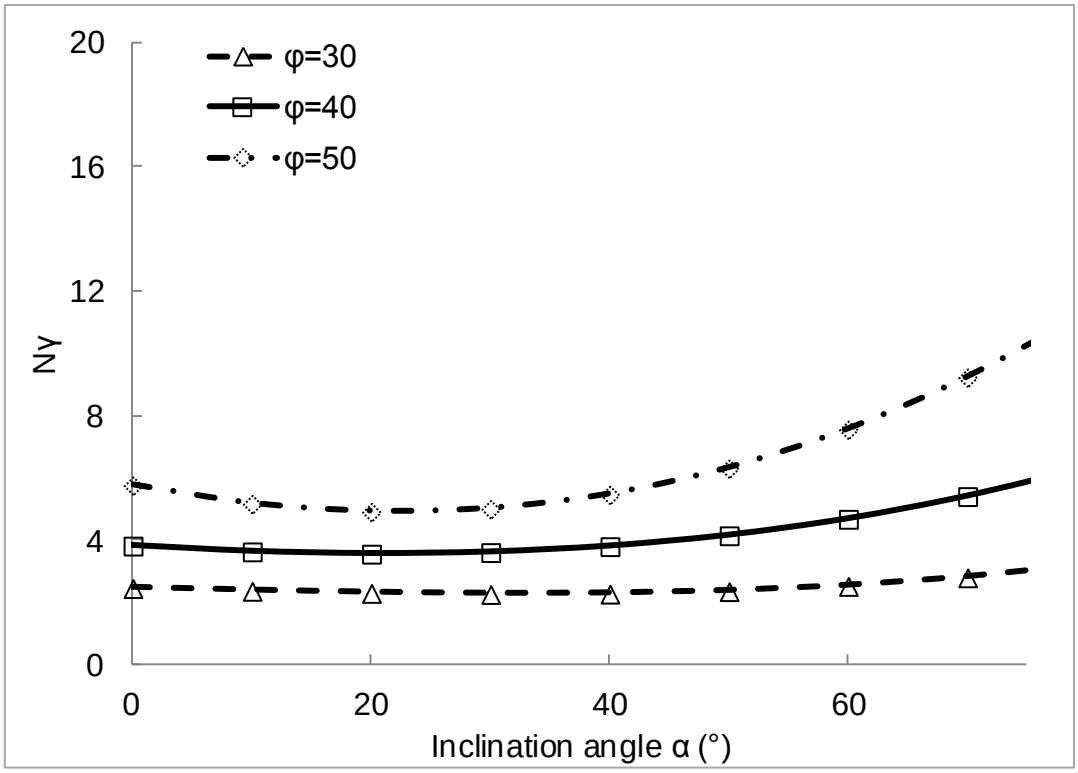

Figure 35- Breakout factor vs. inclination angle Meyerhof (1973)

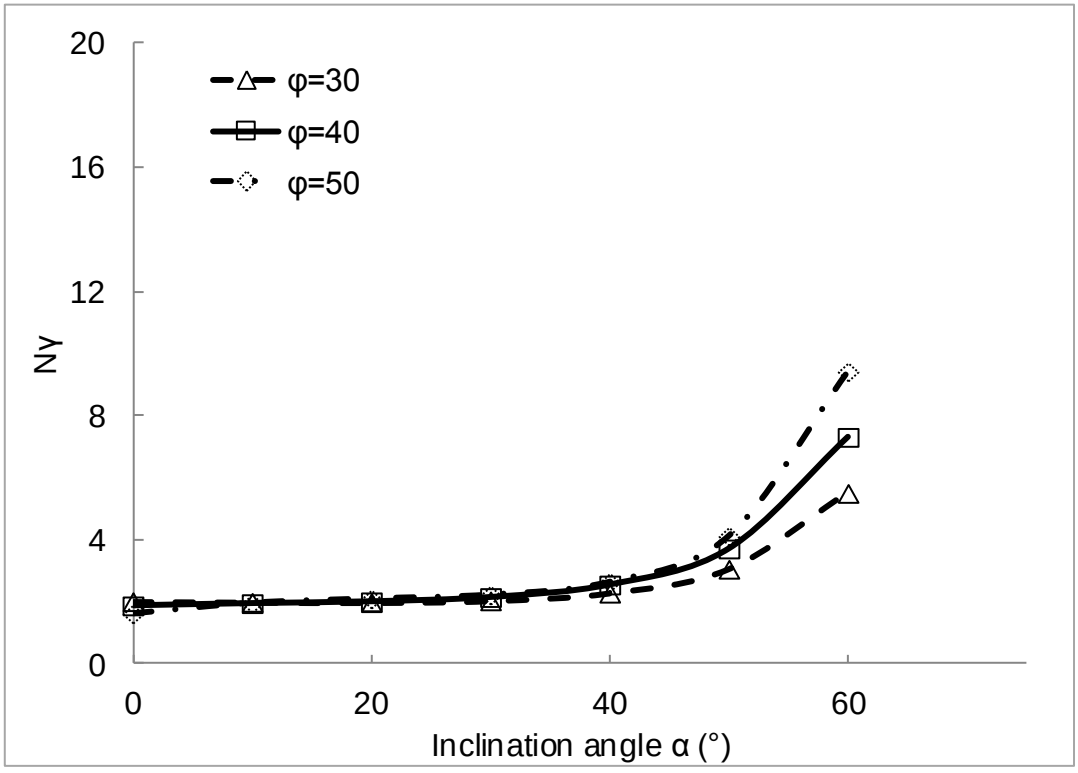

Figure 36- Breakout factor vs. inclination angle Hanna et al. (1988)

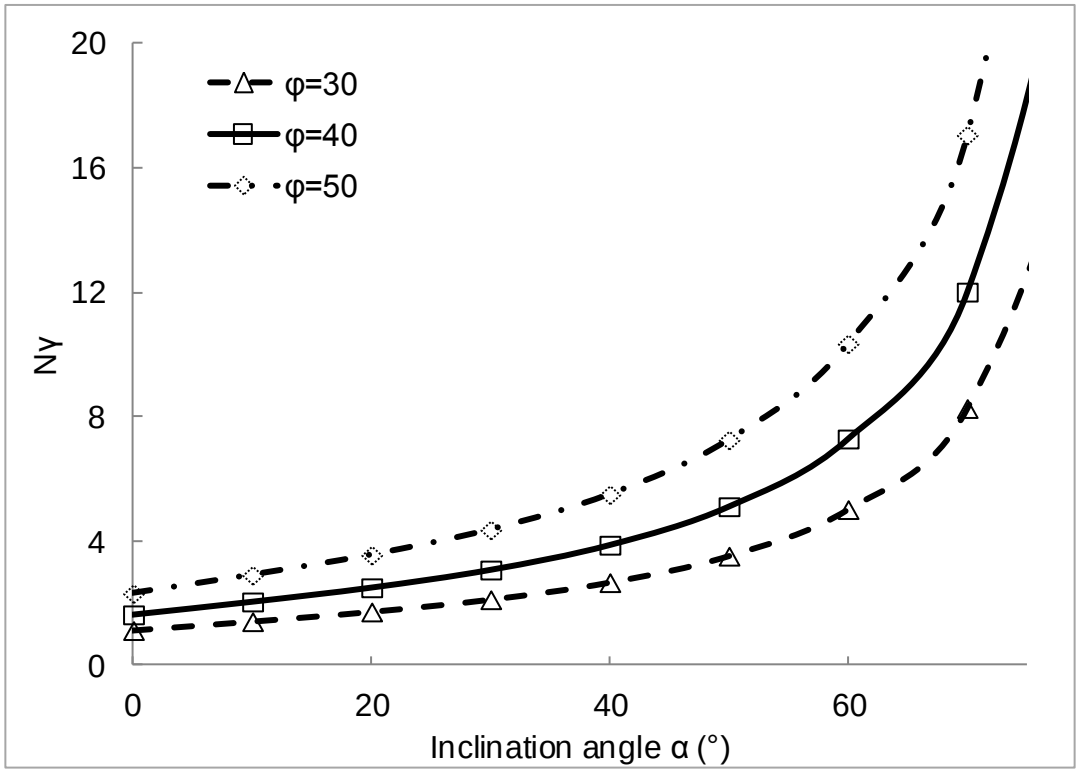

Figure 37- Breakout factor vs. inclination angle Goel et al. (1988)

4.1.2 Effect of embedment ratio

Theoretically, an increase in embedment depth should result in an increase of capacity as the soil mass mobilized above the anchor increases. To model the differences in breakout factors for variations of H/B ratios, the inclination angle was fixed to $\alpha = 40°$, which corresponds to the inclination angles used in the experimental study.

Figures 38, 39, and 40 show the variation of breakout factors with H/B ratios using the theories proposed by Meyerhof (1973), Hanna et al. (1988), and Goel et al. (1988). The Meyerhof factor exhibits an almost linear increase of capacity for loose sands while the denser sand shows an exponential increase. A 4-fold increase in H/B ratio results in an increase in capacity of 520% for the dense sample. The Hanna et al. factor also show an increase of breakout capacity with increasing H/B ratios. The overall increase in capacity is less pronounced than in Meyerhof's theory. For an increase in H/B of 4 the capacity increases by 220% for the dense sand. The Hanna et al. factor shows very little sensitivity to friction angle. The Goel et al. factor exhibits a linear increase of N_γ with increasing H/B ratios. For each friction angle an increase of H/B from 1 to 4 resulted in an increase in capacity of 400%. The breakout factors are higher for higher friction angles.

Generally the observed results capture the same behavior empirical tests have shown. Breakout capacities increase with increasing friction angles, embedment depths and with inclination angles (Hanna et al., 1988; Meyerhof, 1973; Goel et al., 2006; Das and Shukla, 2013; Bull, 2009; Das and Seeley, 1977).

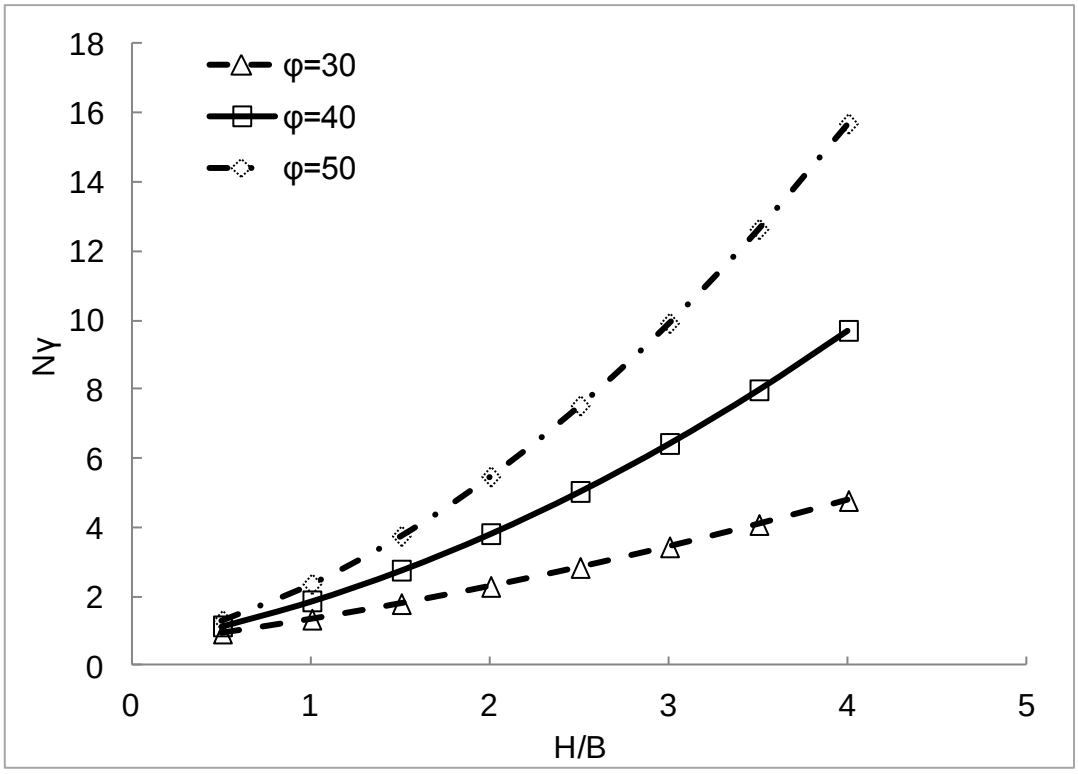

Figure 38- - Breakout factor vs. H/B Meyerhof (1973)

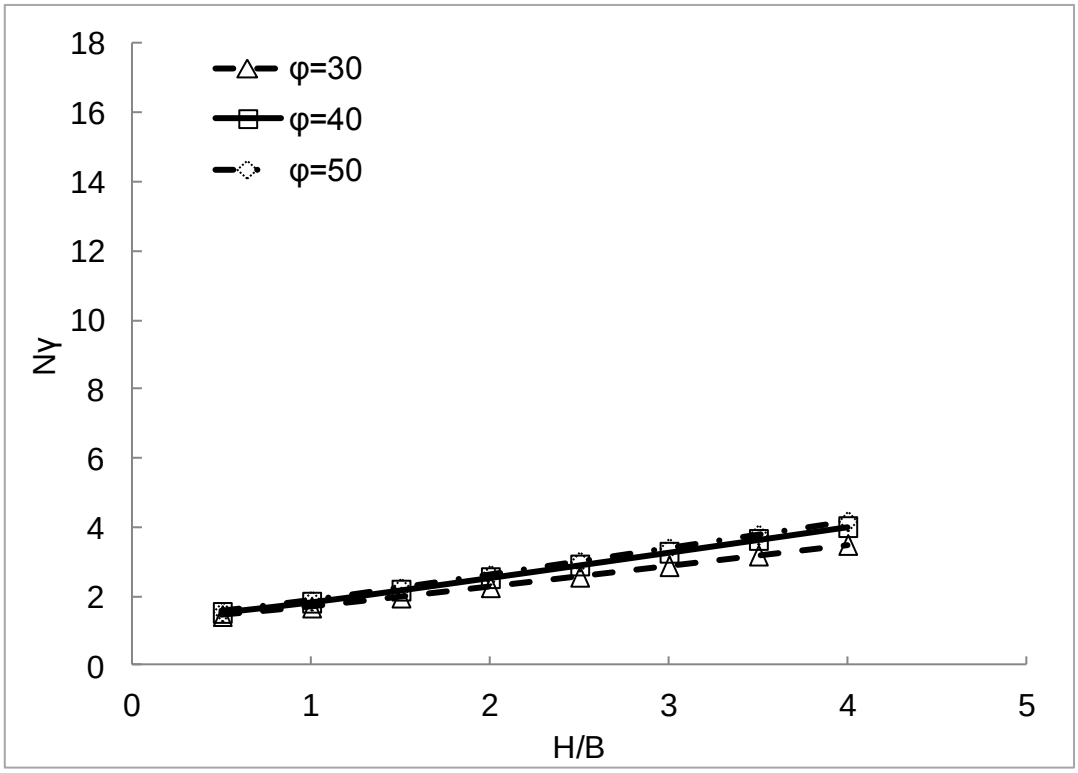

Figure 39- - Breakout factor vs. H/B Hanna et al. (1988)

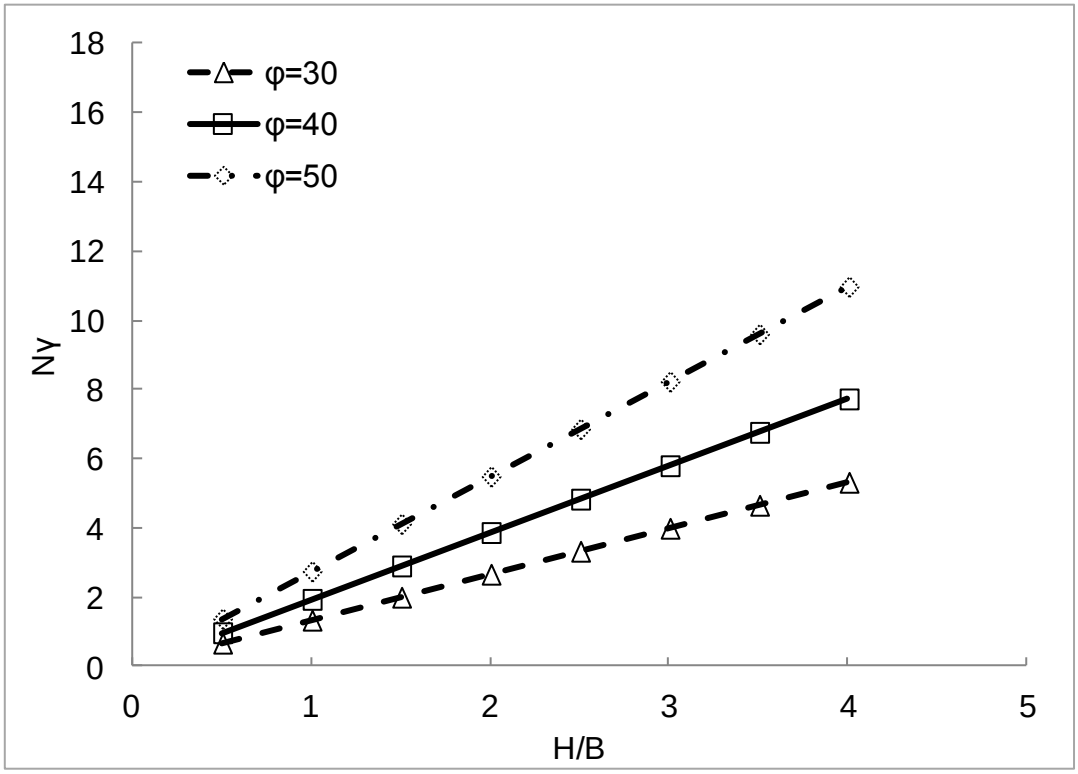

Figure 40- - Breakout factor vs. H/B Goel et al. (2006)

4.2 Evaluation of models

In this section the different theoretical models are compared with the pullout test results described in Chapter 3. The comparison is made using the dimensionless breakout factor.

4.2.1 Drag embedment anchors

The theoretical model used to predict the capacity of a drag embedment anchor for this study was developed by Neubecker and Randolph (1996). As described before, due to the high uncertainty in the positioning of the anchor, drag behavior, and the complexity of the anchor itself, the model contains a lot of variables (see Figures 10, 11, and 12). Neubecker and Randolph give recommendations for specific values and for simplification reasons these values are used in this study as well (i.e. failure wedge angle $\lambda = 60°$). To compare analytical values to experimental tests, the same soil specific properties were used as measured in the experimental tests. These include unit weight, friction angle, and dilatancy angle and are shown in Table 14.

The analytically obtained values of breakout factor are plotted against the experimentally observed values for different H/B ratios in Figure 41. The analytical values are in good agreement with the experimental values. This is also shown in Figure 42 where the bias of the analytical and experimentally obtained breakout factors is plotted. The bias is defined as the analytical values divided by the experimental values. The straight line represents perfect agreement of experimental

and analytical values. The results of the analytical values, experimentally values, and the bias are summarized in Table 15.

Table 15- Summary of Neubecker & Randolph (1996)

Test No.	H/B	Pullout force, measured N	Pullout force, predicted N	Nγ, measured	Nγ, predicted	Bias
10	1	272	366	5.17	6.97	1.35
11	1.5	945	939	11.99	11.92	0.99

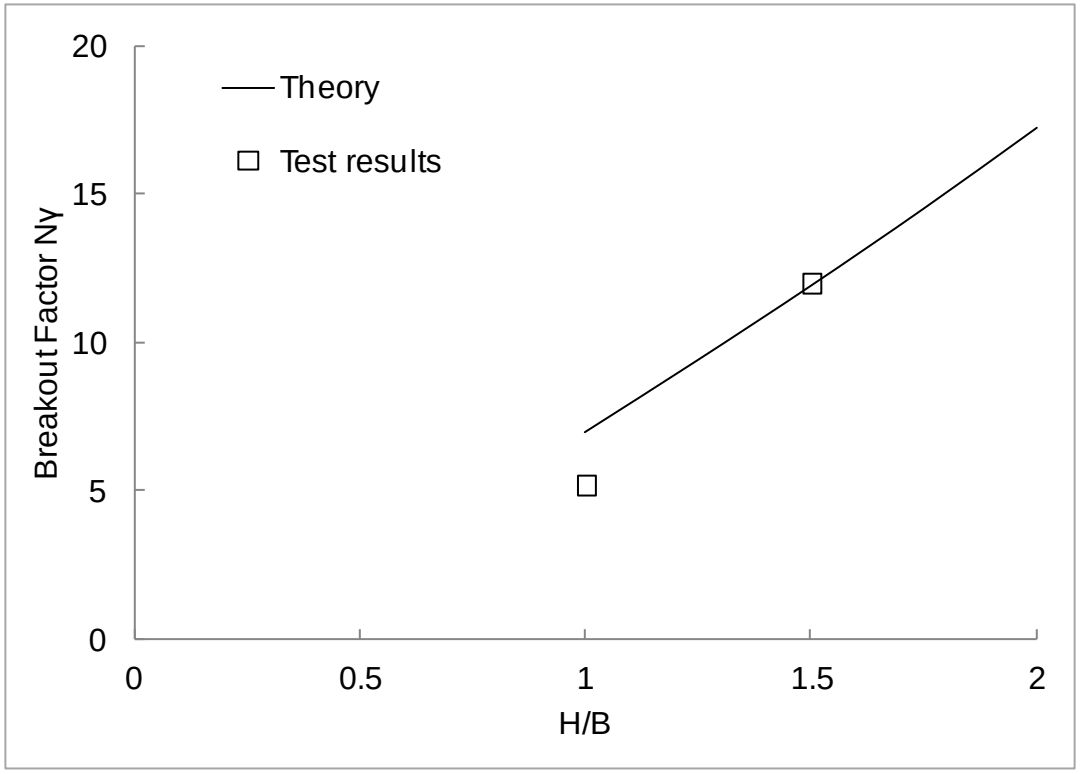

Figure 41- Breakout Factor vs. H/B Neubecker & Randolph (1996)

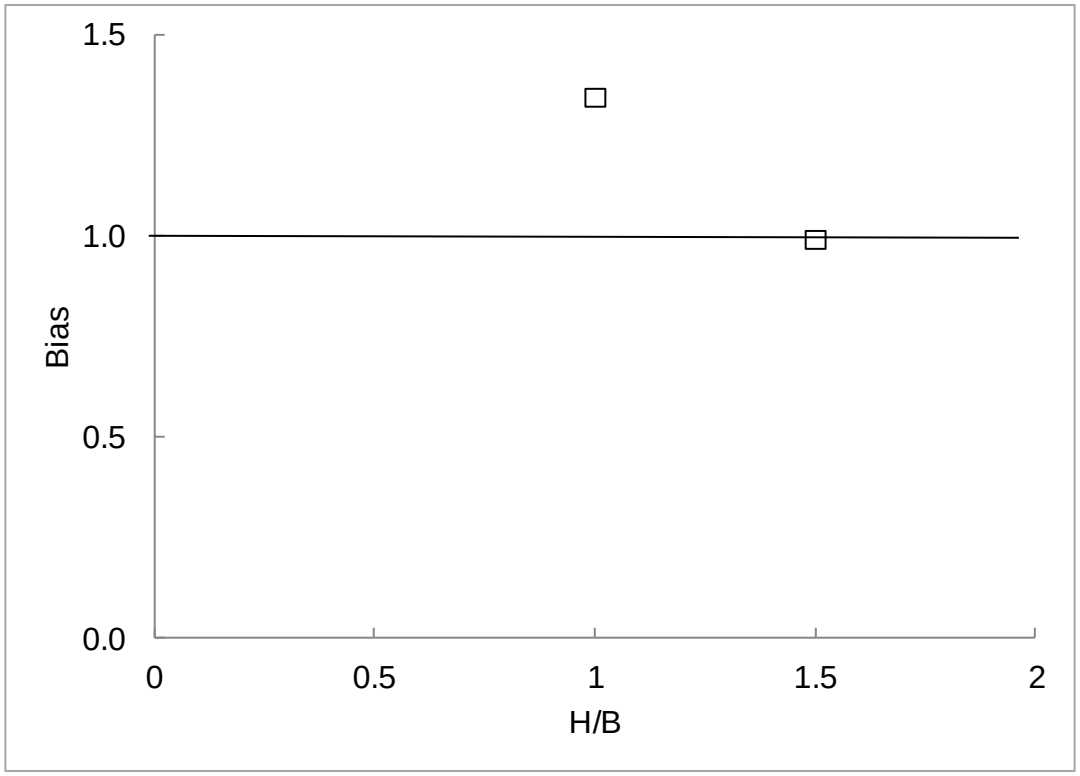

Figure 42- Bias vs. H/B Neubecker & Randolph (1996)

The tests were limited to a ratio of embedment depth over fluke width of 1.5. This ratio is recognized as the maximum penetration depth in practice for sandy soil conditions and drag anchors. Due to the high uncertainties described before and the lack of test results, the applicability of the model as a design standard for drag embedment anchors remains uncertain.

4.2.2 Vertically loaded plate anchors

In this section the results of the vertical pullout test results are compared to the known models for vertically loaded plate anchors. The results of each model and the corresponding plots will be presented first, followed by a discussion for each model. The models are individually evaluated and the model representing the experimental results most accurately is identified.

Meyerhof and Adams (1968)

The limit equilibrium approach developed by Meyerhof and Adams (1968) has been compared to the experimental results and shows an over-prediction on average of capacity of 144% with a coefficient of variation of 0.24. Figure 43 shows the experimental test results plotted against the proposed theory and Figure 44 the calculated bias. A summary of theoretical predictions and experimental results is given in Table 16.

Table 16- Summary of Meyerhof & Adams (1968)

Test No.	H/B	Pullout force, measured N	Pullout force, predicted N	Nγ, measured	Nγ, predicted	Bias
1	1	91	199	1.72	3.75	2.18
3	1	98	179	1.88	3.42	1.82
5	1	727	1458	1.73	3.47	2.01
2	2	258	895	2.45	8.50	3.47
4	3	708	1923	4.52	12.26	2.71

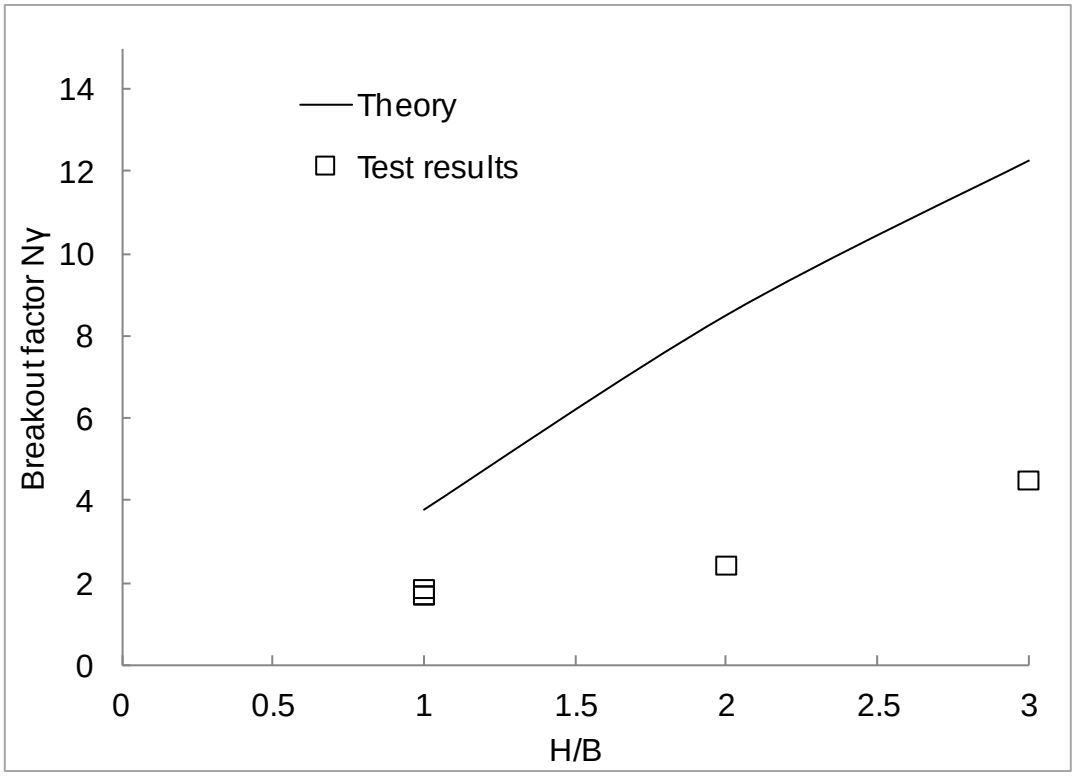

Figure 43- Breakout Factor vs. H/B Meyerhof & Adams (1968)

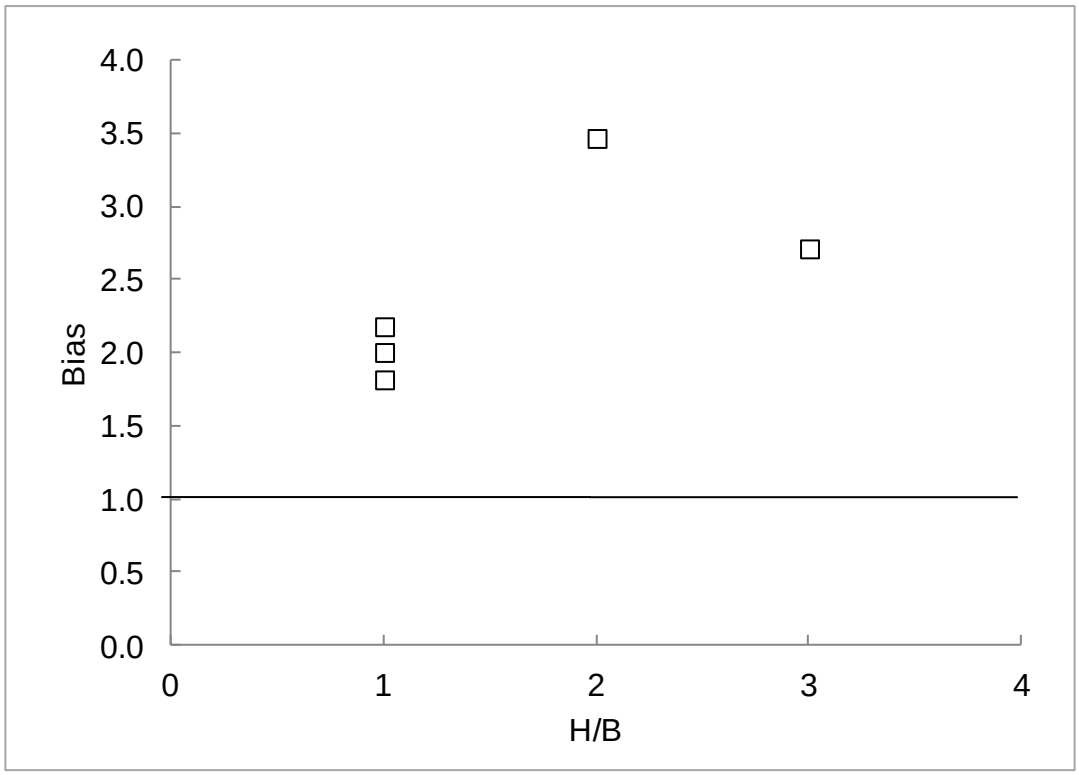

Figure 44- Bias vs. H/B Meyerhof & Adams (1968)

Murray and Geddes (1987)

The limit analysis method presented by Murray and Geddes (1987) is an upper bound solution. It over-predicts breakout factor on average by 100% with a coefficient of variation of 0.23. Figure 45 shows the experimental test results plotted against the proposed theory and Figure 46 the calculated bias. A summary of theoretical predictions and experimental results is given in Table 17.

Table 17- Summary of Murray & Geddes (1987)

Test No.	H/B	Pullout force, measured N	Pullout force, predicted N	Nγ, measured	Nγ, predicted	Bias
1	1	91	156	1.72	2.94	1.71
3	1	98	144	1.88	2.77	1.47
5	1	727	1173	1.73	2.79	1.61
2	2	258	734	2.45	6.97	2.84
4	3	708	1761	4.52	11.23	2.49

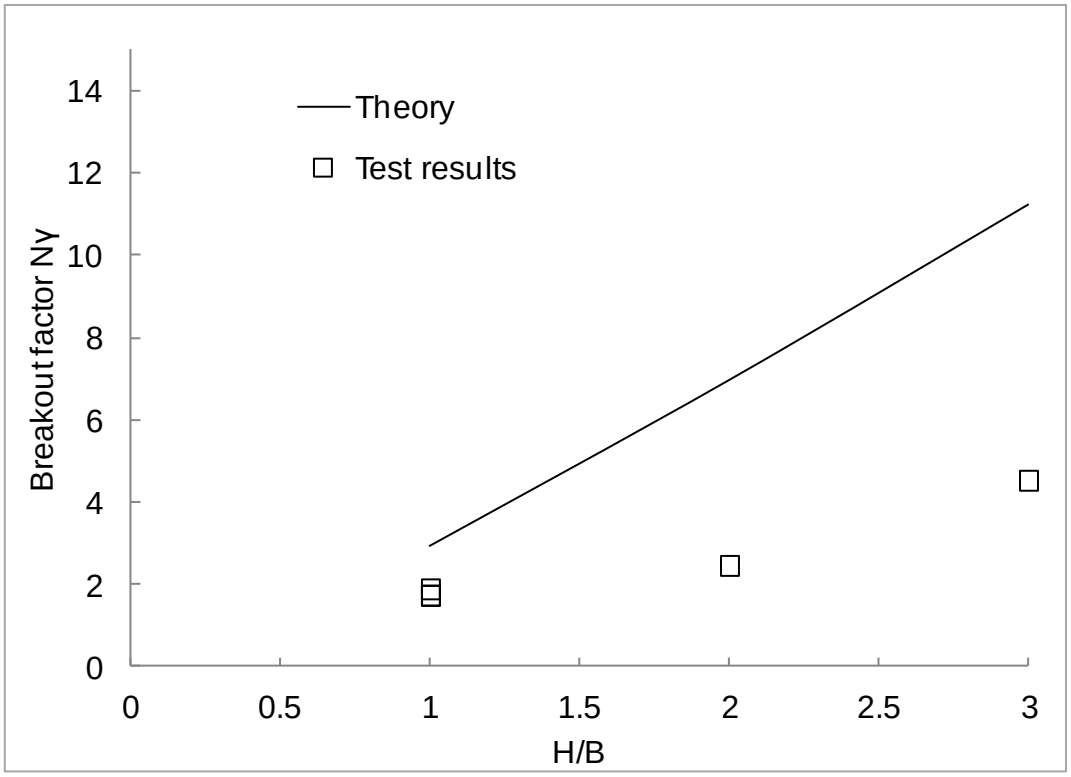

Figure 45- Breakout Factor vs. H/B Murray & Geddes (1987)

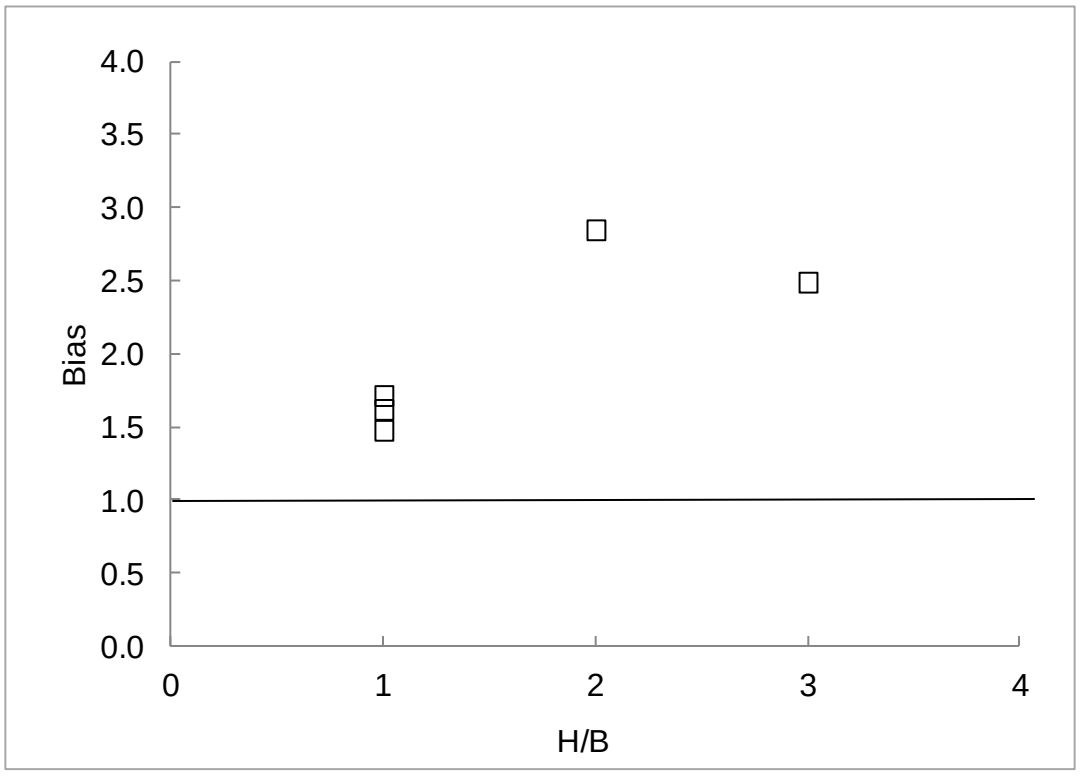

Figure 46- Bias vs. H/B Murray & Geddes (1987)

Sarac (1989)

The limit equilibrium solution by Sarac (1989) over-predicts capacity by 83% on average with a coefficient of variation of 0.2. Figure 47 shows the experimental test results plotted against the proposed theory and Figure 48 the calculated bias. A summary of theoretical predictions and experimental results is given in Table 18.

Table 18- Summary of Sarac (1989)

Test No.	H/B	Pullout force, measured N	Pullout force, predicted N	Nγ, measured	Nγ, predicted	Bias
1	1	91	151	1.72	2.85	1.66
3	1	98	139	1.88	2.68	1.43
5	1	727	1139	1.73	2.71	1.57
2	2	258	634	2.45	6.02	2.46
4	3	708	1452	4.52	9.26	2.05

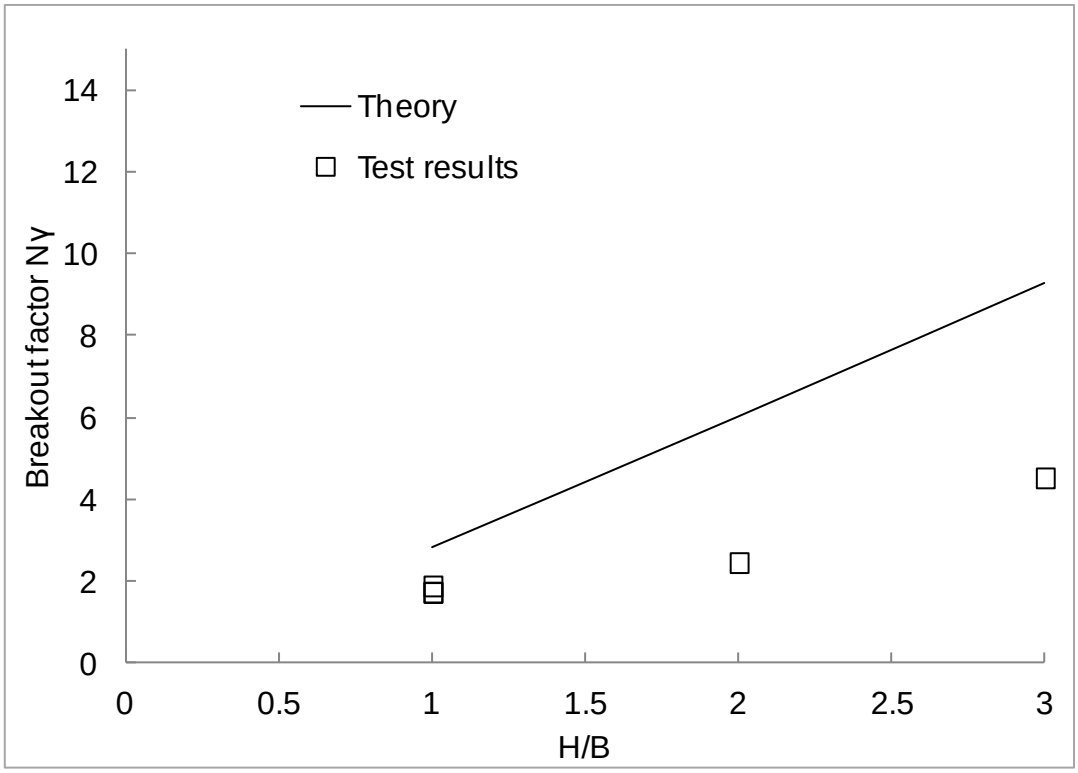

Figure 47- Breakout Factor vs. H/B Sarac (1989)

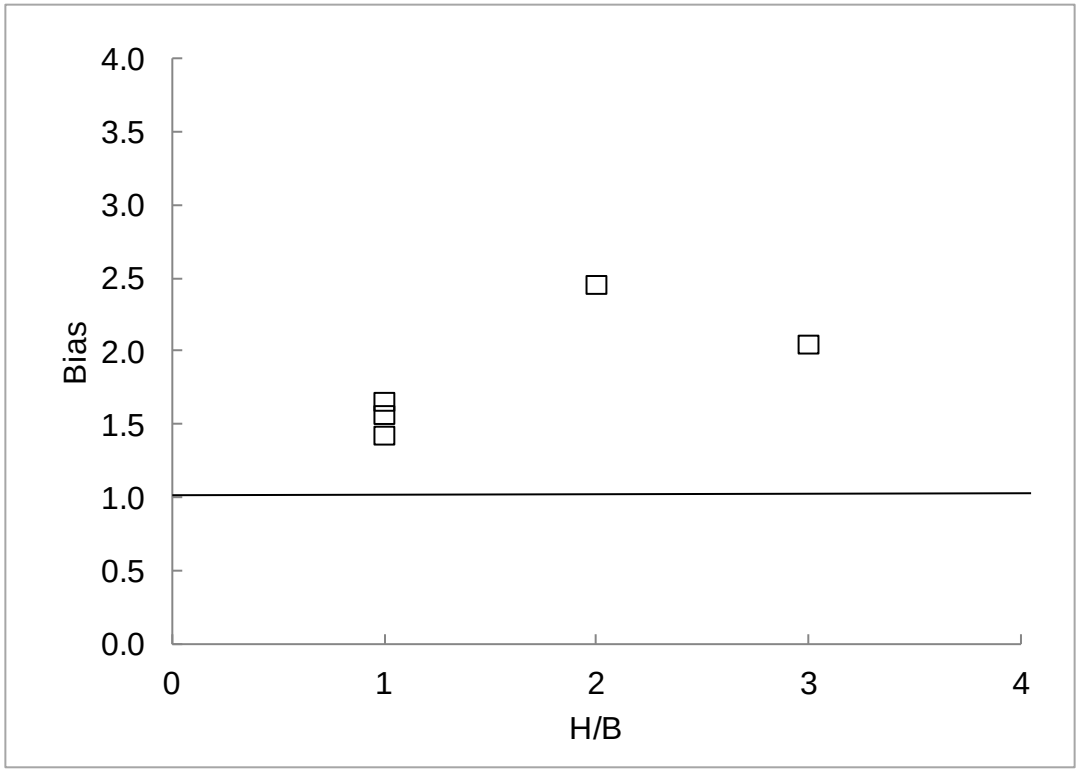

Figure 48- Bias vs. H/B Sarac (1989)

Merifield et al. (2006)

The solution presented by Merifield et al. (2006) uses a limit analysis approach to predict the capacity and a lower bound solution is developed by the authors. The model showed to over-predict capacity by 155% on average with a coefficient of variation of 0.14. Figure 49 shows the experimental test results plotted against the proposed theory and Figure 50 the calculated bias. A summary of theoretical predictions and experimental results is given in Table 19.

Table 19- Summary of Merifield et al. (2006)

Test No.	H/B	Pullout force, measured N	Pullout force, predicted N	Nγ, measured	Nγ, predicted	Bias
1	1	91	220	1.72	4.15	2.41
3	1	98	207	1.88	3.97	2.11
5	1	727	1647	1.73	3.92	2.27
2	2	258	774	2.45	7.34	3.00
4	3	708	2101	4.52	13.40	2.96

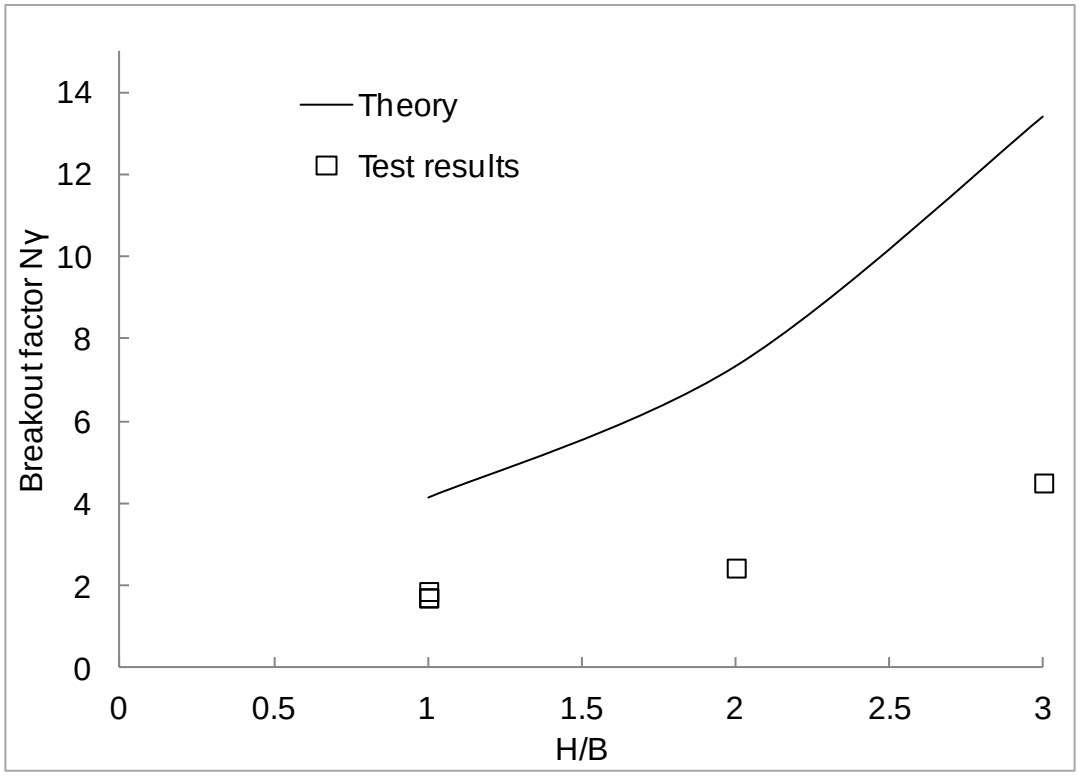

Figure 49- Breakout Factor vs. H/B Merifield et al. (2006)

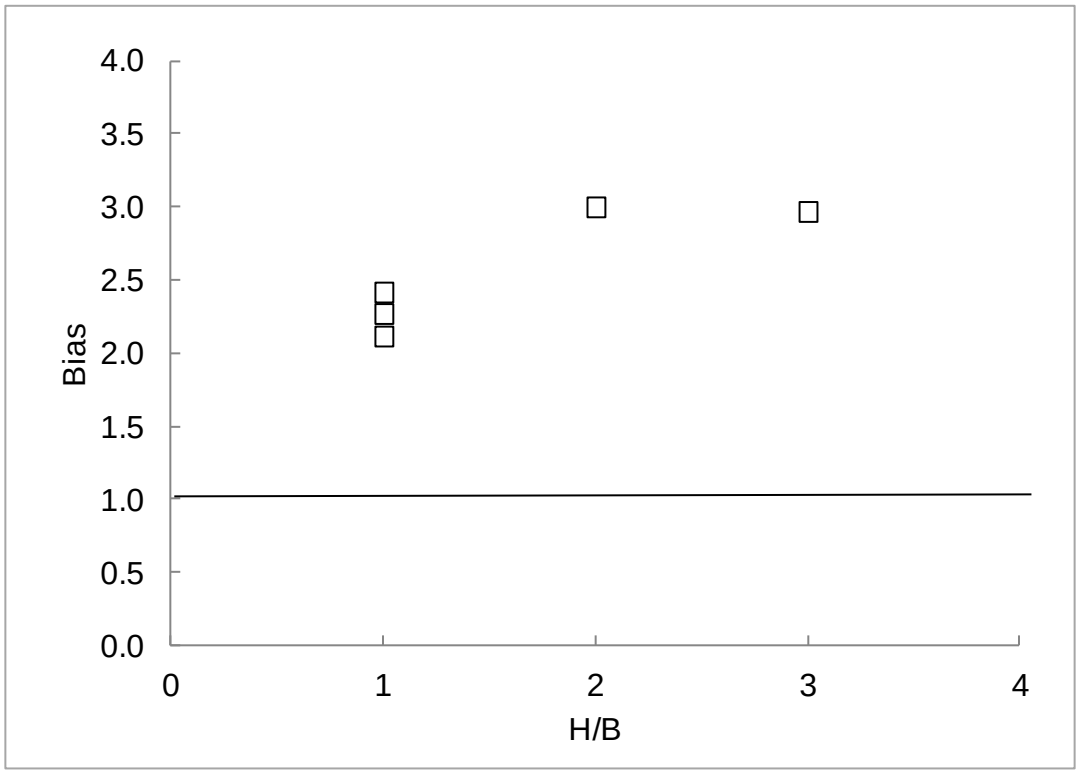

Figure 50- Merifield et al. (2006)

Discussion

As mentioned in Chapter 2.3.2 several assumptions have been made by the authors to define failure and predict capacities.

Meyerhof and Adams assume the average angle of the failure surface to be ϕ'/3 with the vertical. Using the peak friction angle of the experimental tests; this results in inclination angles ~15°. The lateral earth pressure coefficient is assumed to be between 1 and 2. This might over-estimate the stresses and the use of K_0 conditions might be more appropriate.

In the model presented by Sarac, a log spiral failure surface is assumed that meets the ground surface at an angle of 45-ϕ'/2. Using the peak friction angle of the experimental tests, this results in inclination angles ~20°. The earth pressures used are only described briefly and their effect on capacity remains unclear.

The limit analysis methods used in this study utilize the associated flow rule where the dilatancy angle is assumed to be equal to the friction angle and to the inclination angle of the failure wedge (θ= ϕ' =ψ). As a result the assumed failure wedges are oversized and the corresponding models over-predict capacities. The over-prediction of Murray and Geddes solution is consistent with their theory, as the limit analysis gives an upper bound solution and should therefore over-predict. Merifield et al. (2006) presented a lower bound solution and ought to under-predict the capacity. The results indicate that this is not the case and the solution may not be lower bound as it over-predicts breakout factors for all embedment depths.

The described models over-predicted the measured capacity on average by 120%. For this reason a new model was derived based off a model presented by White et al. (2008) for strip anchors and circular pipes.

White et al. (2008)

White et al. (2008) present a limit equilibrium solution for the vertical pullout resistance of both pipes and strip plate anchors in sand. The method is based on observations of model tests performed by Cheuk et al. (2007). The failure plane is determined to be inclined at the dilatancy angle ψ and is illustrated in Figure 51. The authors state that the consideration of the dilatancy angle as the inclination angle of the failure plane results in more realistic capacity predictions.

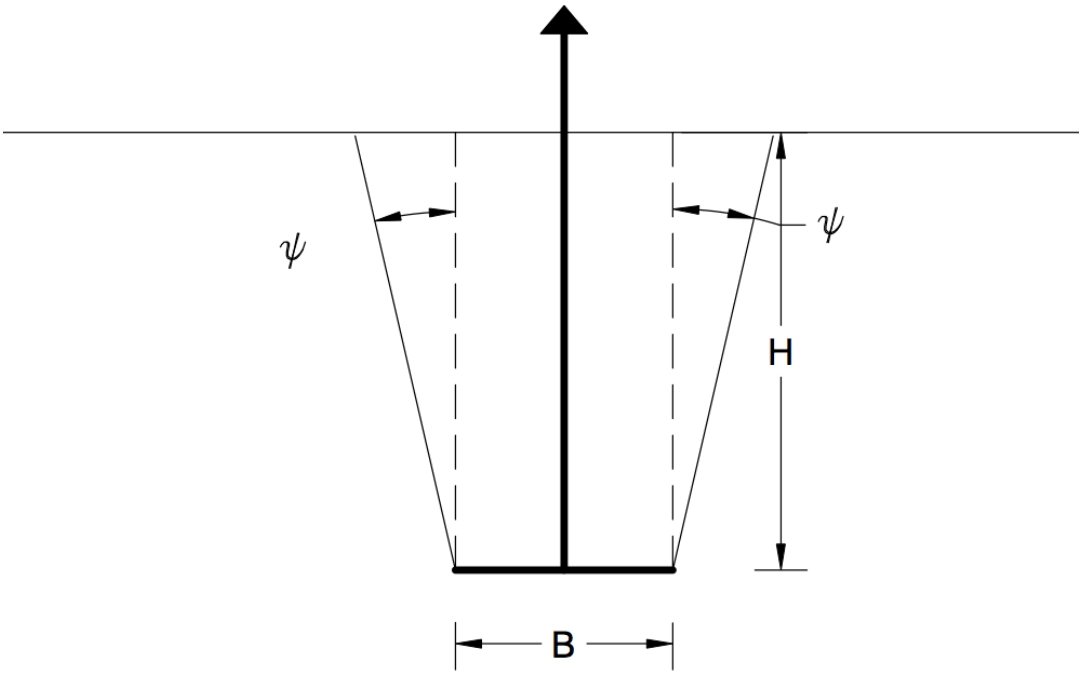

Figure 51- Assumed failure surface (adapted from: White et al., 2008)

Using this model as the starting point, a new model was derived for square plate anchors in sand. A complete derivation of this approach is presented in Appendix A and is summarized below.

The breakout capacity consists of the weight of the soil above the anchor plus the shear resistance along the surface. The soil wedge is assumed to be shaped like a truncated pyramid and can be calculated with Equation (16):

$$W_{Soil} = \frac{1}{3} * \gamma' * H * \left\{ \left(B + 2H \tan\psi \right)^2 + 2B^2 + 2HB \tan\psi \right\} \qquad (16)$$

where γ' is the effective unit weight, H is the embedment depth, B is the plate width and ψ is the dilatancy angle.

It is assumed that the normal stress on the failure planes is equal to the in-situ value obtained from K_0 conditions. Therefore, throughout deformation the normal stress on the failure plane does not change and the peak shear stress on the slip surface can be calculated. Through integration along the slip surface the shear resistance can be calculated using:

$$S_\gamma = 2\gamma' H^2 \tan\phi * \left\{ \left(\frac{1 + K_0}{2} \right) - \left(\frac{\left(1 - K_0\right)\cos 2\psi}{2} \right) \right\} * \left(B + \frac{2}{3} H \tan\psi \right) \qquad (17)$$

The total pullout force is the sum of the shear resistance and the weight of the soil and can be written as:

$$Q_u = \frac{1}{3} * \gamma' * H * \left\{ (B + 2H\tan\psi)^2 + 2B^2 + 2HB\tan\psi \right\}$$
$$+ 2\gamma' H^2 \tan\phi * \left\{ \left(\frac{1+K_0}{2} \right) - \left(\frac{(1-K_0)\cos 2\psi}{2} \right) \right\} * \left(B + \frac{2}{3} H \tan\psi \right) \quad (18)$$

For comparison reasons and clarity, Equation (18) is simplified and brought into the form of the dimensionless breakout factor N_γ.

$$N_\gamma = \frac{Q_u}{\gamma' H B^2} \quad (19)$$

$$N_\gamma = 1 + \frac{H}{B} F_1 + \left(\frac{H}{B} \right)^2 F_2 \quad (20)$$

$$F_1 = 2\left(\tan\psi + (\tan\phi - \tan\psi) c_1 \right) \quad (21)$$

$$F_2 = \frac{4}{3}\left(\tan^2\psi + \tan\psi (\tan\phi - \tan\psi) c_1 \right) \quad (22)$$

$$c_1 = \frac{(1+K_0)}{2} - \frac{(1-K_0)\cos 2\psi}{2} \quad (23)$$

where γ' is the buoyant unit weight, H is the embedment depth, B is the plate width, ψ is the dilatancy angle, ϕ is the friction angle, Q_u is the pullout capacity, and F1 and F2 are uplift coefficients, K_0 is the coefficient of lateral earth pressure at-rest.

The re-derived solution over-predicts capacity by 27% on average with a coefficient of variation of 0.14. This is an excellent agreement of theoretical values and experimental results. For this reason this method is chosen as the best fit for the experimental values. Figure 52 shows the experimental test results plotted against

the proposed theory and Figure 53 the calculated bias. A summary of theoretical predictions and experimental results is given in Table 20.

Table 20- Summary of White et al. (2008)

Test No.	H/B	Pullout force, measured N	Pullout force, predicted N	Nγ, measured	Nγ, predicted	Bias
1	1	91	115	1.72	2.18	1.27
3	1	98	108	1.88	2.07	1.10
5	1	727	878	1.73	2.09	1.21
2	2	258	413	2.45	3.92	1.60
4	3	708	830	4.52	5.29	1.17

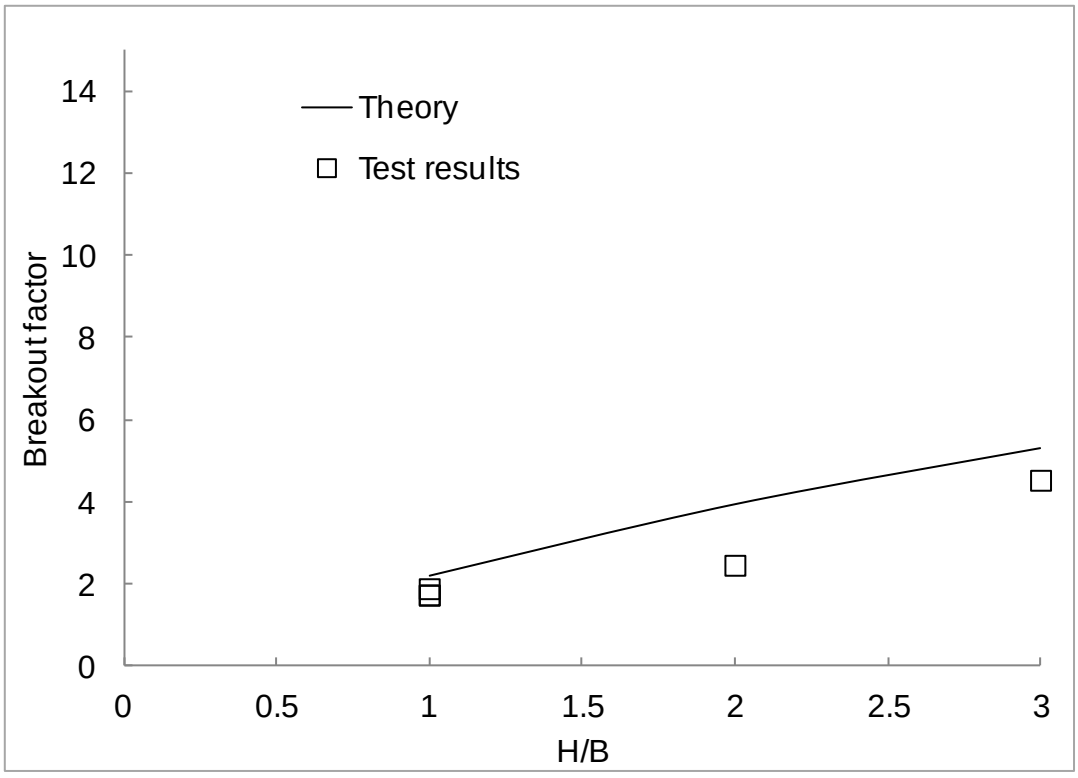

Figure 52- Breakout Factor vs. H/B White et al. (2008)

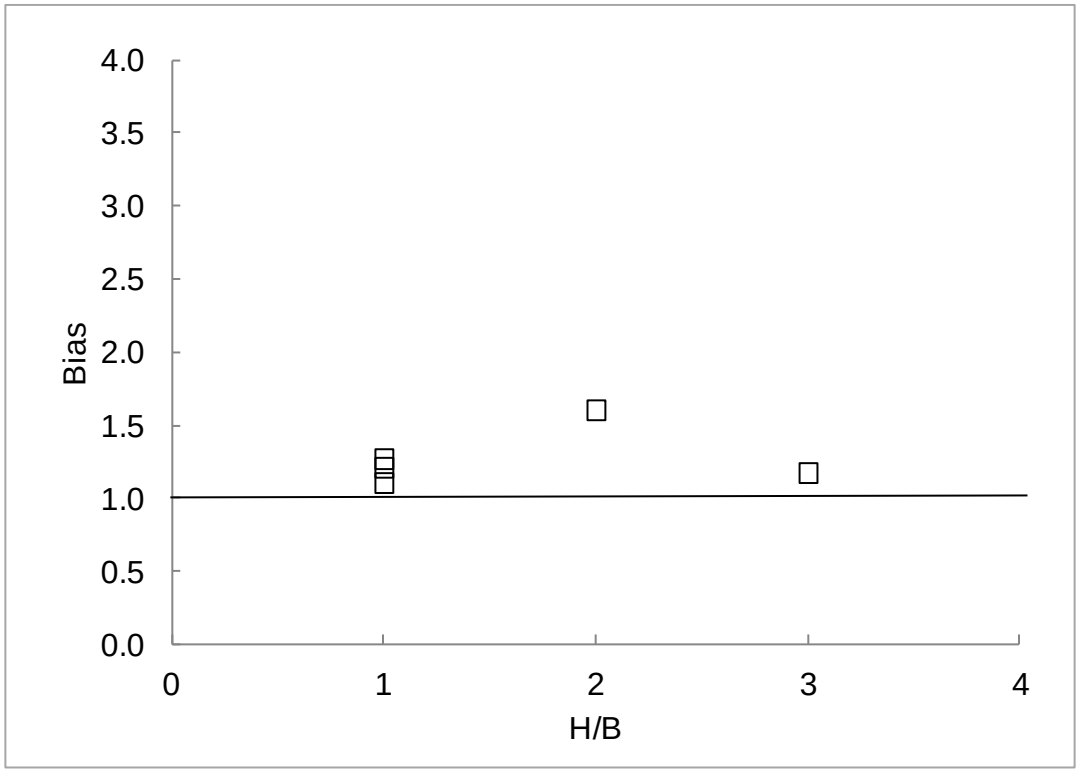

Figure 53- Bias vs. H/B White et al. (2008)

4.2.3 Inclined plate anchors

Three models for predicting the breakout capacity for inclined plate anchors were compared to the experimental results from this study: Meyerhof (1973), Hanna et al. (1988), and Goel et al. (2006). The performance of each model is described separately followed by a discussion of the results.

Meyerhof (1973)

The limit equilibrium method presented by Meyerhof (1973) over-predicts capacity. On average, the breakout capacities were 36% higher than the experimental results with a coefficient of variation of 0.2. Figure 54 shows the experimental test results plotted against the proposed theory and Figure 55 the calculated bias. A summary of theoretical predictions and experimental results is given in Table 21.

Table 21- Summary of Meyerhof (1973)

Test No.	H/B	Pullout force, measured N	Pullout force, predicted N	Nγ, measured	Nγ, predicted	Bias
1	1	103	108	1.95	2.05	1.05
2	1	612	859	1.45	2.03	1.40
3	2	366	443	3.49	4.23	1.21
4	3	627	1126	3.99	7.17	1.80

Figure 54- Breakout Factor vs. H/B Meyerhof (1973)

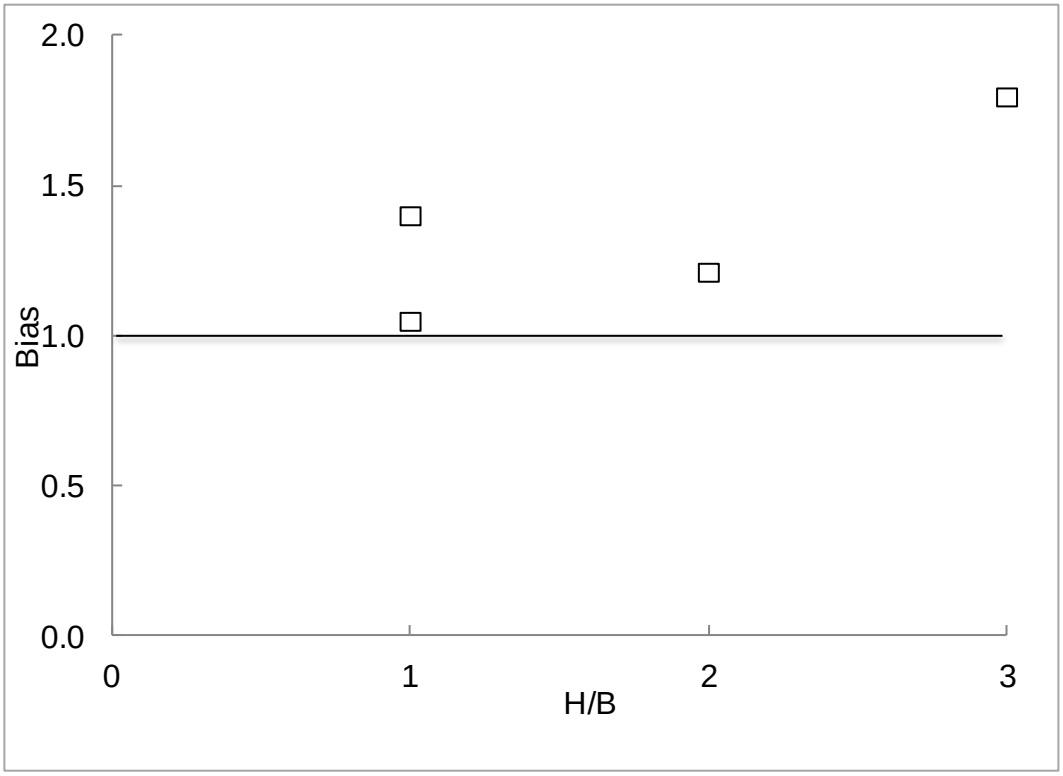

Figure 55- Bias vs. H/B Meyerhof (1973)

Hanna et al. (1988)

In contrast to the other limit equilibrium solutions for inclined plate anchors, the model developed by Hanna et al. (1999) under-predicts capacity. The predictions were 5% lower than the experimental results on average with a coefficient of variation of 0.2 for this study. Figure 56 shows the experimental test results plotted against the proposed theory and Figure 57 the calculated bias. A summary of theoretical predictions and experimental results is given in Table 22.

Table 22- Summary of Hanna et al. (1988)

Test No.	H/B	Pullout force, measured N	Pullout force, predicted N	Nγ, measured	Nγ, predicted	Bias
1	1	103	99	1.95	1.88	0.96
2	1	612	612	1.45	1.83	1.26
3	2	366	273	3.49	2.60	0.75
4	3	627	528	3.99	3.36	0.84

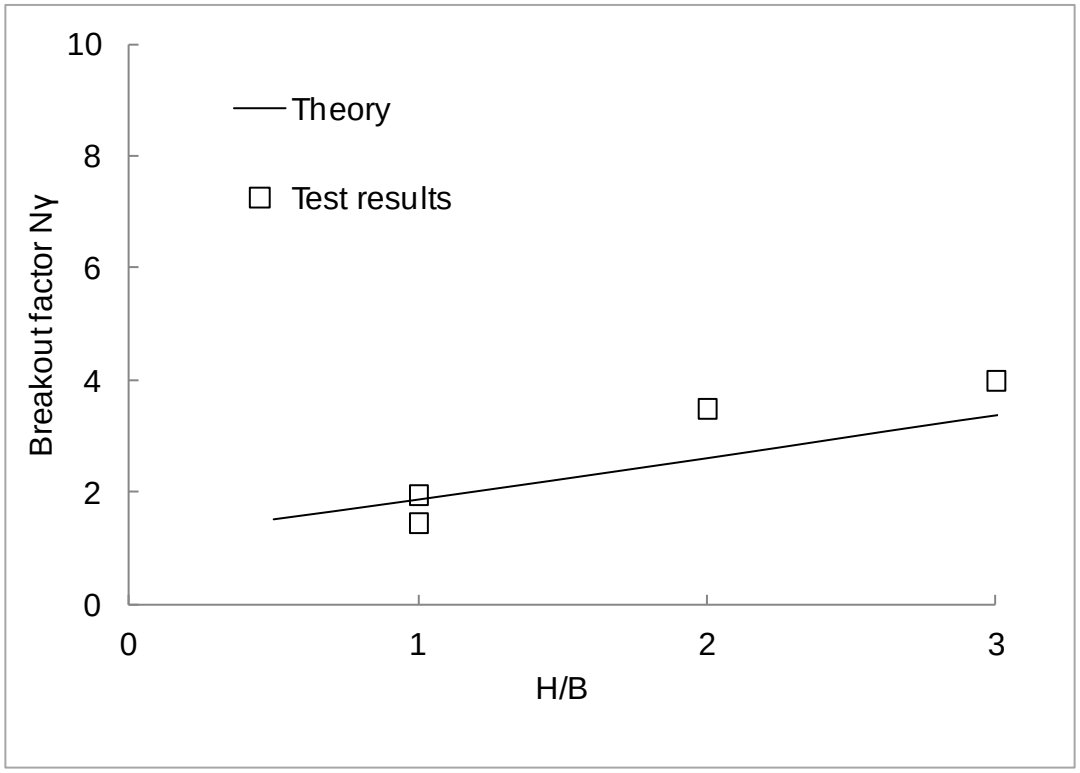

Figure 56- Breakout Factor vs. H/B Hanna et al. (1988)

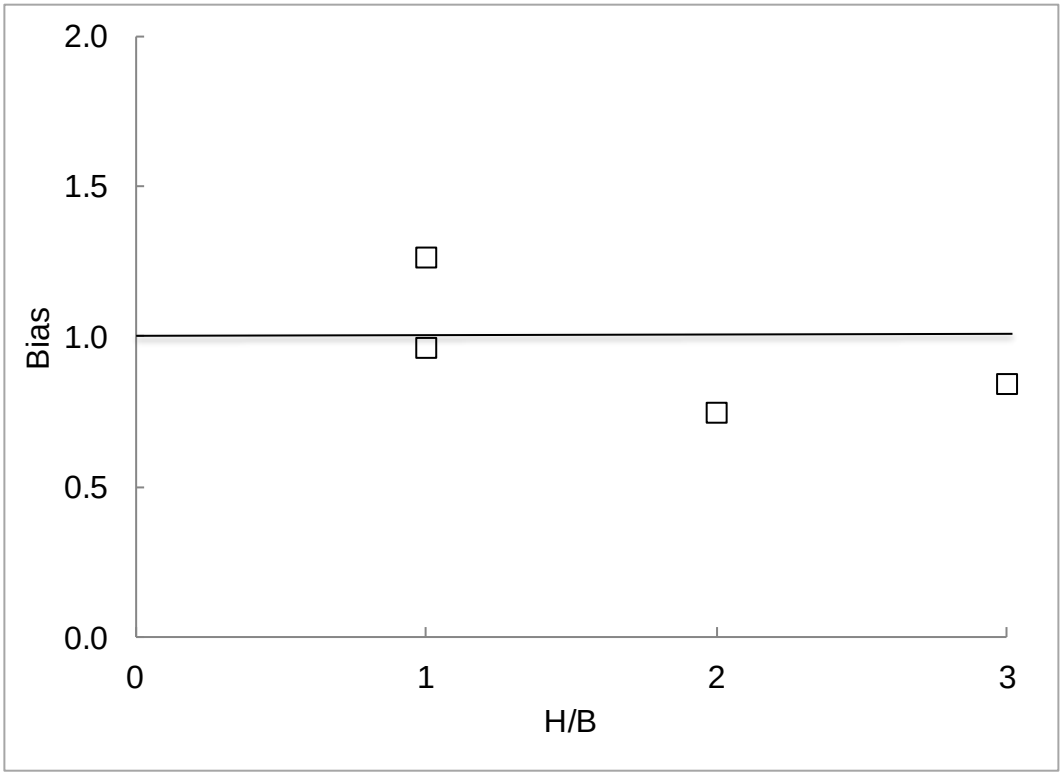

Figure 57- Bias vs. H/B Hanna et al. (1988)

Goel et al. (2006)

Similarly to the solutions of Meyerhof, the limit equilibrium solution presented by Goel et al. (2006) over-predicts capacity by 33% on average with a coefficient of variation of 0.14. Figure 58 shows the experimental test results plotted against the proposed theory and Figure 59 the calculated bias. A summary of theoretical predictions and experimental results is given in Table 23.

Table 23- Summary of Goel et al. (2006)

Test No.	H/B	Pullout force, measured N	Pullout force, predicted N	Nγ, measured	Nγ, predicted	Bias
1	1	103	113	1.95	2.25	1.10
2	1	612	899	1.45	2.13	1.47
3	2	366	437	3.49	4.17	1.19
4	3	627	972	3.99	6.19	1.55

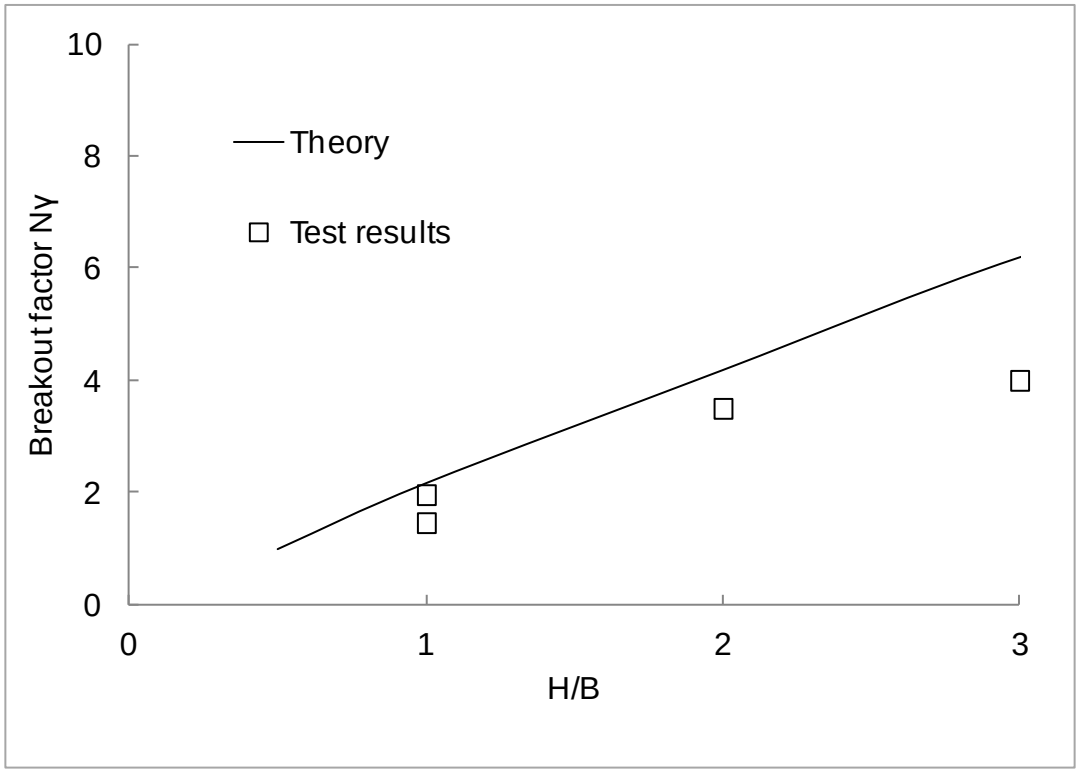

Figure 58- Breakout Factor vs. H/B Goel et al. (2006)

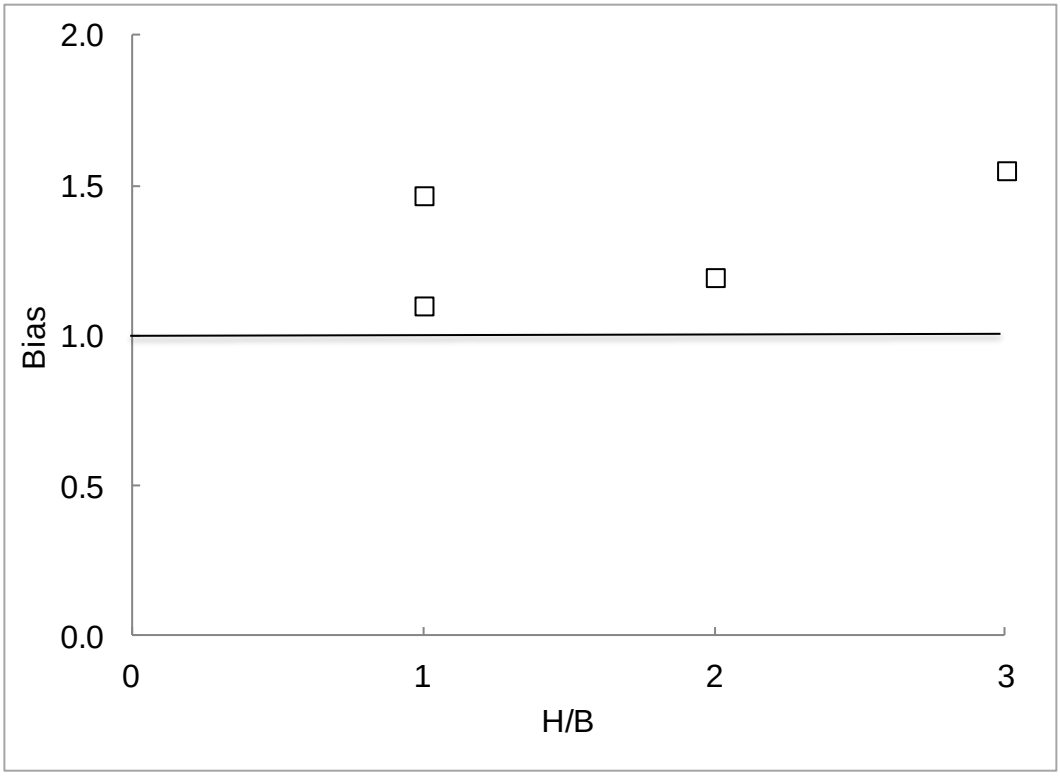

Figure 59- Bias vs. H/B Goel et al. (2006)

Discussion

All three presented models were, in the first place, developed to predict breakout factors for strip anchors. The model presented by Meyerhof can, according to the author, be used for square anchor plates as well. For this reason a shape factor is introduced as described in Chapter 2.3.3. The other two models do not include shape factors to account for different shapes such as square plates. Therefore the results obtained from Hanna et al. (1988) and Goel et al. (2006) must be interpreted with caution. The reason why they are still included in this study is that the authors compare their models themselves to square anchors in their publications.

Meyerhof (1973) utilizes an uplift coefficient K_b, depending on the friction angle of the soil and the inclination angle of the anchor. This coefficient is determined from earth pressure coefficients for inclined walls and increases with increasing friction angle and inclination of the anchor. Meyerhof provides the coefficient in from of a chart for shallow and deep strip and square anchors, respectively. This, in combination with the shape factor, accounts for the inclination of the anchor and the square shape.

The lack of theoretical solutions for square plate anchors in sand complicated the interpretation of the obtained analytical results. A broader range of different methods with various assumptions regarding the failure surfaces and earth pressures would allow a more throughout analysis of the problem and simplify the identification of the most accurate theory. Nevertheless the predictions calculated

with Meyerhof's (1973) approach seem to match the experimental results and thus it appears that the assumptions capture the behavior of inclined anchors. The models derived for strip anchors were neglected even though they showed a smaller bias developed for square anchors in the first place and therefore assume different failure mechanisms. For this reason this model has been chosen as the best fit for inclined anchors in sand.

Table 24 provides an overview of every analyzed model and each calculated bias and coefficient of variation.

Table 24- Summary of all models

Model	α °	Bias	COV
Neubecker & Randolph (1996)	DEA	1.17	0.15
Meyerhof & Adams (1968)	0	2.44	0.24
Murray & Geddes (1987)	0	2.02	0.27
Sarac (1989)	0	1.83	0.20
Merifield et al. (2006)	0	2.55	0.14
This study	0	1.27	0.14
Meyerhof (1973)	40	1.36	0.20
Hanna et al. (1988)	40	0.95	0.20
Goel et al. (2006)	40	1.33	0.14

4.3 Design Analysis

This section is used to demonstrate that plate anchors theoretically can be used to secure offshore wind platforms. A study on the feasibility of floating platforms carried out by Musial et al. (2004) provides an estimation of the anchors loads from an offshore wind platform. For standardization reasons a 5-MW wind turbine developed at NREL was used (Jonkman et al., 2009). Two different floating concepts with different mooring systems are discussed in the analysis: (1) the NREL wind turbine with a tension leg platform and (2) a dutch developed tri-floater concept with a comparable power output. The NREL concept uses vertical tendons to connect the platform to six anchors in the seafloor. These anchors are designed to carry a vertical tension force of 4700 kN. For the dutch concept a system of six anchors in a catenary mooring system is designed. These anchor forces are significantly smaller than the loads in the vertical mooring system as these anchors are only used to restrain platform movement and the heavy anchor chain is taking considerable loads as well. The mooring lines are pre-tensioned at 300 kN for the dutch study (Bulder et al., December 2002).

Sclavounos et al. (2010) presented a study on motion resistant floating wind turbines supporting 3-5 MW offshore wind turbines. Two different concepts are presented in their study: (1) is similar to the NREL concept as it also uses a tension leg platform with a vertical mooring system and (2) a taut leg buoy concept using a semi-taut mooring system. The difference between buoyancy effects of the

platform and weight of the turbine and structure is equal to the uplift capacity of the anchors. To compare the results the 5-MW wind turbine is used to calculate the corresponding capacities. For the tension leg platform the cumulative capacity is equal to 20,000 kN and for the buoy the capacity is 25,000 kN. In both cases a mooring system with six anchors is considered. The floating structures and mooring systems are shown in Figure 60 with the TLB on the left and the TLP on the right hand side.

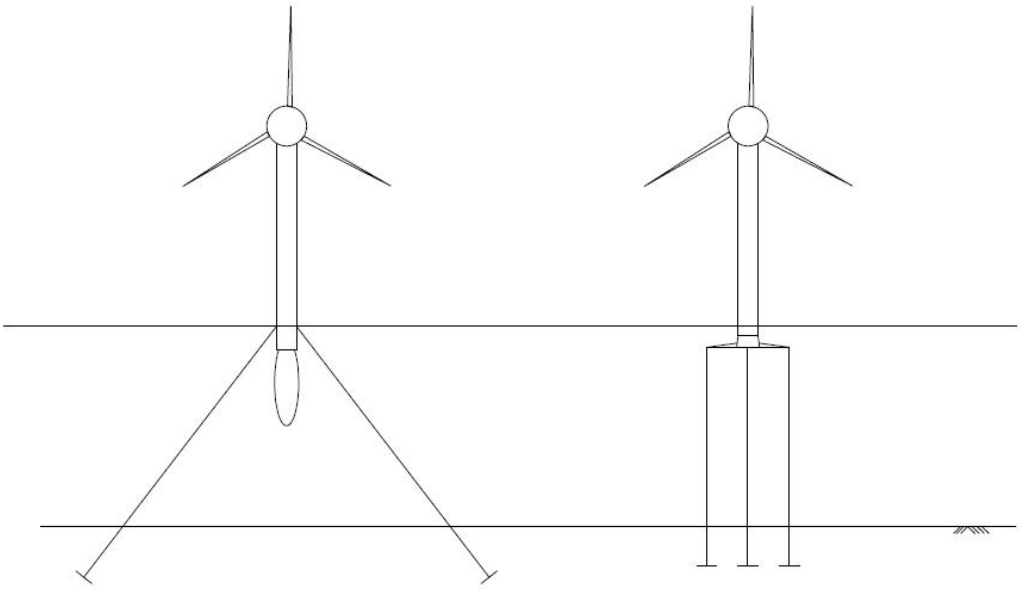

Figure 60- TLB and TLP used (adopted from Sclavounos et al. (2010))

These two studies can be seen as examples on the magnitude of the loads acting on floating offshore platforms. In general a load analysis needs to be carried out for each design project individually as many variables depend on the site (i.e. wind loads, wave heights, current loads) (Matha, 2009; Tong, 1998; Myhr et al., 2011).

The models that best fit the experimental results from this study are used to determine the minimum anchor dimensions for the loads for drag embedment anchors, vertically loaded anchors, and inclined anchors. For vertically loaded anchors it showed that the re-derived model of White et al. (2006) agreed best with the experimental data and for inclined anchors the model proposed by Meyerhof (1973) was used. The calculations are carried out using a loose and a dense sand (D_r= 30% and D_r= 70%). The soil parameters are obtained using the Rhode Island beach sand and Bolton's stress-dilatancy relationship to scale the sand to the desired conditions.

Tables 25 and 26 summarize the loads acting on the anchors in the vertical mooring system and anchor sizes designed to withstand these forces in loose and dense sands, respectively. Sclavounos et al. (2010) determined the forces to be about 3300 kN per anchor in a six anchor mooring system. Three different anchor configurations are presented to meet the required holding capacities. With decreasing plate areas, the embedment depth increase. A factor of safety of 2 has been incorporated in the calculations (Vryhof Anchors, 2010).

A similar calculation has been carried out for the inclined anchors used in a semi-taut mooring system. Sclavounos et al. (2010) estimated the forces to be 4200 kN per anchor, using a six anchor mooring system. Again, three different anchor dimensions are presented in Table 27 and 28 for each soil condition. The capacity of the inclined anchors is, as expected, generally higher than the capacity of the

vertically loaded anchors. The used factor of safety represents the common practice and is recommended by anchor manufacturers.

Table 25- Proposed anchor dimensions for the TLP in loose sand

Loads		Anchor				
Load (kN)	Load/Anchor (kN)	Plate Area (m^2)	Plate Width (m)	Embedment Depth (m)	H/B	Allowable Capacity (kN)
20000	3333	25	5.00	12.82	2.59	3333
20000	3333	15	3.87	14.41	3.72	3333
20000	3333	5	2.24	16.96	7.59	3333

Table 26- Proposed anchor dimensions for the TLP in dense sand

Loads		Anchor				
Load (kN)	Load/Anchor (kN)	Plate Area (m^2)	Plate Width (m)	Embedment Depth (m)	H/B	Allowable Capacity (kN)
20000	3333	25	5.00	11.24	2.25	3333
20000	3333	15	3.87	12.78	3.30	3333
20000	3333	5	2.24	15.28	6.83	3333

Table 27- Proposed anchor dimension for the TLB in loose sand

Loads		Anchor				
Load (kN)	Load/Anchor (kN)	Plate Area (m^2)	Plate Width (m)	Embedment Depth (m)	H/B	Allowable Capacity (kN)
25000	4167	25	5.00	11.23	2.25	8334
25000	4167	15	3.87	11.93	3.08	8334
25000	4167	5	2.24	13.03	5.83	8334

Table 28- Propsed anchor dimensions for the TLB in dense sand

Loads		Anchor				
Load (kN)	Load/Anchor (kN)	Plate Area (m^2)	Plate Width (m)	Embedment Depth (m)	H/B	Allowable Capacity (kN)
25000	4167	25	5.00	8.73	1.75	8334
25000	4167	15	3.87	9.29	2.40	8334
25000	4167	5	2.24	10.13	4.53	8334

Anchor manufacturer like Vryhof or Pelastar indicate that plate anchors with areas between 15 to 30 m^2 have already been used in embedment depth of 20 to 40 meters below the seabed in clay. The proposed anchor dimensions include larger plate areas ($25m^2$) with smaller embedment depths, medium size plate areas ($15m^2$), and small plate areas ($5m^2$) with large embedment depths. None of the proposed anchors exceed the already realized anchor dimensions or embedment depths and with reasonable fluke areas no H/B ratios larger than 7 are needed to mobilize pullout capacities satisfying the demands. Considering this, the use of plate anchors to secure floating offshore wind turbines is technically feasible. Optimization in the design process will require a cost-benefit analysis of the amount of used steel for the anchor and the installation costs (and feasibility) of the anchor for deeper embedment depths.

5 CONCLUSIONS

Summary

In this thesis different anchoring systems associated with floating offshore platforms for wind turbines have been examined. The need for renewable and clean energy resources is pushing the wind industry into deeper water further offshore where there are significant energy resources. This push into deeper water combined with differing soil conditions results in an unavoidable search for new anchoring solutions as the traditional methods become unpractical and inefficient. Moving farther away from the shore does not only result in greater water depths but also in more severe loading conditions such as wind, wave, and tidal forces. Fixed structures, like monopiles, become practically impossible under these new conditions and it seems as if floating platforms are inevitable.

Different theoretical models to predict holding capacities, based solely on soil parameters, have been published over the years for anchors that possibly can be used to stabilize the floating platforms. An accurate capacity prediction is a crucial aspect in designing offshore anchors with respect to the safety and serviceability of these floating structures. The first objective of this thesis was to analyze and evaluate the existing theoretical capacity prediction models for vertical and inclined plate anchors in sand. The second objective was to identify a best fit model for both

anchor types and use this model to assess the technical feasibility of these anchors to secure floating offshore wind turbines in deep water.

An extensive literature review was carried out which included the following topics: sample preparation at large scale, scaling issues in 1g model tests and different anchor shapes. A laboratory testing program involving 1g model pullout tests was performed. Bolton's stress dilatancy concept was used to design the experiment to obtain the same constitutive response in the test tank and prototype. The sand prepared in the test tanks was therefore prepared at lower relative densities than the corresponding prototype (approximately 22% compared with 30% in the prototype) to give it the same volume change characteristics (contractive vs. dilative) as the prototype despite the very different stress conditions.

For the preparation of the samples different pluviators were analyzed. A pluviating concept was chosen that allowed to place both the soil in layers and the anchors at the desired depths without disturbing the soil around or above it. Hand readings and a miniature cone penetrometer were used to ensure the samples were homogeneous. The readings of the miniature cone were correlated to relative densities and a soil profile was developed for each test. Six soil samples were prepared and three different anchor types were tested for a total of 11 tests. The test results were then compared and evaluated to theoretical prediction models.

Conclusions

The following conclusions can be made:

- It is possible to model prototype conditions in a lab when scaling issues are considered properly. The test tank needs to be prepared in a looser state with lower stress levels to achieve the same constitutive response and friction angle in the prototype and model.

- Neubecker and Randolph's (1996) model to predict capacity of a drag embedment anchor in sand compared promisingly with the laboratory model test results. However the development of models to predict the kinematics of these anchors in sand is still ongoing and it is not possible to predict the final embedment depth and orientation beforehand, yet. This, combined with various variables and assumptions incorporated in the model, makes the model highly uncertain and inapplicable for a safe anchor design.

- The presented models to predict the holding capacity of vertically loaded anchors entirely over-predict capacity even though different failure mechanisms are assumed. The upper bound theory of Murray and Geddes (1987) is expected to over-predict capacity, as it is the upper part of a capacity envelope. The second limit analysis method, presented by Merifield

et al. (2006), also over-predicts but was inconsistent with their theory of being a lower bound solution. The two examined limit equilibrium models by Meyerhof and Adams (1968) and Sarac (1989) also over-predict capacities, possibly by using earth pressure coefficients higher than the actual pressures.

- The re-derived model by White et al. (2008) for vertical uplift showed an excellent agreement between experimental and analytical values. It is also the only model that takes the dilatancy angle into consideration when predicting the holding capacity. As it is most precise, it is recommended to be used for vertically loaded anchors.

- For shallow square plate inclined anchors the only model available was a limit equilibrium method presented by Meyerhof (1973). It showed good agreement between the recorded and predicted values. The two other models assessed were developed for strip anchors and did not include a shape factor to account for a square form.

- It was shown that plate anchors generally can be used to secure the applied loads on a floating offshore platform in deep water just from a capacity point of view. The embedment depths needed to mobilize the desired holding capacities have already been realized in clay.

Recommendations for future research

To completely capture the behavior of plate anchors in sand tests more tests need to be carried out. Due to time restrains and technical limitations the testing for this study was limited to H/B ratios of 3. Usually a change in failure mechanism is expected to happen at an H/B ratio greater than 5 and therefore it should be aimed to fill this gap. Also, this study was conducted on very loose sands that represent the lower end of the soil spectrum. A test series on dense sand could provide valuable inside into the behavior of plate anchors in these conditions and finalize the laboratory studies of holding capacities.

Since the behavior of anchors in the process of installation is still researched, a model accounting for different anchor geometries would be useful as they might change. All models are derived for square, circular, rectangular or strip anchor geometries. As it is still unclear to the present day which geometry would be optimal for soil penetration, a model accounting for different anchors shapes would be needed.

Another key point is the kinematic behavior of a plate anchor during embedment. Different installation methods have already been used including jetting and driving but a promising new approach might be to use the self-weight of the anchor to free-fall penetrate the soil. Previous studies on ultimate embedment depth concentrated on clay-like soil conditions and the ultimate embedment depths in sands remain

unknown. An experimental database needs to be developed to verify the theoretical embedment depths required.

It might be an interesting concept to investigate the expended energy in conventional anchor design, manufacture, and installation and compare it to the energy needed for the new anchor concepts. The energy saving potential could be a decisive criterion for the future of offshore wind platforms.

APPENDIX A: Derivation of White et al. (2008)

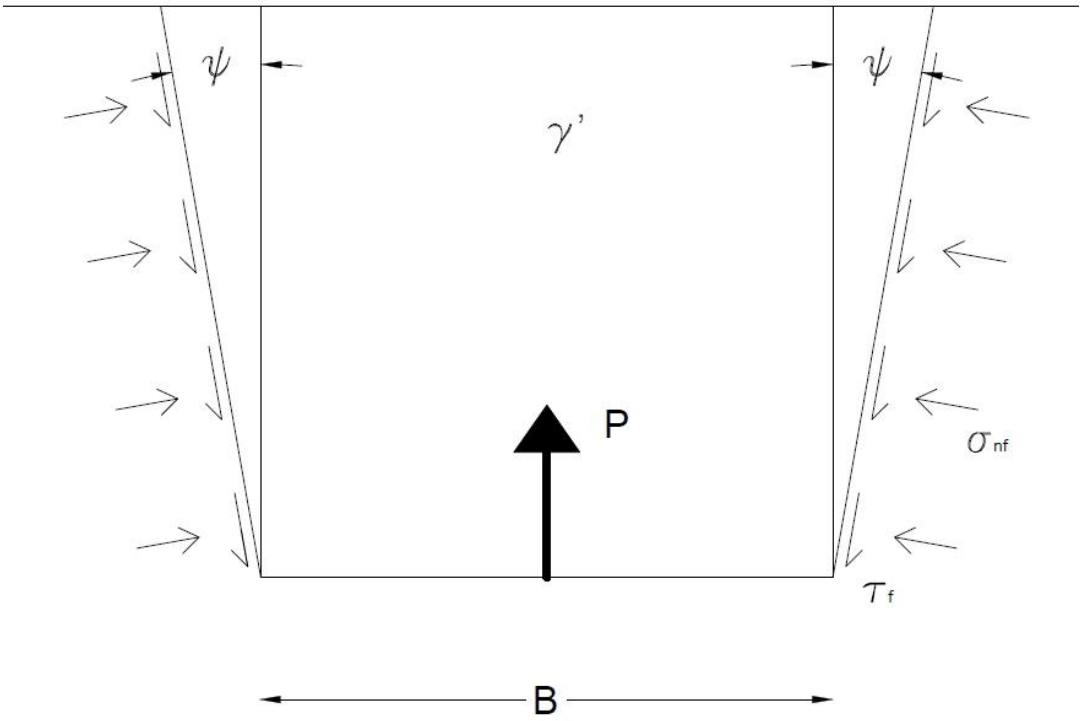

Figure 61- Free body diagram new model

Weight of the soil:

$$\forall = \frac{H}{3} * (B'^2 + B^2 + \sqrt{B'^2 B^2})$$

$$\forall = \frac{H}{3} * (B'^2 + B^2 + BB')$$

$$B'^2 = (B + 2H\tan\psi) * (B + 2H\tan\psi)$$

$$\forall = \frac{H}{3} * \left\{ (B + 2H\tan\psi)^2 + B^2 + (B + 2H\tan\psi)B \right\}$$

$$W = \frac{1}{3} * \gamma' * H * \left\{ (B + 2H\tan\psi)^2 + 2B^2 + 2HB\tan\psi \right\}$$

Shear on the sides:

$$S_\lambda = \int_0^H \tau(z)p(z)dz$$

$$B(z) = B + 2(H - z)\tan\psi$$

$$p(z) = 4(B + 2(H - z)\tan\psi)$$

$$\tau(z) = \gamma' z \tan\phi c_1$$

$$c_1 = \left(\frac{1+K_0}{2}\right) - \left(\frac{(1-k_0)\cos 2\psi}{2}\right)$$

$$F = \int_0^H \left(4\gamma' z \tan\phi c_1 \{B + 2(H - z)\tan\psi\}dz\right)$$

$$F = \int_0^H \left(4\gamma' z \tan\phi c_1 \{B + 2H\tan\psi - 2z\tan\psi\}dz\right)$$

$$F = \int_0^H \{(B + 2H\tan\psi)(4\gamma'\tan\phi c_1)z\}dz - \int_0^H \left(8\gamma'\tan\phi c_1 \tan\psi z^2\right)dz$$

$$F = \frac{1}{2}(B + 2H\tan\psi)(4\gamma'\tan\phi c_1)H^2 - \frac{1}{3}(8\gamma'\tan\phi c_1 \tan\psi H^3)$$

$$F = 2\gamma' H^2 \tan\phi c_1 (B + 2H\tan\psi) - \frac{8}{3}\left(\gamma' H^3 \tan\phi c_1 \tan\psi\right)$$

$$S_\gamma = 2\gamma' H^2 \tan\phi c_1 \left\{B + 2H\tan\psi - \frac{4}{3}H\tan\psi\right\}$$

$$S_\gamma = 2\gamma' H^2 \tan\phi c_1 \left\{B + \frac{2}{3}H\tan\psi\right\}$$

Breakout factor of the soil:

$$N_\gamma = \frac{P}{\gamma' HB^2}$$

$$N_{\gamma W} = \frac{1}{\gamma' HB^2} * \left(\frac{1}{3} * \gamma' * H * \left\{(B + 2H\tan\psi)^2 + 2B^2 + 2HB\tan\psi\right\}\right)$$

$$N_{\gamma W} = \frac{1}{3B^2}\left\{B^2 + 4HB\tan\psi + 4H^2\tan^2\psi + 2B^2 + 2HB\tan\psi\right\}$$

$$N_{\gamma W} = \frac{1}{3} * \left(1 + 4\left(\frac{H}{B}\right)\tan\psi + 4\left(\frac{H}{B}\right)^2 \tan^2\psi + 2 + 2\left(\frac{H}{B}\right)\tan\psi\right)$$

$$N_{\gamma W} = 1 + 2\left(\frac{H}{B}\right)\tan\psi + \frac{4}{3}\left(\frac{H}{B}\right)^2 + \tan^2\psi$$

Breakout factor of the shear:

$$N_{\gamma S} = \frac{1}{\gamma' HB^2} * \left(2\gamma' H^2 \tan\phi c_1 \left\{ B + \frac{2}{3} H \tan\psi \right\} \right)$$

$$N_{\gamma S} = 2\frac{H}{B^2}\tan\phi c_1 \left\{ B + \frac{2}{3} H \tan\psi \right\}$$

$$N_{\gamma S} = \tan\phi c_1 \left\{ 2\frac{H}{B} + \frac{4}{3}\left(\frac{H}{B}\right)^2 \tan\psi \right\}$$

$$N_{\gamma S} = 2\left(\frac{H}{B}\right)\tan\phi c_1 + \frac{4}{3}\left(\frac{H}{B}\right)^2 \tan\psi \tan\phi c_1$$

Combined:

$$N_\gamma = 1 + 2\left(\frac{H}{B}\right)\tan\psi + \frac{4}{3}\left(\frac{H}{B}\right)^2 \tan^2\psi + \left(\frac{H}{B}\right)\tan\phi c_1 + \frac{2}{3}\left(\frac{H}{B}\right)^2 \tan\psi \tan\phi c_1$$

$$N_\gamma = 1 + \left(\frac{H}{B}\right)F_1 + \left(\frac{H}{B}\right)^2 F_2$$

$$F_1 = 2\left(\tan\psi + \tan\phi c_1\right)$$

$$F_1 = 2\left(\tan\psi + \left(\tan\phi - \tan\psi\right)c_1\right)$$

$$F_2 = \frac{4}{3}\left(\tan^2\psi + \tan\psi \tan\phi c_1\right)$$

$$F_2 = \frac{4}{3}\left(\tan^2\psi + \tan\psi\left(\tan\phi - \tan\psi\right)c_1\right)$$

APPENDIX B: Pictures of the anchors and the setup

Figure 62- Small square anchor plate

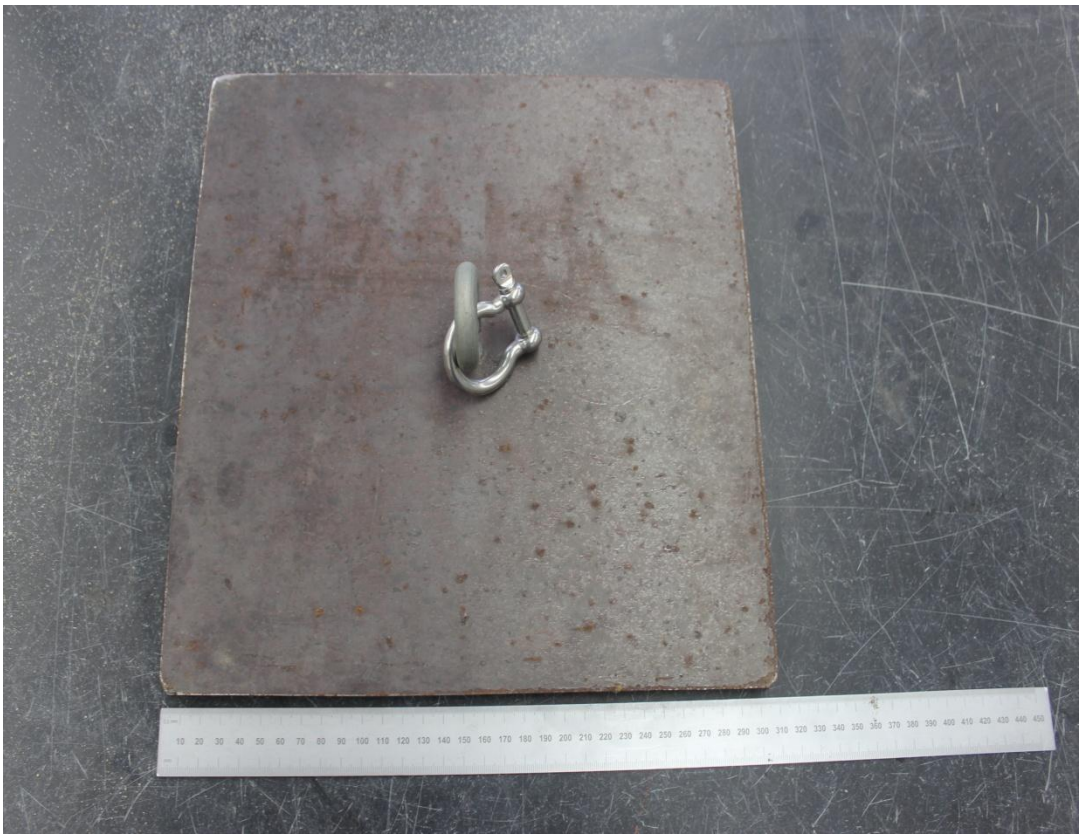

Figure 63- Large square anchor plate

Figure 64- Drag embedment anchor

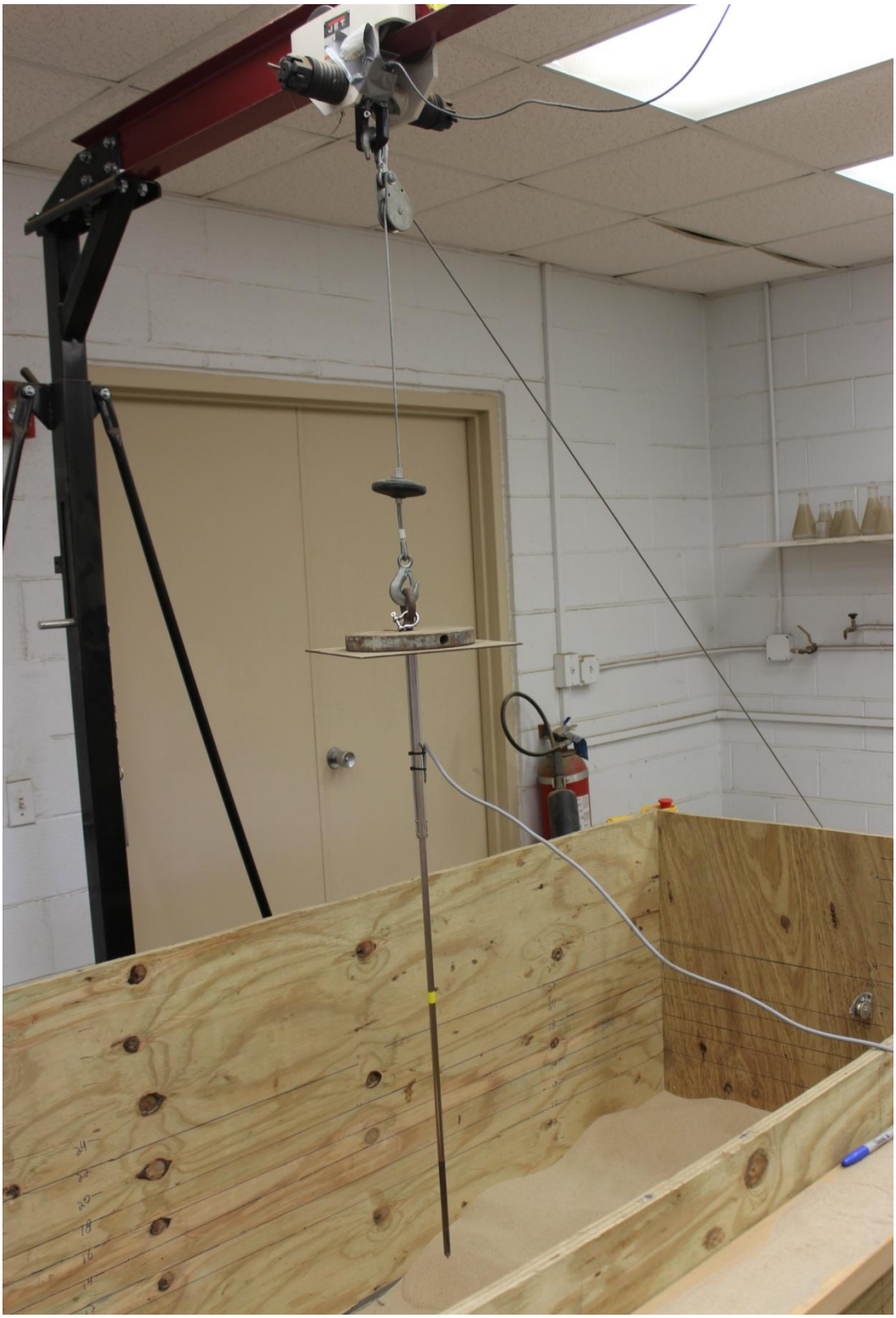

Figure 65- MCPT setup

Figure 66- Inclined pullout test setup

6 BIBLIOGRAPHY

ASTM Standard (2007) *Test Method for Particle-Size Analysis of Soils,* ASTM International, West Conshohocken, PA, DOI: 10.1520/D4513-11

ASTM Standard (2006a) *Test Methods for Maximum Index Density and Unit Weight of Soils Using a Vibratory Table,* ASTM International, West Conshohocken, PA, DOI: 10.1520/D4253-00R06

ASTM Standard (2006b) *Test Methods for Minimum Index Density and Unit Weight of Soils and Calculation of Relative Density,* ASTM International, West Conshohocken, PA, DOI: 10.1520/D4254-00R06E1

Aubeny, C.P., Murff, J.D. and Roesset, J.M. (2001) 'Geotechnical Issues in Deep and Ultra Deep Waters', *The International Journal of Geomechanis*, Vol. 1, No. 2, pp.225–247.

Bolton, M.D. (1986) 'The Strength and Dilatancy of Sands', *Géotechnique*, Vol. 36, No. 1, pp.65–78.

Breton, S.P. and Moe, G. (2009) 'Status, plans and technologies for offshore wind turbines in Europe and North America', *Renewable Energy*, Vol. 34, No. 3, pp.646–654.

Bulder, van Hees, Henderson, Huijsmans, Pierik, Snijders, Wijnants and Wolf (December 2002) *Studie naar halbaarheid van en randvoorwaarden voor drijvende offshore windturbines.* Masterthesis, TU Delft.

Bull, J.W. (2009) *Linear and non-linear numerical analysis of foundations,* Spon, London, New York.

Butterfield, R. and Andrawes, K.Z. (1970) 'An Air Activated Sand Spreader for Forming Uniform Sand Bes', *Géotechnique*, 20(1), pp.97–100.

Butterfield, C.P., Musial, W. and Jonkman J. (2007) 'Overview of Offshore Wind Technology: Preprint', *NREL*.

Butterfield, C.P., Musial, W.P., Scott, G.N. and Simms, D.A. (1992) 'NREL Combined Experimental Final Report - Phase II', *NREL*.

Butterfield, S. and Musial, W. (2004) 'Future for Offshore Wind Energy in the United States: Preprint'.

Butterfield, S., Musial, W. and Jonkman, J. (2005) 'Engineering Challenges for Floating Offshore Wind Turbines', *NREL*.

Casagrande, A. (1936). 'The determination of the pre-consolidation load and its practical significance', *Proceedings of the international conference on soil mechanics and foundation engineering,* Vol. 3, pp.60–64.

Caquot, A. and Kerisel, L. (1949) *Traite de Macanique des Sols,* Gauthier-Villars, Paris.

Cheuk, C.Y., White, D.J. and Bolton, M.D. (2007) 'Large-scale modelling of soil–pipe interaction during large amplitude cyclic movements of partially embedded pipelines', *Canadian Geotechnical Journal*, Vol. 44, No. 8, pp.977–996.

Choudhury, D. and Subba Rao, K S (2005) 'Seismic uplift capacity of inclined strip anchors', *Canadian Geotechnical Journal*, Vol. 42, No. 1, pp.263–271.

Das, B.M. and Seeley, G.R. (Eds.), (1977) *Uplift capacity of shallow inclined anchors*.

Das, B.M. and Shukla, S.K. (2013) *Earth anchors,* J. Ross Publishing Inc, Plantation, Florida.

Dave, T.N. and Dasaka, S. (2012) 'Assessment of portable traveling pluviator to prepare reconstitued sand specimens', *Geomechanics and Engineering - An International Journal*, Vol. 4, No. 2, pp.79-9-.

Dickin, E.A. and Leung, C.F. (1985) 'Evaluation of Design Methods for Vertical Anchor Plates', *Journal of Geotechnical Engineering*, Vol. 111, No. 4, pp.500–520.

Dickin, E.A. and Leung, C.F. (1983) 'Centrifugal Model Tests on Vertical Anchor Plates', *Journal of Geotechnical Engineering*, Vol. 109, No. 12, pp.1503–1525.

Fellenius, B.H. and Altaee, A. (1994) 'Physical modeling in sand', *Canadian Geotechnical Journal*, Vol. 31, pp.420–431.

Gade, V.K., Dave, T.N., Chauhan, V.B. and Dasaka, S. (2013) 'Portable Traveling Pluviator To Reconstitute Specimens Of Cohesionless Soils'.

Ghaly, A.M. (1997a) 'Load displacement prediction for horizontally loaded vertical plates', *Journal of Geotechnical and Geoenvironmental Engineering*, Vol. 123, No. 1, pp.74–76.

Ghaly, A.M. (1997b) 'The static equilibrium of drag anchors in sand: discussion', *Canadian Geotechnical Journal*, Vol. 34, No. 4, pp.635–636.

Ghosh, P. (2010) 'Seismic uplift capacity of inclined strip anchors in sand using upper bound limit analysis', *Geomechanics and Geoengineering*, Vol. 5, No. 4, pp.267–275.

Giampa, J.R. (2014) *Interpretation of Shallow Helical Anchor Capacity in Sand.* Masterthesis, University of Rhode Island, Kingston, Rhode Island.

Goel, S., Shalini and Patra, N.P. (2006) 'Break out resistance of inclined anchors in sand', *Geotechnical and Geological Engineering*, Vol. 24, No. 6, pp.1511–1525.

Green, R. and Vasilakos, N. (2011) 'The economics of offshore wind', *Energy Policy*, Vol. 39, No. 2, pp.496–502.

Hanna, A.M., Das, B.M. and Poriero, A. (1988) 'Behavior of shallow inclined plate anchors in sand', *Special Topics in Foundations*, pp.54–72.

Hensel, J., Sharma, R., Baxter, C. and Hu, J. (2012) 'Development of a technology type factor for jacket structures for offshore wind turbines in Rhode Island', *Journal of Renewable and Sustainable Energy*, Vol. 4, No. 6, p.63120.

Heronemus, W.E. (Ed.), (1972) *Pollution-Free Energy From Offshore Winds*.

Holtz, R.D., Kovacs, W.D. and Sheahan, T.C. (2011) *An introduction to geotechnical engineering*, 2nd ed., Pearson, Upper Saddle River, NJ.

Houlsby, G.T. (Ed.), (1991) *How the dilatancy of soils affects their behaviour*.

Jefferies, M. and Been, K. (2002) *Soil liquefaction,* Spon, London.

Jonkman, J., Butterfield, S., Musial, W. and Scott, G. (2009) 'Definition of a 5-MW Reference Wind Turbine for Offshore System Development'.

Jonkman, J.M. (2007) 'Dynamics Modeling and Loads Analysis of an Offshore Floating Wind Turbine'.

Jonkman, J.M. and Buhl, M.L. (Eds.), (2007) *Loads Analysis of a Floating Offshore Wind Turbine Using Fully Coupled Simulation: Preprint*.

Kim, J., Nadukuru, S.S., Pour-Ghaz, M., Lynch, J.P., Michalowski, R.L., Bradshaw, A.S., Green, R.A. and Weiss, W.J. (2012) 'Assessment of the Behavior of Buried Concrete Pipelines Subjected to Ground Rupture: Experimental Study', *Journal of Pipeline Systems Engineering and Practice*, Vol. 3, No. 1, pp.8–16.

Kirsch, A. (2009) *On the face stability of shallow tunnels in sand. Advances in Geotechnical Engineering and Tunneling,* Logos-Verl, Berlin.

Kulhawy, F.H. and Mayne, P.W. (1990) 'Manuel on Estimating Soil Properties for Foundation Design', *Cornell University*.

Laudahn, A. (2005) 'An approach to 1g modelling in geotechnical engineering with soiltron', Logos-Verl, Berlin, Vol. 11.

Leblanc, C., Houlsby, G.T. and Byrne, B.W. (2010) 'Response of stiff piles to long term cyclic loading', *Géotechnique*, Vol. 60, No. 9, pp.715–721.

LeLievre, B. and Tabatabaee, J. (1981) 'The performance of marine anchors with planar flukes in sand', *Canadian Geotechnical Journal,* No. 18, pp.520–534.

Liu, H., Li, Y., Yang, H., Zhang, W. and Liu, C. (2010) 'Analytical study on the ultimate embedment depth of drag anchors', *Ocean Engineering*, Vol. 37, 14-15, pp.1292–1306.

Liu, H., Liu, C., Yang, H., Li, Y., Zhang, W. and Xiao, Z. (2012a) 'A novel kinematic model for drag anchors in seabed soils', *Ocean Engineering*, Vol. 49, pp.33–42.

Liu, J., Liu, M. and Zhu, Z. (2012b) 'Sand Deformation around an Uplift Plate Anchor', *Journal of Geotechnical and Geoenvironmental Engineering*, Vol. 138, No. 6, pp.728–737.

Masciola, A., Robertson, A., Jonkman, J. and Driscoll, F. (Eds.), (2011) *Investigation of a FAST-OrcaFlex Coupling Module for Integrating Turbine and Mooring Dynamics of Offshore Floating Wind Turbines: Preprint*.

Matha, D. (2009) 'Model Development and Loads Analysis of an Offshore Wind Turbine on a Tension Leg Platform with a Comparison to Other Floating Turbine Concepts: April 2009', *NREL*.

Matha, D., Fischer, T. and Kuhn, M. (2009) 'Model Development and Loads Analysis of a Wind Turbine on a Floating Offshore Tension Leg Platform'.

Merifield, R.S., Lyamin, A.V. and Sloan, S.W. (2006) 'Three dimensional lower bound solutions for the stability of plate anchors in sand', *Géotechnique*, Vol. 56, No. 2, pp.123–132.

Meyerhof, G.G. (1973) 'Uplift Resistance of Inclined Anchors and Piles', *International Conference on Soil Mechanics and Foundation Engineering*, Vol. 21, No. 1, pp.167–172.

Meyerhof, G.G. and Adams, J.J. (1968) 'The Ultimate Uplift Capacity of Foundations', *Canadian Geotechnical Journal*, V, No. 4, pp.225–244.

Miedema, S.A., Lagers, G. and Kerkvliet, J. (2005) 'An oveview of drag embedded anchor holding capacity for dredging and offshore applicaions'.

Monaco, T. (May 2013) *Experimental Studies of Scale Model Drag Embedment Anchors (DEAs) Subjected to Impulse Forces.* Master thesis, Syracuse University, Syracuse, NY.

Murray, E. and Geddes, J. (1989) 'Resitance of passive inclined anchors in cohesionaless medium', *Géotechnique*, Vol. 39, No. 3, pp.417–431.

Murray, E. and Geddes, J. (1987) 'Uplift of Anchor Plates in Sand', *Géotechnique*, Vol. 113, No. 3, pp.202–215.

Musial, W. and Butterfield, S. (2004) 'Future for Offshore Wind Energy in the United States: Preprint', *NREL*.

Musial, W., Butterfield, S. and Boone, A. (2004) 'Feasibility of Floating Platform Systems for Wind Turbines: Preprint', *NREL*.

Musial, W., Butterfield, S. and Ram, R. (2006) 'Energy from Offshore Wind: Preprint', *NREL*.

Myhr, A., Maus, K.J. and Nygaard, T.A. (Eds.), (2011) *Experimental and Computational Comparisons of the OC3-HYWIND and Tension-Leg-Buoy (TLB) Floating Wind Turbine Conceptual Designs*.

NAVFAC (Ed.), (2012) *Handbook for Marine Geotechnical Engineering,* NAVFAC, Port Huneme, California.

NCEL (1987) *Drag Embedment Anchors for Navy Moorings,* Port Huneme, California.

Neubecker, S.R. and Randolph, M.F. (1996a) 'The kinematic behaviour of drag anchors in sand', *Canadian Geotechnical Journal*, Vol. 33, pp.587–594.

Neubecker, S.R. and Randolph, M.F. (Eds.), (1995) *Performance of Embedded Anchor Chains and Consequences for Anchor Design*.

Neubecker, S.R. and Randolph, M.F. (1996b) 'The static equilibrium of drag anchors in sand', *Canadian Geotechnical Journal,* Vol. 33, pp.574–583.

Okamoto, M. and Fityus, S. (2006) 'An evaluation of the dry pluviation preparation technique applied to silica sand samples', *Geomechanics and Geotechnics of Particulate Media,* CRC Press.

Poulos, S.J. (1981) 'The steady state of deformation', *ASCE Journal of Geotechnical Engineering*, Vol. 107, pp.553–562.

Prezzi, M. (2009) 'Implementation of Laterally Loaded Piles in Multi-Layer Soils'. Purdue University, West Lafayette, Indiana.

Rad, N.S. and Tumay, M.T. (1987) 'Factors affecting sand specimen preparation by raining', *Geotechnical Testing Journal*, Vol. 10, No. 1, pp.31–37.

Randolph, M.F., Gaudin, C., Gourvenec, S., White, D.J., Boylan, N. and Cassidy, M.J. (2011) 'Recent advances in offshore geotechnics for deep water oil and gas developments', *Ocean Engineering,* No. 38, pp.818–834.

Randolph, M.F. and Gourvenec, S. (2011) *Offshore geotechnical engineering*, 1st ed., Spon Press, Abingdon, Oxon, New York, NY.

Roscoe, K.H. and Poorooshasb, H.B. (1963) 'A Theoretical and Experimental Study of Strains in Triaxial Compression Tests on Normally Consolidated Clays', *Géotechnique*, Vol. 13, No. 1, pp.12–38.

Roscoe, K.H., Schofield, A. and Wroth, C.P. (1958) 'On the yielding of soils', *Géotechnique*, Vol. 8, pp.22–53.

Rowe, R.K. and Booker, J.R. (Eds.), (1979) *The analysis of inclined anchor plates*.

Rowe, R.K. and Davis, E.H. (1982) 'The behaviour of anchor plates in sand', *Géotechnique*, Vol. 32, No. 1, pp.25–41.

Salgado, R., Bandini, P., and Karim, A. (2000) 'Shear Strength and Stiffness of Silty Sand', *Journal of Geotechnical and Geoenvironmental Engineering*, Vol. 126, pp.451–462.

Santamarina, J.C. and Cho, G.C. (2001) 'Determination of Critical State Parameters in Sandy Soils- Simple Procedure', *Geotechnical Testing Journal*, Vol. 24, No. 2, pp.185–192.

Sarac, D.Z. (1989) 'The Uplift Capacity of Shallow Buried Anchor Slabs', *International Conference on Soil Mechanics and Foundation Engineering*, Vol. 12, pp.1213–1218.

Schneider, J. and Senders, S. (2010) 'Foundation Design: A Comparison of Oil and Gas Platforms with Offshore Wind Turbines', *Marine Technology Society Journal*, Vol. 44, No. 1, pp.32–51.

Schofield, A.N. and Wroth, P. (1968) *Critical state soil mechanics,* McGraw-Hill, London, New York.

Sclavounos, P.D., Lee, S., DiPietro, J., Potenza, G., Caramuscio, P. and Michele, G. de (Eds.), (2010) *Floating Offshore Wind Turbines Tension Leg Platform and Taught Leg Buoy Concepts Supporting 3-5 MW Wind Turbnies*.

Snyder, B. and Kaiser, M.J. (2009) 'Ecological and economic cost-benefit analysis of offshore wind energy', *Renewable Energy*, Vol. 34, No. 6, pp.1567–1578.

Thorne, C.P. (1998) 'Penetration and Load Capacity of Marine Drag Anchors in Soft Clay', *Journal of Geotechnical and Geoenvironmental Engineering*, Vol. 124, No. 10, pp.945–953.

Tong, K. (1998) 'Technical and economic aspects of a floating offshore wind farm', *Journal of Wind Engineering and Industrial Aerodynamics*, 74-76, pp.399–410.

Tufenkjian, M.R., Yee, E. and Thompson, D.J. (Eds.), (2010) *Comparison of cone and minicone penetration resistance for sand at shallow depth*.

Vaid, Y.P. and Negussey, D. (1984) 'Relative Density of Pluviated Sand Samles', *Soils and Foundations,* Vol. 24, No. 2, pp.101–105.

Vryhof Anchors (2010) *Anchor Manual 2010*, 4th ed., Vryhof Anchors, Capelle a/d Yssel, Netherlands.

Wang, M.C. and Wu, A.H. (Eds.), (1980) *Yielding load of anchor in sand. Applications of Plasticity and Generalized Stress-Strain in Geotechnical Enginerring*.

White, D., Cheuk, C.Y. and Bolton, M.D. (2008) 'The uplift resistance of pipes and plate anchors buried in sand', *Géotechnique*, Vol. 58, No. 10, pp.771–779.

Yan, L. and Byrne, P.M. (1989) 'Application of hydraulic gradient similitude method to small-scale footing tests on sand', *Canadian Geotechnical Journal*, Vol. 26, pp.246–259.